Fundamental Analysis of the Interaction of Low Pressure Plasmas with Polymer Surfaces

by

Markus Bach

Thesis

Presented to the

Department of Physics

University of Osnabrück

Osnabrück

June, 2003

Thesis Advisor:

apl. Prof. Dr. Manfred Neumann

Table of Contents

1. Introduction

Polymers are an interesting kind of material. The word polymer comes from the Greek words *polys* (many) and *meros* (part) and describes a natural or synthetic compound combined by a multiplicity of small molecules (monomers). While the most simple structures from a chemical point of view only consist of hydrogen and carbon atoms, the ability of the carbon to build up different forms of bonds leads to a multiplicity of these compounds. Next to the hydrocarbon compounds other atoms like oxygen and nitrogen may be incorporated, which form new chemical groups with different properties. The physical and chemical properties of this class of material therefore refers to aspects of structure and composition.

Polymers play an important role in industry. As raw materials are cheap, the total world production of polyolefines (including Polyethylene and Polypropylene) will rise from 53.6 mio.t in 1995 up to 79.6 mio.t in 2005 [KAMI97]. They are also quite easy to produce and can be formed through various processes such as injection moulding. For different applications the composition of the polymer material can be engineered. However, sometimes the specifications for a product or production process vary for different areas of the material (e.g. bulk and surface properties) and some properties like adhesion or wettability need to be changed according to the requirements of the engineers.

To overcome these problems several techniques of surface modification have been developed. Plasma technology with its non-equilibrium chemistry is very promising for fulfilling the demands of finishing processes. A plasma can briefly be described as an ionised[1] gas, consisting therefore of ions, electrons and neutral species. Due to relaxation and recombination processes various radiation wavelengths occur down to ultraviolet (UV). Their properties change dramatically when coming into contact with the surface. One can distinguish basically two effects of such encounters: an *activation* of the surface occurs by a loss of energy and charge of the plasma species and a *functionalisation* by a direct incorporation of the molecular components of the process gas to the surface or bulk material.

In the process of *activation* a noble gas and its compounds cause polymer bonds to break, thereby creating radicals on the surface. These sites are chemically reactive and participate in subsequent reactions. The radicals can also react with one another, therefore creating double bonds or cross-linkage.

In the case of *functionalisation*, one can think of gases like oxygen or nitrogen coming into contact with the activated surface and participating in chemical reactions.
An even more reactive form of *functionalsiation* will occur when these gases generate fragments inside the plasma and yield functional groups after penetrating into the polymer. Using oxygen as a process gas leads to the production of hydroxyl, carbonyl, and ester groups. These functional groups are useful in the industry because such pre-treated products are receptive to further surface processes like painting or adhering.

However, the modification of polymers becomes a complex task because of the various interactions within the plasma and between the plasma and the material. As it is so far impossible to model all conceivable reactions theoretically, a new approach has been accomplished in this work by splitting the plasma into its basic components. Additionally the system complexity has been reduced by choosing accurate parameters for the discharge, eliminating the influence of the ions. These parameters have been found by theoretical considerations and testing special experimental aspects, leading to effective modification processes only through electrons and photons.
Furthermore, modifications were so far only analysed as a completed process by identifying and evaluating the new chemical groups afterwards, but in this work some of the preceding reactions, such as the origin of different types of radicals, have been determined after applying a kind of conservation reaction. With those analytical methods reactions can be investigated at a molecular level.

The new idea of this work is to describe microscopic changes in chemical composition and structure of a polymer surface caused by the separated plasma species electrons and photons.

The challenge to distinguish different effects in the modification process will be tackled by observing the chemical and structural changes of the polymer surface. The composition of the sample was investigated with *x-ray photoelectron spectroscopy (XPS)*, in which emitted electrons have been analysed. The surface structure was detected with an *atomic force microscope (AFM)*, where a tiny tip screens the polymer and records the forces between tip and sample. From this signal structural data like topography or elasticity can be calculated.

[1] It was used here the British form of orthography, leading to some unfamiliar spelling like “ionisation”

The modification of the material has been accomplished with a microwave plasma as well as with electrons and UV-light to induce different reactions in the surface region. Therefore a basic description of a physical plasma is found in chapter 2 – *Theory and Experimental Testing*.

The modification experiments required a very precise understanding of the plasma's behaviour, and so the basic inner plasma reactions and possible interactions between the plasma and the polymer surface are introduced and discussed according to the simplified treatment conditions. The plasma electrons especially have been studied in these preliminary stages leading to basic considerations for the experiments and analysing methods. After these preparations the plasma can be experimentally modelled. Those aspects and their measurements will be presented in chapter 3 – *Plasma Analysis*.

Surface modifications with electrons, photons and plasmas of different process gases lead to several interactions when the sample later comes into contact with air. One of these interactions is the incorporation of different elements and therefore the creation of new chemical groups, which were partly determined according to their depth distribution. Also structural changes, such as the creation of double bonds, are discussed. To understand some initial reactions of the modification process, different types of radicals were traced after electron treatment in a chemical labelling reaction. These and further measurements are presented in chapter 4 – *Results and Discussion*.

This assignment will end with a *Summary and Conclusions* (chapter 5), A*cknowledgements* (chapter 6) and further aspects in an *Appendix*.

2. Theory and experimental testing

This work refers to polymer surfaces modified by plasma treatment and the separated effects through electrons and UV-light, so first of all the question arises what a surface is and how it can be characterised. As there is no universal definition, a surface will often be described as the border between two thermodynamical phases [NeKo00]. An answer also depends on experimental techniques which give information about chemical and structural aspects within different depths. In the microscopic approach there are basically two ways how a surface can be characterised: with spectroscopic and imaging techniques. Next to these kinds of techniques, there are also macroscopic methods to describe surface properties (e.g. measurements contact angles or the fractal dimension).

In spectroscopy an excitation is applied to a sample and the interaction according to a probe is detected. The excitation can be induced by radiation with different wavelengths or particles (ions, electrons, ...). Also the variety of probes is manifold and the different types of analysers gives various insights to the sample. According to the excitation and the probes, spectroscopic methods can be distinguished by the obtained information, detection limit, lateral resolution and analysis depth (see figure 1).

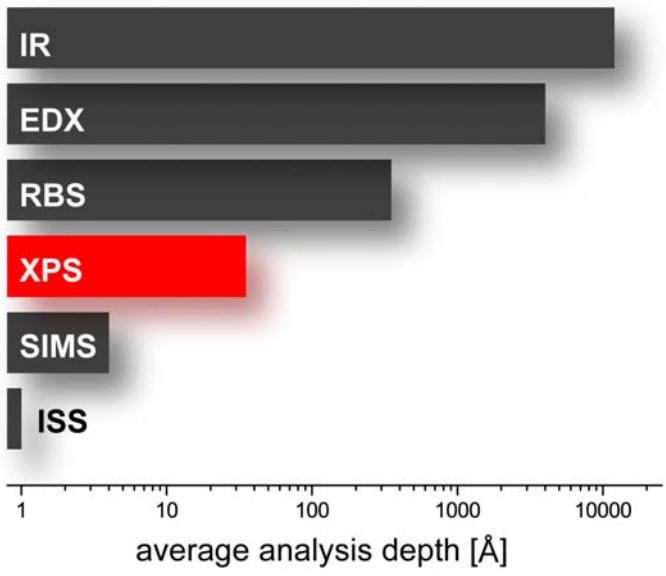

Figure 1: analysis depths of several spectroscopic techniques like infrared spectroscopy (IR), energy dispersive x-ray spectroscopy (EDX), RUTHERFORD backscattering spectroscopy (RBS), secondary ion mass spectroscopy (SIMS), and ion scattering spectroscopy (ISS)

Also aspects like the quantification of the measured values and a possible destruction of the sample can be taken into account.

Imaging techniques visualise the structures of a sample in a direct, calculated or reciprocal way. These methods include optical imaging (like from a classical microscope), electron-optical imaging, diffraction methods, and various scanning methods. They also differ in their specific parameters like lateral resolution and analysis depth.

In this work a combination of a spectroscopic and an imaging technique was used to obtain information about untreated and modified surfaces. *X-ray photoelectron spectroscopy* investigates electronic properties of atoms by detecting electrons as probes and therefore identifying the chemical composition of the sample. This technique is sensitive for the first atomic layers and mainly non-destructive (see red bar in figure 1).

For a structural analysis of the sample (as well as some mechanical aspects) *atomic force microscopy* was used. The occurring forces between a tiny tip and the sample are measured and from this signal the topography can be calculated. This technique is also non-destructive with a high resolution (about some nm), depending on the different forces.

In this chapter the basic theories of the experimental techniques are introduced as well as some aspects of microwave discharges.

2.1 Chemical composition of a sample

A main aspect is to investigate the chemical composition of a sample. On one hand it can be used to verify the purity of the sample. On the other hand the change in composition due to the modification can be traced. Therefore the theory and experimental aspects of high resolution x-ray photoelectron spectroscopy must be discussed.

Nowadays an important and widely used experimental technique is photoelectron spectroscopy. Based on the photoelectric effect discovered by HERTZ in 1887, respectively HALLWACHS in 1889, where photons with a sufficient amount of energy interact with a solid emitting electrons, these so called photoelectrons provide information about the occupied electronic states in the surface area of the sample [Hert87][Hall89]. In 1905 EINSTEIN interpreted this process by granting the photons a quantified energy $h\nu$ proportional to their frequencies [Eins05], being transferred in this case to an electron. In the process the energy is sufficient for stripping the electron away from the atom overcoming a binding energy E_{bin} as well as for accelerating it up to the kinetic energy of the photo-emitted electrons (E_{kin}). The last value is measured in photoelectron spectroscopy and refers to core or valence orbitals.

Depending on whether ultraviolet or x-ray radiation is used, the techniques are called ultraviolet photoelectron spectroscopy (UPS) or x-ray photoelectron spectroscopy (XPS). With UPS ($h\nu$ ~ 10...100eV) the valence band of a sample can be examined with high

accuracy because of the small line width of the used gas discharge lamps. For the chemical analysis of materials XPS ($h\nu$ ~ 100...10000eV) is an appropriate technique with a high sensitivity for the chemical environment. This method is therefore also called ESCA as an abbreviation for *Electron Spectroscopy for Chemical Analysis* [Sieg67]. Today, an increasing usage of synchrotron radiation for photoelectron spectroscopy dissolves the border between UPS and XPS with tuneable frequencies for the radiation at small line-widths.

2.1.1 Theory of XPS

The balance in regard to energy conservation for a free atom (or molecule) before and after ***photoemission*** is:

$$E_{in} + h\nu = E_{kin} + E_{fin}\,, \tag{1}$$

where $h\nu$ is the photon energy, E_{in} and E_{fin} are the total initial and final energies of the atom before and after photoemission, and E_{kin} is the kinetic energy of the photoelectron. For a given electron the binding energy E_{bin} is defined as the energy necessary to remove an electron without kinetic energy to infinity. Considering the vacuum level with its energy E_v as reference (i.e. E_v=0), one can write:

$$h\nu = E_{kin} + E_{bin}\,. \tag{2}$$

For conducting materials the spectrometer and the solid can be connected in order to keep the system at a common potential during photoemission. In this case the FERMI level of the spectrometer and the solid become the same [Deke73].
The calibration for non-conducting samples, as it will be shown below, can be carried out by comparing the signals with references.

A simple, phenomenological approach to describe the photoemission process is the ***three-step model*** [PlEb82][Spic58][BeSp64][Luet93]. This model describes the process in three independent events for the photoelectron:

- photoionisation;
- propagation through the sample to the surface;
- penetration through the surface and emission into the surrounding vacuum.

As the photoemission process implies a full quantum-mechanical processing in which an electron is removed from an occupied state within the solid before it is detected, a more sophisticated description is the ***one-step model*** [Bors85]. Here Ψ_{in} and Ψ_{fin} are considered as wave functions corresponding to the initial and final states, while the transition probability between these two eigen functions of the same HAMILTONIAN H_0 obeys FERMI'S golden rule:

$$\omega \sim \left|\left\langle \Psi_{fin} \left| H^* \right| \Psi_{in} \right\rangle\right|^2 \delta\left(E_{fin} - E_{in} - h\nu\right). \tag{3}$$

It is assumed that the perturbation H^* is small when applied to the system. The incident radiation, characterised by the vector potential A and scalar potential Φ, causes the perturbation of the system so that the initial HAMILTONIAN H_0 becomes H:

$$H = H_0 + \frac{e}{2mc}(A \cdot P + P \cdot A) - e\Phi + \frac{e^2}{2mc^2}\left|A\right|^2 \tag{4}$$

In this formula e and m denote the electron charge and mass, c is the speed of light and P stands for the momentum operator. While in the initial state N electrons occupy the system, the initial and final wave functions can be written in a ***sudden-approximation*** because of the fast-emitted photoelectrons. The interaction with the remaining (N-1) electron system is negligible:

$$\Psi_{in}^{(N)} \sim \Psi_{in}^{k} \Psi_{in}^{(N-1)} \tag{5}$$

$$\Psi_{fin}^{(N)} \sim \Psi_{fin}^{E_{kin}} \Psi_{fin}^{(N-1)} \tag{6}$$

Ψ_{in}^{k} is the wave-function of the k orbital and $\Psi_{fin}^{E_{kin}}$ the wave-function of the photoelectron having left the level k with the kinetic energy E_{kin}. Hence, the matrix element $\left\langle \Psi_{fin} \left| H^* \right| \Psi_{in} \right\rangle$ is the product of a one-electron matrix, $\left\langle \Psi_{fin}^{E_{kin}} \left| H^* \right| \Psi_{in}^{k} \right\rangle$ and an (N-1) electron overlap integral, $\left\langle \Psi_{fin}^{(N-1)} \middle| \Psi_{in}^{(N-1)} \right\rangle$.

Assuming the orbitals remain unmodified during the photoemission process, this ***frozen-orbital*** leads to $\Psi_{fin}^{(N-1)} = \Psi_{in}^{(N-1)}$, and the transition matrix element equals the one-

electron matrix element. KOOPMANS' theorem gives the binding energy measured in an XPS process [Koop33]:

$$E_{bin}(k) = -\varepsilon k \,. \qquad (7)$$

Even in this more precise theory other aspects like relaxation, correlation and relativistic effects have to be considered [Holl82].

After photoionisation the excited atomic system has to relax into a state of minimal energy. An inner shell electron-hole recombination can reach this state. There are several ways for such a ***recombination***, illustrated in the next figure.

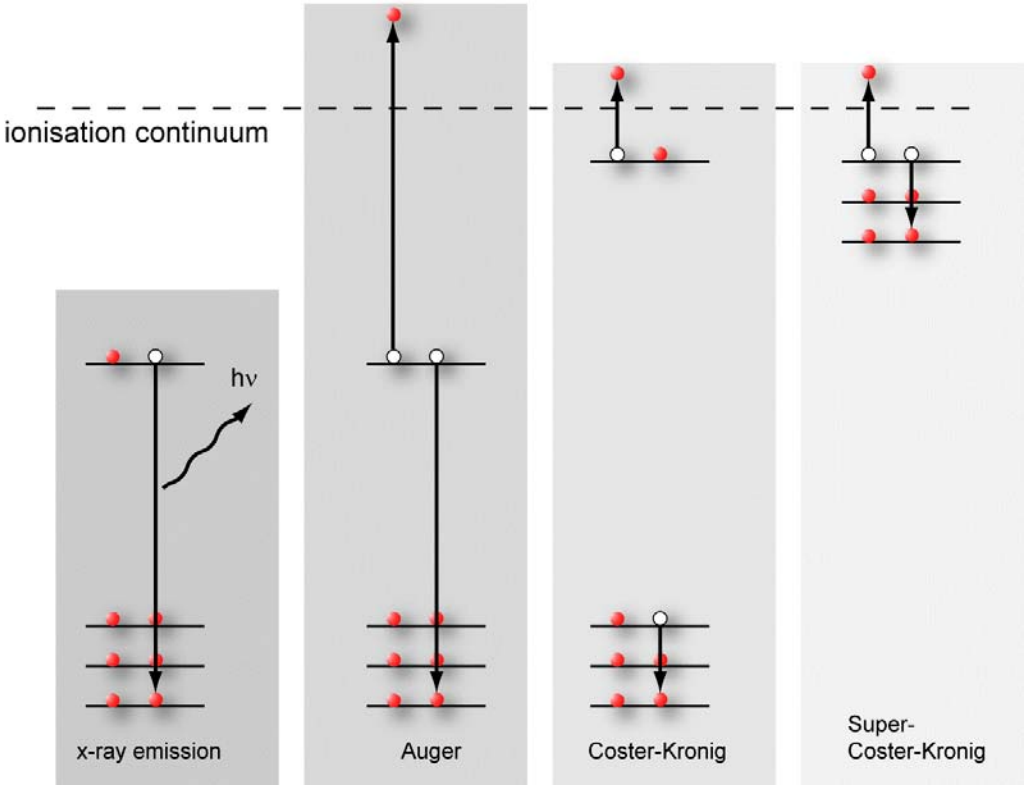

Figure 2: different recombination processes [Schn01]

In the process of ***x-ray emission***, the relaxation energy is emitted as a photon. Taking only the electric dipole vector of the radiation into consideration, the x-ray emission obeys the following selection rules: $\Delta l = \pm 1$ and $\Delta j = \pm 1$ or 0.

The probability of relaxation via dipolar emission is more than two times greater than that corresponding to electric quadrupoles or to the magnetic dipole vector, therefore these can usually be neglected [BrBa79].

The x-ray emission is named after the shell in which the initial vacancy was created (K for l = 0, L for l = 1, etc.). This capital is followed by a Greek letter (α, β, ...) and numerical subscripts, as indicated in the next figure.

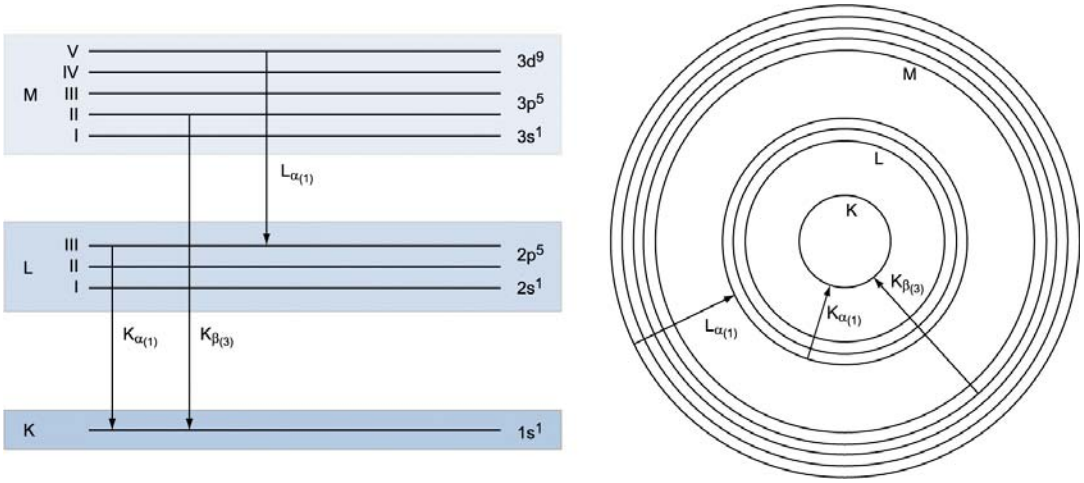

Figure 3: x-ray emission lines – left: term diagram, right: quasi-atomic model [Voge97]

The probability of relaxation rises with the ordinal number [Deme01] and therefore the method is not suitable for investigated hydrocarbons.

With smaller ordinal numbers the probability of a second way of ion relaxation rises: the ejection of a second electron in an ***AUGER process*** [Auge25]. In this two electron process (named after P. AUGER who discovered this process in 1925) one electron transfers the freed energy to another electron in the same shell. If the second electron has enough energy to leave the solid, it may be analysed next to the photoelectron. The process then leaves two secondary electron holes. For an energy transfer to electrons of other shells, these are called COSTER-KRONIG [Kuzm98] and SUPER-COSTER-KRONIG [DaFe81] transitions.

In the nomenclature used for this process the first letter stands for the hole's shell, the second denotes the shell from where the recombination starts and the third letter labels the shell from where the AUGER electron is emitted. So K is used for the 1s levels, L_1, L_2 and L_3 for 2s, $2p_{1/2}$ and $2p_{3/2}$ respectively[2] [Deke73]. For example, the kinetic energy of a KL_3L_1 Auger electron is

$$E_{kin} = E(K) - E(L_3) - E(L_1)^* - \phi . \qquad (8)$$

[2] some authors use Roman numbers instead of Arabic ones

As the equation is independent from the excitation, photoelectrons and Auger electrons can be distinguished by using two different x-ray energies. Equation 8 and the notations above are also valid for the COSTER-KRONIG and the SUPER-COSTER-KRONIG transitions.

The photoelectron lines associated with ***core levels*** are usually sharp, may have variable intensities and widths and, except the s levels, are doublets. The spectroscopic notation of a state is nl_j, where n and l are the principal and orbital quantum numbers and $j=l\pm s$ (s=1/2). For a given principal quantum number, l can take n values: 0, 1, 2, 3, ... (n-1) and the corresponding levels are denoted as s, p, d, f, ... respectively. The doublet character of the core lines arises through the spin-orbit (j-j) coupling.
The width of a core line depends upon several factors such as the lifetime of the core hole created during photoemission, unresolved chemically-shifted peaks, multiple final states and x-ray line width, the finite resolution of the analyser etc. [BrSe83]. The peak width (FWHM = full width at half-maximum) can be written as

$$\Delta E = \sqrt{(\Delta E_n)^2 + (\Delta E_p)^2 + (\Delta E_a)^2} \tag{9}$$

where ΔE_n represent the natural width of the core level, ΔE_p and ΔE_a being due to the spectrometer, namely the width of the x-ray line and the analyser resolution, respectively.
For metals, the lines have an asymmetric form, due to the screening effect by the conduction electrons [Kuzm98] and are well described by the DONIACH-SUNJIC formula [DoSu70]. For insulators and semiconductors the lines have a LORENTZ-type shape.

The binding energies of a certain core level are different for non-equivalent atoms. This results from different oxidation states, the surrounding chemical environment or different lattice sites. The difference in binding energy is called ***chemical shift*** in analogy of nuclear magnetic resonance spectroscopy. It can be regarded as the result of a change in the spatially averaged COULOMB and exchange potentials exerted upon an electron by its environment. The next figure shows different chemical surroundings for carbon groups in a three-dimensional plot with the corresponding values for the shift in binding energy.

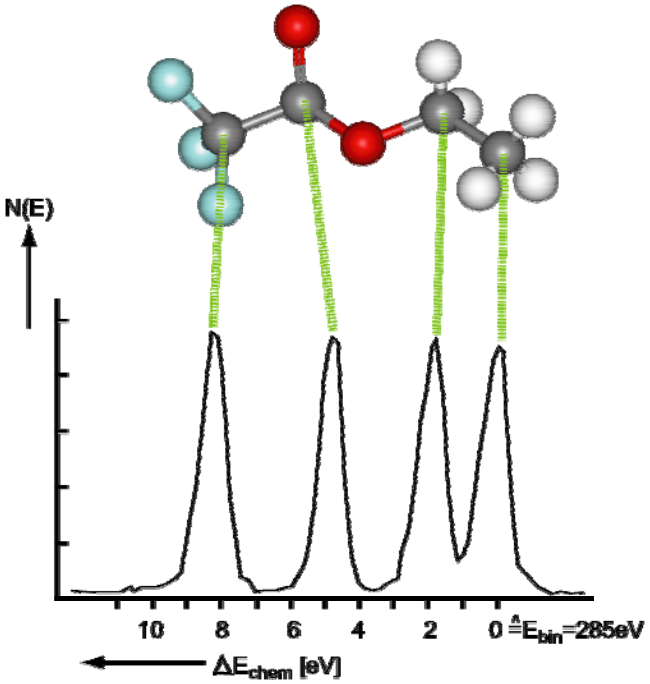

Figure 4: chemical shifts referred to the (hydro-)carbon 1s line at 285eV binding energy

Several theoretical methods for calculating chemical shifts can be carried out like the self-consistent field (SCF) approach, using the non-relativistic HARTREE-FOCK formalism or the relativistic DIRAC-FOCK method [Deke73]. An accurate binding energy can be calculated by extending equation 7 with relaxation, correlation and relativistic effects:

$$E_{bin} = -\varepsilon k - \delta E_{relaxation} + \delta E_{correlation} + \delta E_{relativistic} . \qquad (10)$$

An alternative is the so called charge potential model, in which the core binding energy is considered to depend on the potentials created by the valence electrons of the considered atom and also by electrons from the neighbouring atoms [Ghos83].

Valence band spectra are characterised by many closely spaced levels [BrSe83]. Its electrons are de-localised or sojourn in bonding orbitals which have low binding energies and effect the electronic structure of the investigated material [Zubr95]. Because of lower cross-sections, the intensity of valence band spectra, excited by x-rays, appears to be much lower than that of core level spectra. More about this theme with a special focus on polymers was published by FOERCH and MÄHL [FBB91] [Mähl99].

Multiplet (exchange) ***splitting*** of core level lines can occur for systems with unpaired electrons in valence levels. More about the exchange splitting can be found with [Vlec34] [FaSh70] [OkKo92].

Besides the previously described effects involving one electron, effects with more electrons occur [Carl67][KrCa67]. Here two electron processes dominate [Fadl78], in which, simultaneously with the removal of the photoemission electron, a second electron can be transferred to a higher orbital in a ***shake-up process*** or be completely removed in a ***shake-off process***, leading to a second emitted electron (see next figure).

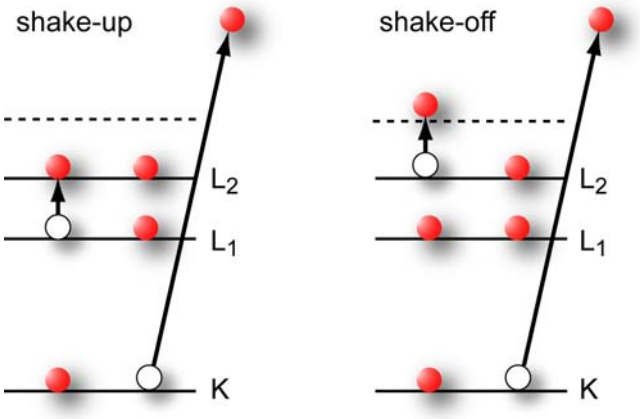

Figure 5: Electron shake-up and shake-off processes following ionisation [Holl82].

The energy necessary for either process is supplied from the kinetic energy of the photoelectron produced during initial ionisation. Therefore, the corresponding satellites in the XPS spectrum will appear on a higher binding (lower kinetic) energy side of the main peaks. For the electron involved in a shake-up or shake-off process the selection rules $\Delta l=0$, $\Delta s=0$, $\Delta j=0$ have to be fulfilled and therefore a change of n can occur [Holl82].

While the photoelectron spectra offer a lot of information, the peak areas and shapes need to be determined for a ***quantitative analysis*** of the XPS spectra. The radiation of the x-rays penetrates the solid some µm and electrons in this depth are thereby excited. However, some of them lose a part of their energy through inelastic scattering processes during on their way to the surface and end up at a lower energy in the spectrum, giving rise to a ***background*** signal. This signal must be corrected in order to determine the true line areas from which the relative concentrations of the elements will be calculated. Next

to this interference the background can also give information about layer systems [Toug90] [Simo99] or nanostructures [Toug96].
Only the electrons from the highest atomic layers reach the analyser with their full kinetic energy. For the others the distance between two collisions defines a mean free path λ. Experimental aspects of this to analyse different layer thickness' will be discussed below.
The easiest way to remove the background is to fit and to subtract a linear function. This method is independent of physical parameters and is often applied when a large number of spectra are evaluated. The error of this method is constant and therefore influences all measurements in the same way.
SHIRLEY proposed a purely numerical method where the background intensity within a peak is proportional to the integrated intensity at higher energy [Shir72]. It is presumed that the background matches the spectrum outside the peak region.
Different from that TOUGAARD implies a physical basis of his algorithm [Toug90][ToSi82], in which the measured spectrum j(E) is seen as photoelectron data F(E) and background signal, as given in the next equation:

$$j(E) = F(E) + \lambda(E) \cdot \int_{E}^{\infty} K(E,E-E') \cdot j(E) \cdot dE' . \qquad (11)$$

In this formula the term K(E,E-E') describes the probability that an electron with the energy E loses the energy (E-E') during a mean free path travel λ(E). The loss function can experimentally be evaluated by *Reflection Electron Energy Loss Spectroscopy* (REELS) [Stei83]. The excitation energy should therefore be in the same region as the kinetic energy of the electrons from the level examined [Lütk97].
Because measurements show the same shape of the loss function for different solids and different states, TOUGAARD suggests a universal loss function for same cases [Toug89] [Toug97]:

$$\lambda(E) \cdot K(E,E\text{-}E') \cong \frac{B(E,E\text{-}E')}{\left[C + (E-E')^2\right]^2} \qquad (12)$$

with constants B=2886eV^2 and C=1643eV^2 found experimentally.
One can also think of the inelastic scattering effects of electrons at the nuclei, which mainly influences the photoelectron spectra of ordered crystal structures [Schn01].

After correcting the obtained data, the intensity of the photoelectrons can be used for an analysis of the proportions of different elements. Additionally, the proportion of different functional groups can be investigated by dividing the intensities of core level spectra into areas with corresponding chemical shifts.
A simple model can be used for evaluation [Ghos83], where the number of emitted electrons amounts to

$$N_0 = I_0 n \frac{d\sigma}{d\Sigma} \tag{13}$$

with I_0 being the intensity of primary radiation, n the concentration of the element and $d\sigma/d\Sigma$ the differential cross-section. The electron transport through the solid to the surface has to be evaluated with the mean free path λ and the emission angle Θ between surface normal and analyser:

$$N(E) = I_0 n \frac{d\sigma}{d\Sigma} \lambda \cdot \cos\Theta \,. \tag{14}$$

The measured intensity is also influenced by the characteristics of the spectrometer, which can be dependent on photoelectron energy. MÄHL therefore specified a so-called spectrometer function Q(E) for the used XPS-system, which is a multiplication factor for the number of emitted electrons [Mähl94].

Next to the discussed aspects of XPS, there are some more which also influence the measurement. For details about the surface structure, scattering and inner potentials of the sample see [Fadl84].

2.1.2 Experimental conditions of XPS

Photoelectron spectroscopy was carried out by using a commercial Perkin Elmer PHI 5600ci multi-technique x-ray spectrometer, which is equipped with monochomatised Al K_α radiation and a dual Al/Mg anode. The energies of Al $K\alpha$ and Mg $K\alpha$ radiation are 1486.6eV and 1253.6eV and the widths for the unmonochromatised radiation 0.85eV and 0.7eV respectively. With such a dual anode, ambiguous lines can be distinguished by comparing measurements for both x-ray energies. As there were no such lines for the investigated materials, all photoelectron spectra in this work were obtained by using Al $K\alpha$ monochromatic radiation.

A hemispherical analyser and a multi-channel detector record the spectra of emitted electrons and investigate the sample within a spot diameter of about 0.4mm. The measurements were performed at a base pressure of 3 x 10^{-10}mbar. The main components of this spectrometer are shown in the next figure, for further details see [PeEl91].

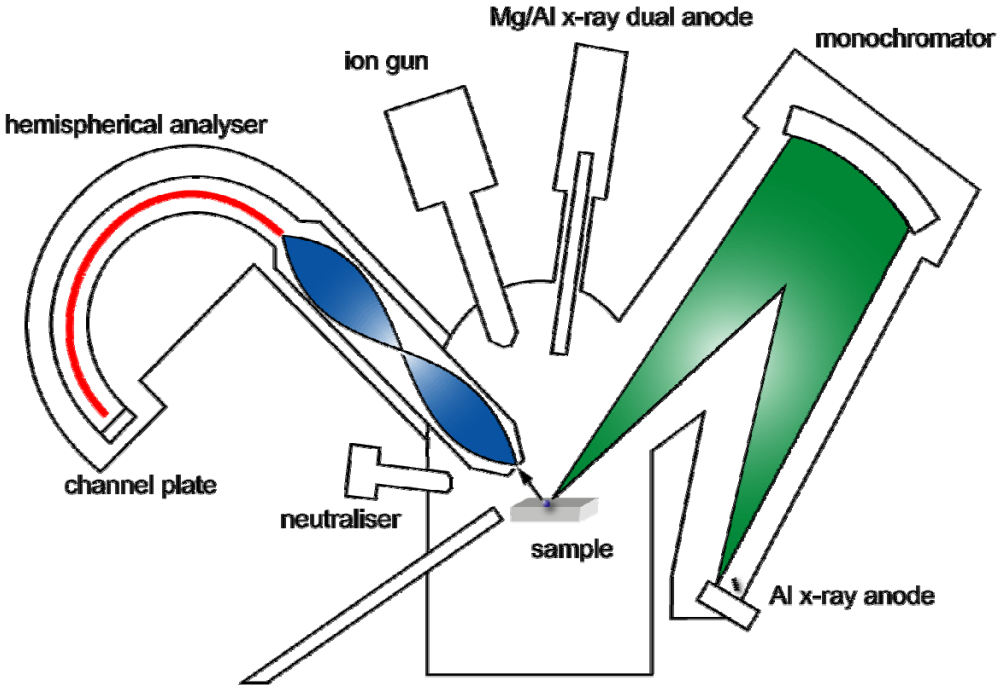

Figure 6: schematic diagram of the PHI 5600 spectrometer

By using a monochromator, the half-width of the Al Kα radiation was reduced to about 0.3eV. The monochromator works on the basis of the constructive interference from crystal diffraction, as given by the BRAGG equation:

$$n\lambda = 2d \sin\theta\,, \qquad (15)$$

where d represents the distance between lattice planes, λ is the radiation wave length and θ is the angle between the incident radiation and the detecting planes.

For investigating polymeric materials, it is necessary to supply low-energy electrons to the samples. This neutraliser compensates charges caused by the photoelectric effect of the x-ray bombardment, leading otherwise to a shift in binding energy of the measured photoelectron lines. It was used here to adjust the carbon 1s line for hydrocarbons to a binding energy of 285eV for a later comparison of the results with other authors.

As the distribution of the newly created chemical groups through the plasma modification should be non-uniform according to the different penetration depths of radiation and

particles, there are basically two ways to get some kind of depth information in photoelectron spectroscopy.

The ***sputter depth profile*** method is based on the following procedure: first an x-ray photoelectron spectrum is obtained. Then the examined layer is sputtered away in a noble gas ion beam. The volume of the ablated material is proportional with the time of sputtering. Afterwards the newly created layer is examined. This procedure can be repeated, so that the examined layers show depths down to several 100nm.

During the surface modification, the changes in the highest layers are mainly from interest. Here the sputter depth profile method could not be used because of two reasons: on one hand the ion bombardment influences the structure of the layer in a chemical and physical way. On the other hand, the removal of atoms depends on the kind of element, i.e. the sputtering cross sections are different for oxygen, nitrogen and carbon and therefore atoms with a smaller cross section accumulate.

The method of ***concentration depth profiles*** examines the surface under different angles of emission for the photoelectron in reference to the surface normal. Angle resolved XPS measurements (ARXPS) are non destructive to the surface as long as the radiation does not affect the sample. The surface sensitivity of this technique results from the short escape depths of the photoelectrons although the x-rays deeply penetrate the sample. Considering a density of 0.95g/cm^3 for PE and 0.90g/cm^3 for PP, the x-ray attenuation length for 1486eV photons can be estimated to be 17.09µm for PE and 18.04µm for PP from the next figure.

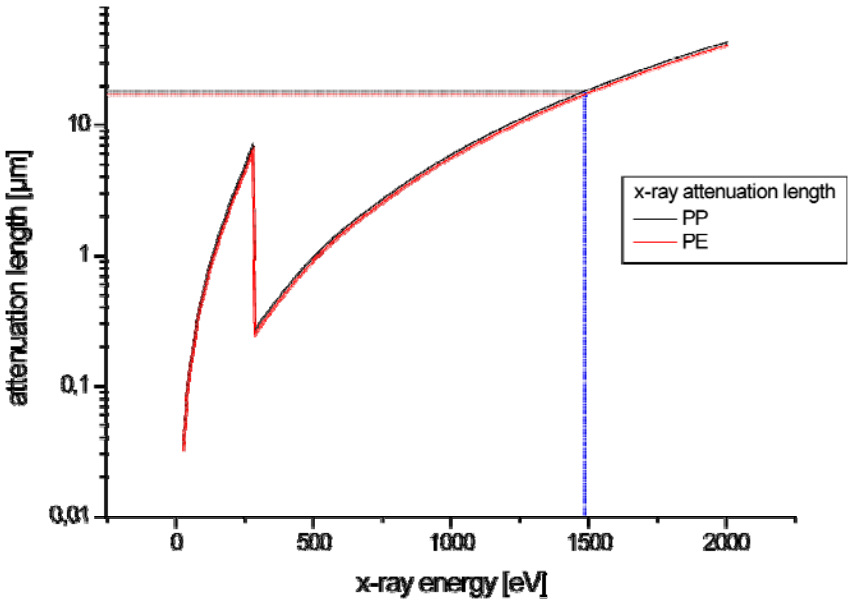

Figure 7: x-ray attenuation length for PP and PE [www00]

Assuming a uniform detachment depth of the electrons, which is basically valid for polymeric materials, differently thick layers were analysed. The surface normal of the sample spans an angle of 45° to the spectrometer, also called normal emission in the following. Concentration profiles from the different angles θ_1, θ_2, ... θ_n of the emitted photoelectrons lead to information about the composition down to a depth of about 10nm. For an analytic description several methods have been developed [ACW90] [BuHo85] [Grab93].

In the following illustration the geometrical aspects are schematically clarified. The symbols γ, ϕ and θ describe the angles between the x-rays and the spectrometer, the x-rays and the surface normal and the surface normal and the spectrometer. The co-ordinates x and y refer to the plane, while z describes the depth of the sample.

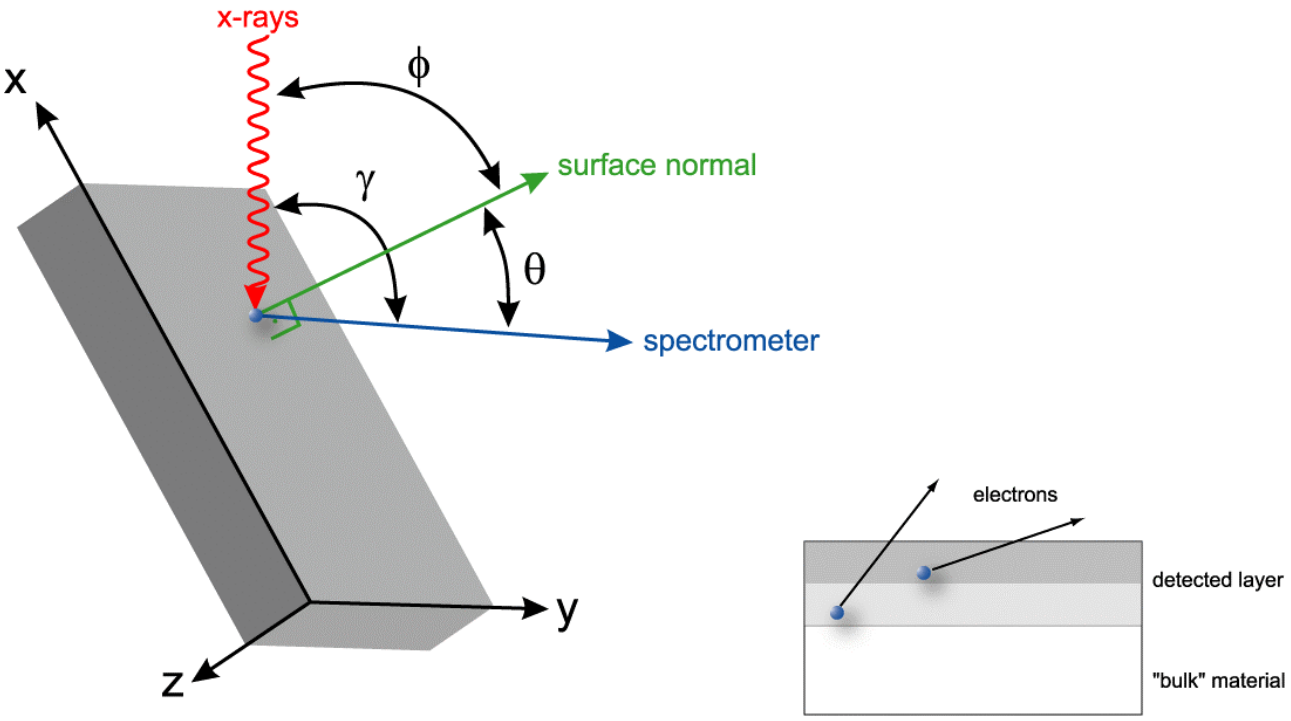

Figure 8: geometrical aspects of angle resolved x-ray photoelectron spectroscopy (ARXPS)

The disadvantages for the concentration depth profiles are on one hand a poor resolution, which has under the best experimental conditions a ratio of $\Delta z/z=0.81$ [Cump95]. On the other hand, the depth profiles can only be analysed up to the mean free path of the electrons and therefore with a depth of only some nm.

Some presumptions for a precise evaluation of the measurements have been published by CUMPSON [Cump95] and are reflected in the following:

- the material of the sample is amorphous or polycrystalline within the analysed volume;
- the acceptance angle for electrons of the analyser is small;
- the sample material is homogeneously distributed within the XY plane;
- the used algorithm had to evaluate peaks with varying intensities and poor resolutions.

The experimental set-up as well as the modified and investigated materials fulfil these assumptions at least in approximation, so that for a distribution of atomic concentrations in depth this behaviour can be determined. According to these assumptions and the experimental set-up, the peak area F can be calculated as

$$F(\theta) = TA\sigma L(\gamma)\int_0^\infty c(z)e^{-\frac{z}{\lambda\cos\theta}}\cdot dz \qquad (16)$$

with T as the transmission function of the instrument, A as the area of analysis, the asymmetry factor $L(\gamma)$, the photo-ionisation cross-section σ, the attenuation length λ, and c(z) as the atomic concentration in the depth z. As the data for the attenuation length λ of polymers varies by different between 2nm [Robe80] and to 7nm [CGS78], only the angles will be displayed below.

Different approaches for angle resolved measurements can be distinguished:

- the area of analysis A is defined by the detection area, i.e. $A = \frac{A_0}{\cos\theta}$ where A_0 is the analysed area at normal emission;
- the area of analysis A is defined by the irradiated area, i.e. $A = \frac{A_0}{\cos\phi}$ where A_0 is area of the primary beam at normal incidence (monochromatic systems);
- systems without a constant $L(\gamma)$, so there is a changing in γ as soon as θ is changed.

The PHI 5600 spectrometer allows a small photoelectron detection area (first point) and the analysed area therefore was smaller than the irradiated one for each angle. Defining a reduced intensity $I(\theta) = \frac{F(\theta)}{TA\sigma L(\gamma)}$, some of the geometrical factors become no longer necessary (so the intensity for a pure material would be $I(\theta) \propto \cos\theta$). Important for the evaluation of the data is then the precise knowledge of the factor $TA\sigma L(\gamma)$ for all angles θ.

A common mistake is made in the adjustment for the radiated and analysed area. If these cover the same area for a given angle, one has to take care of the same areas for other angles, too.

Next to the chemical composition of the sample, knowledge of its structure is also important. This point will be introduced in the following.

2.2 Structural aspects of a sample

Imaging methods cover a different kind of information than spectroscopic ones and lead to a knowledge of structural aspects of a sample. Historically it started with magnifying glasses and later with microscopes. While these methods give a direct image of a sample, they are in a way limited by the wavelength of the light (see figure 9).

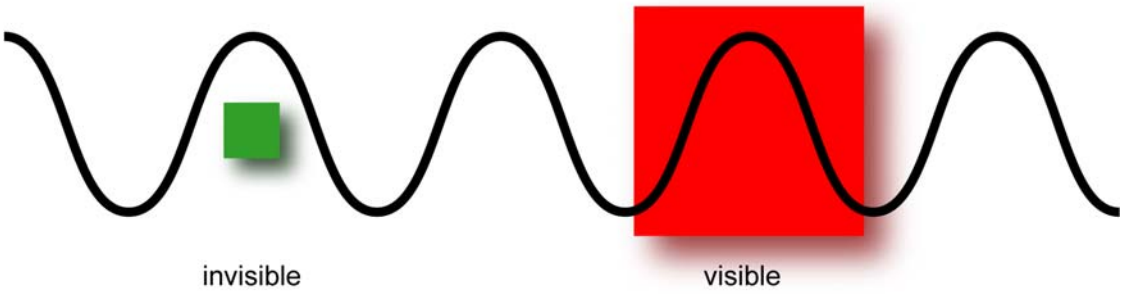

Figure 9: simplified correlation between object size and wavelength - only objects larger than the used wavelength are visible

To achieve information about geometrical composition at an atomic size, one can also think of diffraction experiments like *low energy electron diffraction* (LEED) and *reflection high energy electron diffraction* (RHEED) which provide a reciprocal picture of a surface. This reciprocal picture must be transferred into real space, but as those methods require ordered structures, they cannot be used for unordered polymer structures.
Electron microscopy uses electrons instead of light to image small structures. This leads to a higher resolution because of the shorter wavelengths of electrons, but gives only qualitative depth information and samples must be also conducting (this can be archived for polymers by covering them with a thin film of gold).

When BINNING and ROHRER invented the *scanning tunnelling microscope* in 1982, a new approach to a direct imaging was born. In this kind of microscopy a tip scans over the

surface and its electronic structure can be obtained down to atomic resolution [BRGW82]. The basics refer to the quantum-mechanical tunnel effect which is based on the finite probability that electrons can overcome the gap between the metal tip and the surface. In order to scan a surface within the nanometer scale, the tip is moved by piezo-crystals. The received data of charge densities can be computed into a topography of the surface. More detailed descriptions of this method are given in various articles and books [GüWi92] [WiGü92] [WiGü93].

Next to the tunnelling current other "nanoscopic" effects take place. The optical resolution limit of λ/2 after ABBE [Voge97] is avoided within the *optical near field microscopy*. That is because here not the optical far field is detected, but the optical near field of the sample. An object which is substantially smaller than the wavelength of the used light influences the wave propagation only in the way that it creates a HUYGENS secondary wave. This scattering wave is dependent on the size of the object, but the propagating far field is always spherical and therefore independent from the shape of the object. But the non propagating near field contains the structural information about the object [Hörs99]. Apart from the transmission and reflection measurements also the fluorescence can be measured.

Another variable is the deflection of a cantilever in *atomic force microscopy* (AFM)[3]. Such a microscope uses the interaction forces between a fine tip mounted at the end of a plate-spring and the sample surface [BQG86] [Binn87]. This method is therefore suitable for both electrically conducting and non conductive samples. An image of the surface topography can be archived by screening over the surface with a constant force. For the following experiments this technique was chosen because of the high resolution in all three dimensions, the practicability with non-conducting samples (polymers) and further experimental aspects like measurements of elasticity.

2.2.1 Theory of AFM

In scanning probe microscopy, a tip interacts with the surface of a sample and this force interaction is determined. On the basis of the distance between tip and sample, MOLITOR suggests the distinction of interacting forces between short-distance and long-distance effects [Moli00]. For both length scales attractive and repulsive interaction forces occur, leading to a very complex force - distance behaviour. Table 1 summarises the interactions

[3] Sometimes also called *scanning force microscopy*

between tip and sample surface while in the following paragraph each of those forces will be described briefly.

Force of interaction	Distance and effect of interaction	Range
PAULI-repulsion	Short-distance, repulsive	0.1nm
COULOMB-repulsion	Short-distance, repulsive	0.1nm
Covalent bondage	Short-distance, attractive	0.1nm
Metallic bondage	Short-distance, attractive	Up to 1nm
Ionic bondage	Short-distance, attractive	Up to 1nm
Capillary forces	Medium-distance, attractive	Up to 10nm
Van der Waals forces	Long-distance, attractive	Up to 100nm
Electrostatic forces	Long-distance, attractive or repulsive	Several 100nm
Magnetic forces	Long-distance, attractive or repulsive	Several 100nm

Table 1: survey of forces between tip and surface according to their effect and range in atomic force microscopy [Moli00]

When the tip is very close to the surface, the electron wave functions of atoms at the lower end of the tip and atoms at the sample surface can overlap. Between those atoms two strongly repulsive forces occur: ***Pauli-repulsion*** and ***COULOMB-repulsion***.
According to the PAULI exclusion principle, electrons with the same quantum numbers cannot be at the same place. Therefore these electrons are raised energetically and the resulting repulsion prevents any deeper penetration of the tip into the sample.
The other repulsive strength, which correlates with atomic positions, is given by COULOMB-repulsion, where the nuclei are no longer shielded because of strongly overlapping electron wave functions.

If wave functions of bonding electrons from different atoms overlap, a ***covalent bond*** can develop. Two neighbouring atoms then possess a common pair of electrons. From the exchange interaction of these electrons an attractive force, whose range is typically around 0.1nm. The strength of these forces can be seen in the hardness of diamond and boron nitride and likewise extreme melting temperatures.
With the exception of noble gas atoms all atoms have one or more valences for covalent bonds according to their position in the periodic system. These bonds determine the symmetries of many crystal lattices as well as angles in molecules. In the contact mode of the scanning force microscope a covalent bond between the tip and the surface is possible, which can lead to a destruction of the sample surface due to its strong adhesiveness [HLMG95]. If the binding energy between tip and sample atoms is smaller

than between the atoms within the sample or the tip itself, a non-destructive measurement is possible and the attraction leads to an interaction, which varies on atomic scale.

If two metals approach each other, their bonding electrons form a free electron gas. This short-distance attraction, called ***metallic bond***, is caused by exchange interaction. It can be strong as in the case of an iridium probe over an iridium surface [DZP90]. The attraction varies exponentially with the distance between metal tip and metal surface and these adhesion forces were theoretically described by FERRANTE and SMITH [FeSm85] for different metals.

Electrostatic forces occur on a long range between charged particles or planes and are also named COULOMB forces. The force between two point charges q_1 and q_2 with the distance r between them can be described by:

$$F = \frac{1}{4\pi \cdot \varepsilon \cdot \varepsilon_0} \cdot \frac{q_1 \cdot q_2}{r^2} \tag{17}$$

where ε_0 is the electrical field constant and ε the dielectric constant of the medium between the charges. Depending on the polarity of the charge the COULOMB force can be attractive or repulsive. When insulators are investigated, surface charging leads to such interactions. For a conducting sample image charges are induced which leads to an attractive force between sample and tip.

Interactions between dipoles likewise are electrostatic forces. As the strength of dipole fields decrease with the third power of the distance, these forces decrease with r^{-6} and therefore substantially faster than COULOMB forces. Such interactions can also occur between non-polar molecules and atoms. These so-called ***VAN DER WAALS - forces*** are responsible for many effects (e.g. surface tension of liquids, certain characteristics of gases, capillary forces and the wetting of surfaces). They basically occur between all atoms or molecules. VAN DER WAALS - forces can be divided into three different groups:

- dipole - dipole – forces where molecules with permanent dipole moments interact electrostatically;

- dipole - induced dipole – forces where the field of a permanent dipole induces a dipole moment in a nonpolar molecule, such that the permanent and induced dipole moments interact;
- dispersion - forces based on interaction between fluctuating dipoles and the field that these induce.

The entire VAN DER WAALS - potential is the total of three contributions:

$$V_{vdW} = V_{pol} + V_{ind} + V_{disp} . \tag{18}$$

The first two contributions are of electrostatic nature. The dispersion has its origin in quantum mechanics. Since the forces interacting between permanent and induced dipoles are not subject to retardation, these generally exert their influence at a greater distance than the dispersion forces.

Although smaller than COULOMB forces, VAN DER WAALS - forces with their range of approximately 100nm influence the interaction between tip and sample substantially because volumes have to be taken into consideration here. This applies to the contact as well as to the dynamic mode. In the contact mode short-distance forces play an important role. Although the strength per atom for VAN DER WAALS - forces is very small, the total force achieves a scale around an order of magnitude above the short-distance attraction [GoGa91]. In the dynamic mode the VAN DER WAALS - forces are the determining factor between probe and sample. Only at the reversal point of the oscillatory movement of the tip short-distant forces can become important.
VAN DER WAALS - interactions between the same materials are always attractive no matter what the medium, even for measurements in vacuum [BuCo93].

Capillary forces occur between tip and sample if a liquid film is present. The radius of the tip is small enough that a meniscus can be formed. This effect occurs for measurements in air, although the humidity plays a crucial role. Dipole - dipole - interactions and VAN DER WAALS - forces are likewise responsible for these forces. This additional adhesive force can influence the measurements substantially.

In order to be able to examine ***magnetic forces*** and interactions on a small scale, magnetic force microscopy (MFM) was developed, where the tip consists of a magnetic material. The force on a magnetic dipole with the magnetic moment μ in the field B is:

$$F = \nabla(\mu \bullet B) \tag{19}$$

The magnetic fields are long-distance and for a constant magnetic moment the force depends on the gradient of the magnetic field. Magnetic forces play no role in the investigated polymers, but more details can be found elsewhere [MMB97] [GAM95].

2.2.2 Experimental conditions of AFM

The *atomic force microscope* measurements were performed on the different commercial systems Quesant Q-Scope 250 and Omicron AFM/STM. Although the excitation of the cantilever is different, the primary set-up for both instruments is illustrated schematically in figure 10.

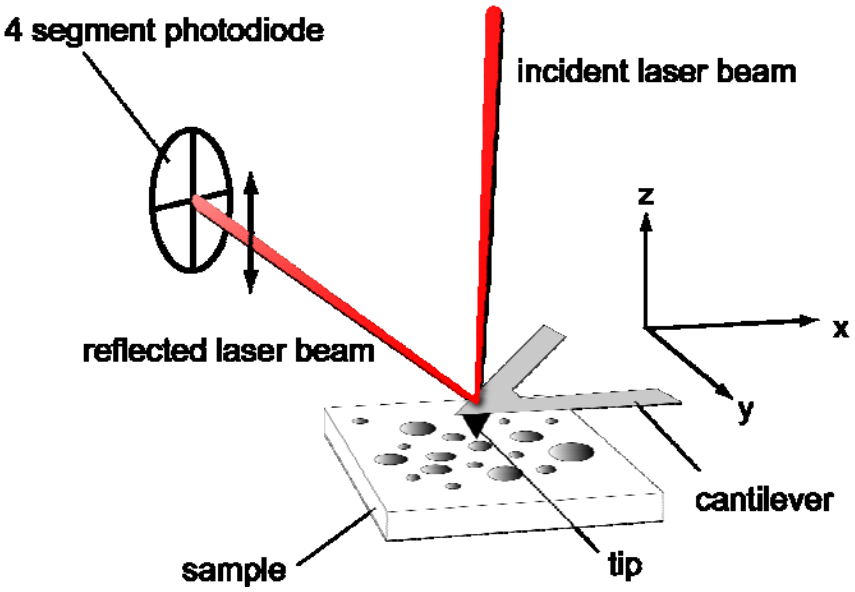

Figure 10 : schematic set-up of an atomic force microscope

While the cantilever scans the surface in plane x and y direction, the reflection of a laser beam upside of the tip is detected at a photodiode. Depending on the segment of the photodiode where the reflection is measured, information about the deflection of the cantilever is obtained. A typical commercial tip depicted by an electron microscope is shown in the next picture.

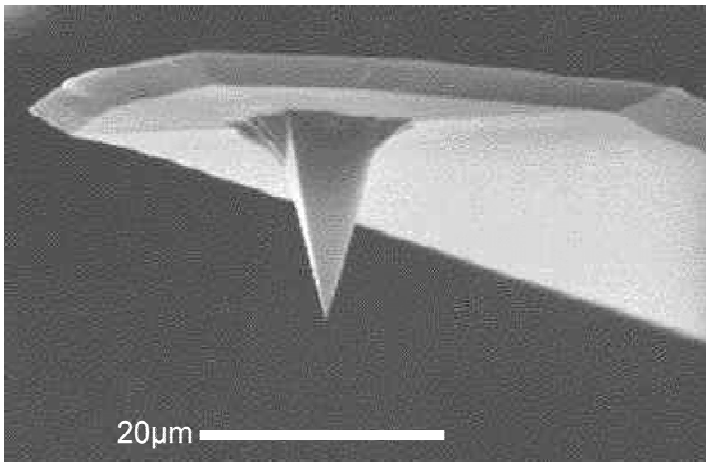

Figure 11: microscopic view of an AFM tip [Nano03]

Atomic force microscopy basically operates within two modes: *contact* and *non-contact mode*. In the *contact mode*, the normal force can be seen as the deflection of the cantilever and the lateral force (friction force) as the torsion of the cantilever. The tip and the sample are approached, until they get “in contact”. The force then has a strength of about 10^{-9}N and the deflection is used as control signal. The surface is scanned while the feedback control system adjusts the distance between tip and sample. When this adjustment passes very fast, the measurement corresponds to a *constant force mode*, while a low feedback leads to a *constant height mode* measurement of the surface.
The deflection of the cantilever is in good approximation proportional to the force between tip and surface and therefore obeys HOOKE's law

$$\Delta l = \alpha \cdot F_N \frac{l}{A} \tag{20}$$

with the length of the cantilever l, Δl as the change of the length, α the linear extension coefficient, F_N the normal force and A the cross section area of the cantilever.

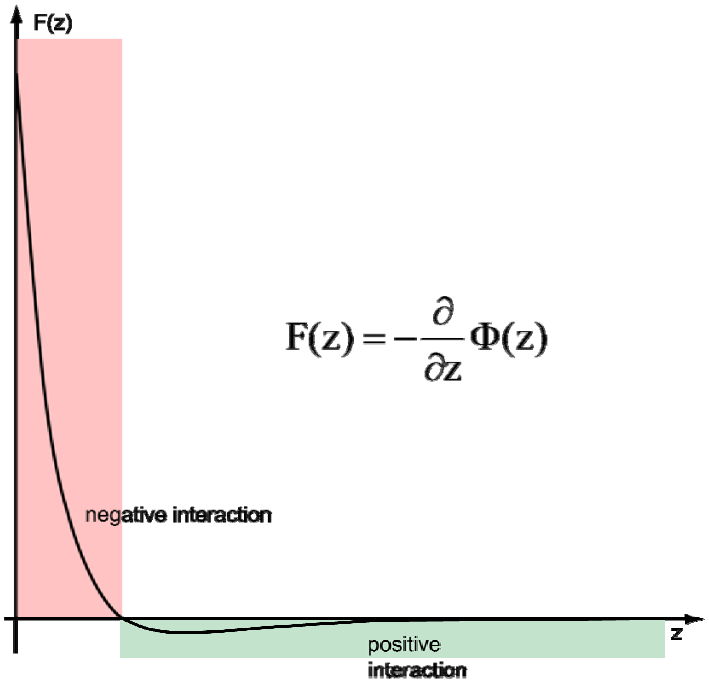

Figure 12: force curve [Rein01]

The force curve shown in figure 12 is the negative derivative of the interaction potential and describes the behaviour of the force F_N in dependence of the distance between tip and surface.

In *contact mode* also the torsion back and forth of the cantilever can be measured. It will be influenced by the topography and friction, while the main interest focuses on the second aspect. The strength of the friction signal depends on the condition of the surface and inner stresses of the cantilever make an evaluation of this signal very complicated.

In the *intermittent mode* is a kind of soft contact mode where the amplitude of the cantilever is dynamically modulated near the resonance frequency. When the tip approaches the surface, the damping is used as a feedback signal for the distance. At the reversal point of the oscillation, the cantilever touches the surface. Because the penetration of this mode into the material is less deep compared with the contact mode, this method will primary be used for the measurements on soft materials. The obtained signal will also be used for analysing the phase shift of the sample.

With the *intermittent contact mode* a phase signal can be measured which helps to differentiate materials according to their hardness. Figure 13 shows the response of the cantilever being externally excited at frequencies near its natural resonance frequency, f_0.

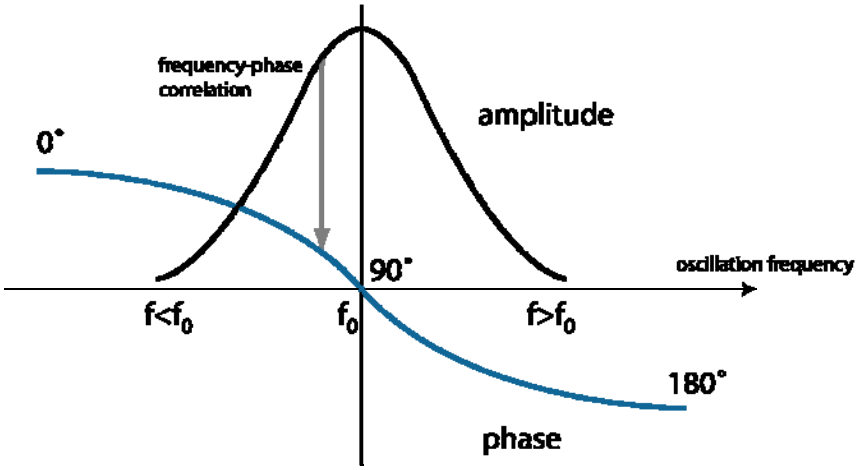

Figure 13: phase imaging - the frequency of an external vibrator can sweep across the cantilever's resonance [Ques02]

The amplitude of the cantilever's motion has a maximum at the resonance frequency with a phase of 90° behind the external vibration. From the *intermittent contact mode* where a frequency below the resonance is locked, the phase shift, at this frequency, is less than 90°. Lowering the probe towards the surface will lead to a different force field and therefore a change in the phase signal, while the direction of the phase change will depend on the nature of the interaction between tip and polymer.
A homogenous surface material lets the cantilever experience a constant phase shift at each position of the scanning process, resulting as a flat plane in the phase image. On one hand the phase measurement will be influenced by the surface geometry - scanning an ascent will cause slight shifting to lower frequencies respectively; slightly higher frequencies result when scanning a descent. On the other hand adhesive forces between tip and surface have an impact on the phase image.

In *non-contact mode* the cantilever is excited to oscillate with its resonance frequency while the sample is ramped along the z axis. An image of the surface and the contrast behaviour of the sample is harder to obtain in this mode, so this technique requires UHV conditions. Several models have been developed to describe the contrast behaviour [Gies97].
In contrast to the *contact mode*, not the deflection but the influence of the force gradient caused by the surface is used as adjustment signal. The mean distance here between tip and surface is between 1nm and 100nm and therefore a measurement can be performed without "contact" to the surface. When the oscillating cantilever is approaching the

surface, the tip is exposed to an attractive force field which leads to a decrease of the resonance frequency.

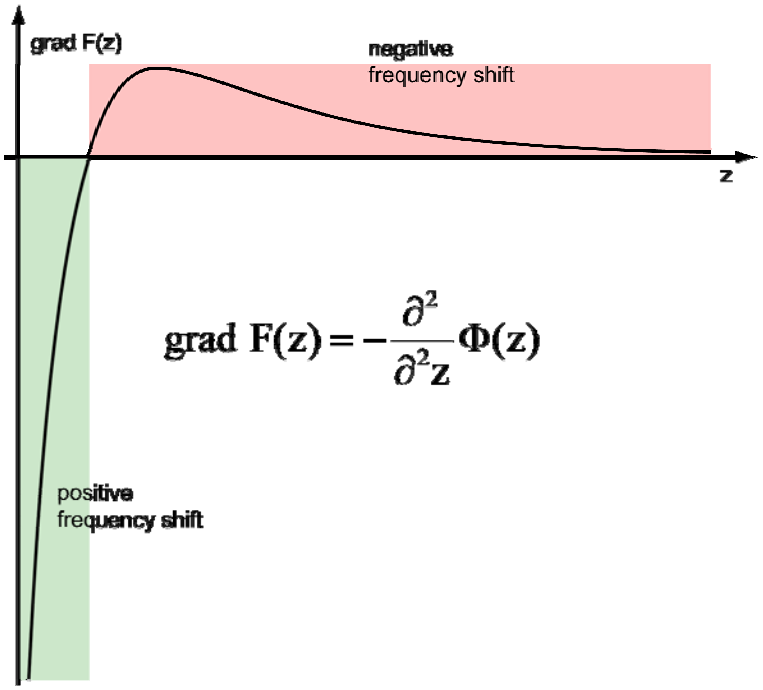

Figure 14: force gradient [Rein01]

The operation of the *non-contact* mode of an atomic force microscope can be divided into small (about 1nm) and large amplitudes (10-100nm) of the cantilever oscillation. For small amplitudes, the tip crosses the force field where the gradient can nearly be seen as constant, so the tip will follow a harmonic movement. Larger amplitudes span areas where this assumption is not valid anymore. Practically a small amplitude has a positive influence on the sensitivity of the surface while larger amplitudes show a better stability of the oscillation itself approaching the surface as well as scanning the sample.

The Omicron microscope uses a method, where the cantilever is driven with an active feedback system with its resonance-frequency according to the actual force-gradient [UGM97]. The amplitude of the oscillation maintains at a fixed value and the outer force-field will be detected by the shift of the resonance-frequency.
The reason for the frequency shift results from the force gradient near the sample surface. This gradient is determined by the LENNARD JONES potential and therefore acts as a distance control. This potential is a superposition of a repulsive short-distance and an attractive long-distance VAN DER WAALS – potential and can be written after [Greu98] as

$$\phi(z) = \frac{c_1}{z^{12}} - \frac{c_2}{z^6} \qquad (21)$$

In this formula c_1 and c_2 are constants while z represents the distance between tip and surface. This semi-empirical approach is acceptable for investigation on polymers although it neglects magnetic and electrostatic interactions. The short-distance repulsive forces determine the lateral resolution while the long-distance attractive forces have only a minor influence.

This behaviour of the force gradient leads to a change of the frequency in the cantilever, which does not occur for an uniform force gradient because then the derivative becomes constant and is therefore not well-defined. The sign of the frequency shift refers to the sign of the force gradient (see figure 14). Approaching the tip to the surface crossing the zero passage $F(z_0)$, the frequency shift changes from negative to positive.

One further aspect is the surface ***elasticity***, which can be recorded as a function of force vs. distance. This does not lead to lateral images as the topography does but records the forces at one location towards the tip when being pressed into the sample material and then later withdrawn. The next figure shows the basic idea of such force-distance curves.

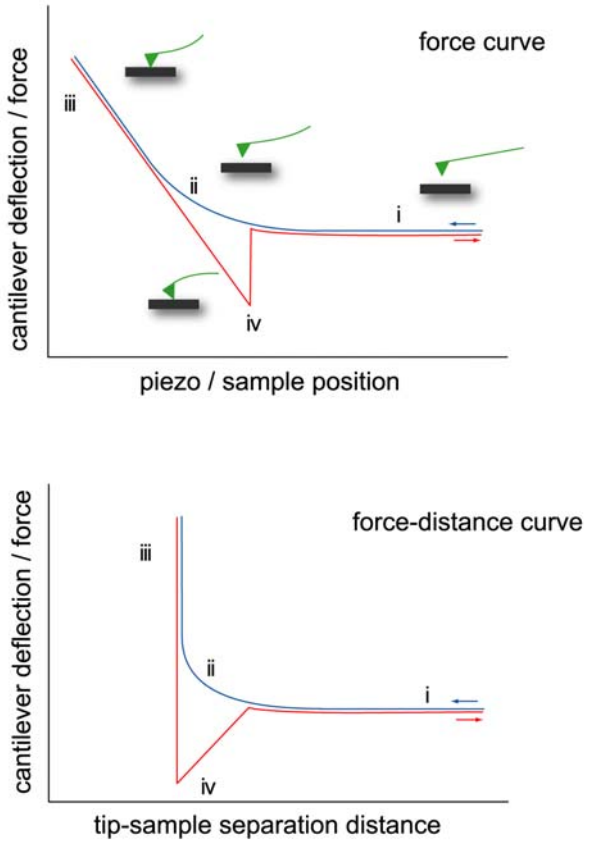

Figure 15: schematic force - piezo position curve respectively distance curve [HeHo99]

The characteristic begins at the right edge of the picture, when the tip is far away from the sample and no deflection occurs (i). Approaching the tip, the gradient of the attractive force suddenly becomes stronger than the spring constant and this force bends the cantilever (ii). An edge in the characteristic is called “snap in” because the tip is in contact with the polymer at this point. Tip and surface are further approached until the reversal movement of the piezo (iii) is reached. The decreasing deflection of the plate-spring when drawing back does not show the same curve as for the approaching deflection because of the non-linearity of the piezo. The curve intersects the normal force (baseline without force) and becomes negative (a sticking between tip and surface through the adhesion forces between them). At the point (iv) the contact breaks down (called “snap off”) and the cantilever swings with its resonance frequency around the intermediate position. Later in the measurements, the approaching lines will be coloured in blue and retraction lines are coloured in red.
Further information about the different contact models can be found at [BuCo93] [GAM95] [CaDi99].

After describing the surface analysing techniques in great detail, the focus will now shift to some aspects of the modification process by a microwave plasma. The basics of such a discharge will be presented in the following text.

2.3 Plasma State

In the experiments the polymer will be exposed to the influence of a plasma, and therefore it is important to understand the processes inside such a discharge. From a physical point of view, it can be defined as a mixture of free electrons, ions (mostly positive) and neutrals of a gas in different energetic and excited states, which interact with photons and among themselves [Dros78] [Ruts84] [Fran94]. It is also referred as the 4^{th} aggregation state like figure 16 suggests.

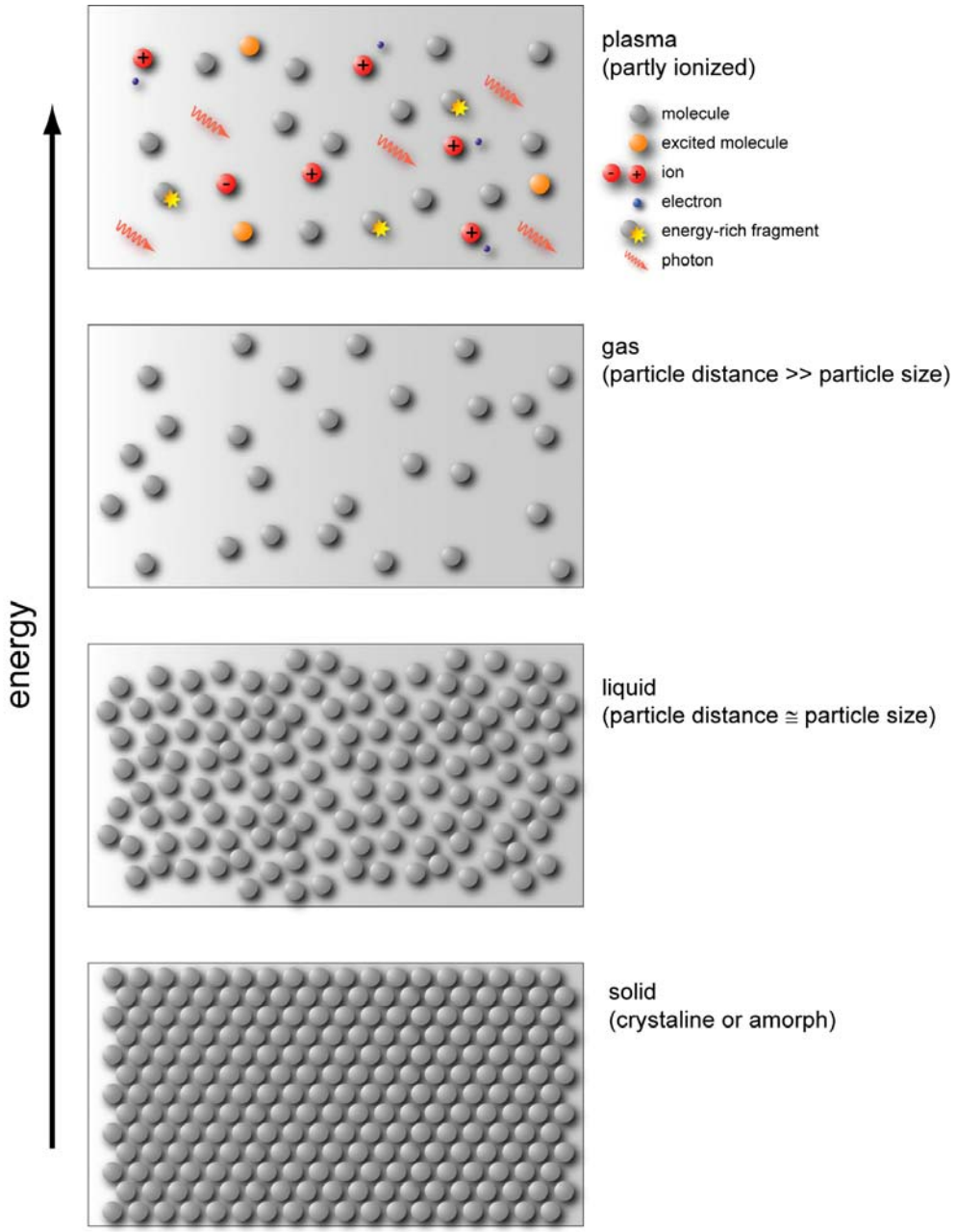

Figure 16 : different aggregation states according to the inner energy

Most publications describe such a plasma by its outer parameters like the kind of process gas, its pressure and flow, the excitation frequency and power consumption [CGNS95]. A more realistic description can be given by inner parameters like density numbers of charged species or the distribution of kinetic energy for the particles. This approach gives ideas of the physical processes and this can lead to a more detailed understanding of the modification. It is also necessary to see later where simplifications of the process can be made in order to model the treatment process correctly. And further more it allows a kind of optimising the reactive species of such a discharge.

2.3.1 Theoretical aspects of the discharge

In order to create plasma a lot of aspects have to be taken into consideration. First, there are large populations of gas atoms or molecules with their particular distributions of movement (direction and speed) and pressure. Temperature is another measure for the mean kinetic energy of molecules [Voge97], therefore the mean value for the translation energy is given by

$$\overline{W}_{trans} = \frac{1}{2} m \overline{v^2} = \frac{3}{2} kT \tag{22}$$

with k as the BOLTZMANN constant. The pressure p is defined as a measure for the number of particles per unit volume n_g, so it gives the density of thermal energy

$$p = n_g \cdot k \cdot T \tag{23}$$

This concept can easily be transferred to charged particle populations. While charge is the cause for an electric field, every charged particle exerts forces to any other charge in inversely squared proportion. An external electric or magnetic field will also apply forces to the charged (and moving) particles within the area of its influence.

The average speed of an argon atom (40 a. u.) at room temperature T is

$$\overline{v} = \sqrt{\frac{2kT}{M}} = 3.5 \cdot 10^2 \frac{m}{s} \tag{24}$$

If work is done on a charged particle it gains a certain energy by moving a given distance x through an electric field $eV = \int_0^x eE \cdot dx$.

Binary collisions occur almost exclusively when pairs of particles collide. The conservation laws for energy and momentum allow three classes of events:

- elastic collisions where the total kinetic energy remains unchanged while momentum is transferred between the particles;
- inelastic collisions when momentum is transferred between the particles, too, but a part of the kinetic energy is transferred to internal energy;

- super elastic collisions in which internal energy is transferred into kinetic energy, while momentum is conserved (the third kind of collision will be neglected here because it does not occur in low pressure discharges).

In elastic collisions the motion paths of the particles are randomised leading to an average speed. Elastic collisions favour the creation of a plasma, therefore some concepts have to be defined (neglecting details like effects of charge, scattering angles, and impact parameters). Considering the path of an electron through a stationary gas such as argon, the target atoms can be seen as hard spheres. The number of target atoms n_g in a volume $x \cdot y \cdot z$ depends on the pressure of the gas. Each atom presents a collision cross section with circular area of $\pi \cdot r_{argon}^2 = \sigma$. To examine the movement along the z-axis from the view of an electron, the blocked area by the argon atom is $n_g xyz\sigma$. The depth z gives the mean free path $\lambda = \frac{1}{n_g \sigma}$ when the x-y-plane is completely blocked. This simplified calculation gives a cross section of $3 \cdot 10^{-20} m^2$, but realistic considerations show an energy dependence for inelastic collisions like in figure 17.

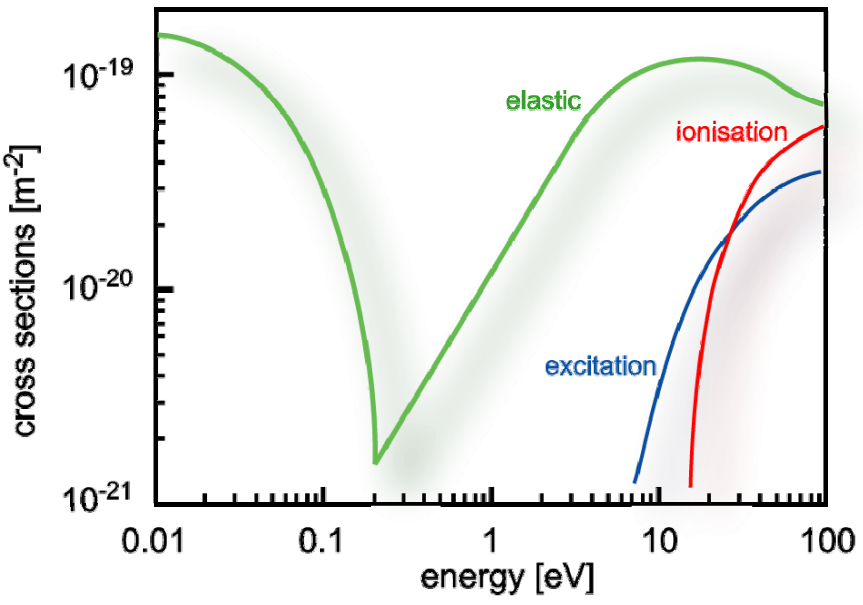

Figure 17 - cross sections for argon [Brai00]

The formation of plasmas can now be achieved by providing enough energy for excitation and ionisation. This can be done by alternating electric fields, leading to this kind of equilibrium beyond the conditions of a gas.

The microwave excitation with its high-frequency alternating field at 2.45GHz accelerates the charged particles. While the light electrons can follow this field, increasing their kinetic energy, the heavy ions seem to be immobile and therefore this kind of plasma with different kinetic energies for its species is called non-equilibrium plasma.

A plasma shows significant changes in its behaviour referred to the gaseous phase because of the concentration of charge carriers, even if the numbers of positive and negative charges in a certain volume are in equilibrium (called quasi neutrality). This volume is characterised by the distance between ions and electrons and it is measured in the term of DEBYE length (more precise this means the electronically screening of the ion)

$$\lambda_D = \sqrt{\frac{\varepsilon_0 k T_e}{e^2 n_{e0}}}. \qquad (25)$$

In the formula n_{e0} represents the mean density of electrons while T_e stands for the electron temperature [Schr00].
Although all kinds of plasmas have some of the above features in common, they must be distinguished according to their density of charge carriers and energy distribution of these ions and electrons. Referring to these values a classification by a two-dimensional plasma parameter space can be made (see figure 18).

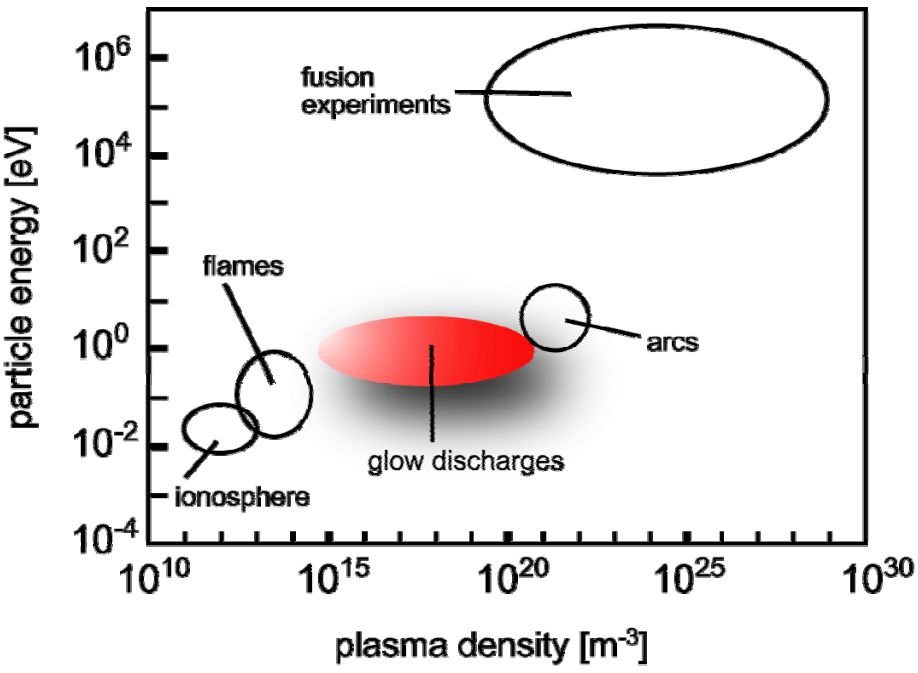

Figure 18: different natural and artificial plasma states [Brai00]

Concerning the glow discharges, the plasma parameters space in the figure above ranges by six magnitudes for the plasma density and nearly two magnitudes for the electron energy. Therefore the sole statement that a glow discharge was used for a modification process is not informative as there are innumerable distinctly different plasma states.
Additionally an argon plasma is distinguishable from one containing negative and positive ions formed from fragments of a molecule like sulphur hexafluoride, so the process gas is also crucial.

As laboratory plasma is confined or in other words it has physical boundaries, charged particles are created and lost both within the volume and at confining surfaces to varying degrees. However, just as amorphous solids appear to be steady-state solids, so laboratory generated plasmas often exist as steady, non-equilibrium states, too. It must be noted that the lifetime of individual particles in laboratory plasmas may only be a small fraction of a second, so that the steady state is a kind of dynamic, but non-thermal equilibrium [Mare00].
Since there are different influences on plasma parameters, these factors can interact, giving rise to an extremely complex system of variables. WILHELM summarises the basic processes in the next figure.

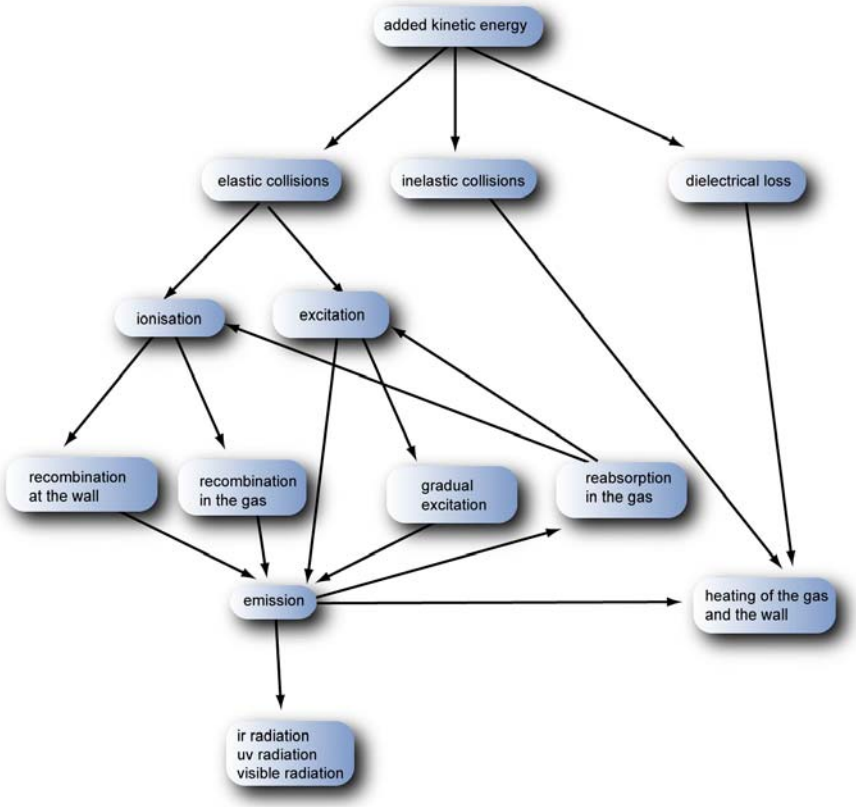

Figure 19: reactions in a plasma [Wilh95]

Next the different influences will be discussed for an argon microwave plasma. In the case of a microwave excitation the degree of ionisation is comparably high with $\frac{n_i}{n} \approx 10^{-2}\text{-}10^{-1}$ as well as the electron energy. Because of the low energy of the ions[4] (some authors call them "cold"), their proportion of energy transfer to the surface is very small and this corresponds to a poor modification of the polymer. The energy of electrons and ions are ideally MAXWELLIAN distributed, and this theory will be compared in the following paragraphs with the experimental results.

Noble gases like argon are chemically non reactive among themselves and therefore the induced energy will change the physical properties of the gas. The next table lists typical values for a microwave argon excitation, while the data for the neutrals match the ones for a normal gas at room temperature.

Species	Physical properties	Values
Neutrals	Density (0.1 mbar) Temperature Velocity	$2.4 \cdot 10^{15} cm^{-3}$ 293K (0.03eV) $4 \cdot 10^{2} m/s$
Ions	Density (0.1 mbar) Temperature Velocity	$5 \cdot 10^{9} – 5 \cdot 10^{10} cm^{-3}$ 500K (0.04eV) $5 \cdot 10^{2} m/s$
Electrons	Density (0.1 mbar) Temperature Velocity	$5 \cdot 10^{9} – 5 \cdot 10^{10} cm^{-3}$ 23000K (2eV) $9.5 \cdot 10^{5} m/s$
UV-Emission	Wavelength of the most intense Argon-(I)-Lines	104.82nm (11.62eV) 106.67nm (11.83eV)

Table 2: typical characteristics of an argon discharge [Chap80] [Haef91]

As soon as the plasma comes into in contact with the sample, sputtering reactions occur and the resulting fragments may enter the discharge, leading to complicated inner plasma reactions. To minimise this possibility, the process gas flow is set rather high so that mainly pure argon will be ionised. Nevertheless, these impurities have to be taken into consideration.

The power consumption of the discharge can be divided into the maintenance of the generator and the power transferred into the discharge. For the second aspect, different steps of excitation can be distinguished. In a pure argon plasma the main forms of power consumption are excitation and ionisation. When hydrocarbons are present in the discharge, additional fragmentation reactions occur. The following table summarises the reactions for such a process gas mixture.

[4] indicated by the difference between the floating and the plasma potential V_{fl} and V_{pl},

Energy	Form of power consumption
<0.5eV	Excitation of rotational and vibrational states in hydrocarbons
2.7eV	Excitation of electronic states, e.g. fracture of double bonds $CH_2=CH_2 + e^- \rightarrow \bullet CH_2\text{-}CH_2\bullet + e^-$
3.6eV	Fracture of ordinary bonds (fragmentation) $CH_3\text{-}CH_3 + e^- \rightarrow 2\bullet CH_3 + e^-$
10.0eV	Ionisation of hydrocarbon fragments $\bullet CH_3 + e^- \rightarrow \bullet CH_3^+ + 2e^-$
11.6eV	Limiting energy for argon excitation $Ar + e^- \rightarrow Ar^* + e^-$
12.0eV	Ionisation of ethylene $C_2H_4 + e^- \rightarrow C_2H_4^+ + 2e^-$
15.8eV	Ionisation of argon $Ar + e^- \rightarrow Ar^+ + 2e^-$

Table 3: different forms of power consumption for an argon-hydrocarbon plasma [GeSc87]

Since photons, ions and electrons are responsible for the surface modification, their formation and disappearance must be observed. The photons are created by recombination processes within the plasma or by plasma-wall interactions. When previously excited electrons relax again, photons are emitted according to the selection rules. In the case of argon the highest energies can be received by a transition from the $3p^5 4s$ state to the ground state, resulting in photon energies of 11.83 or 11.62eV. Figure 20 shows those energy levels and further transitions.

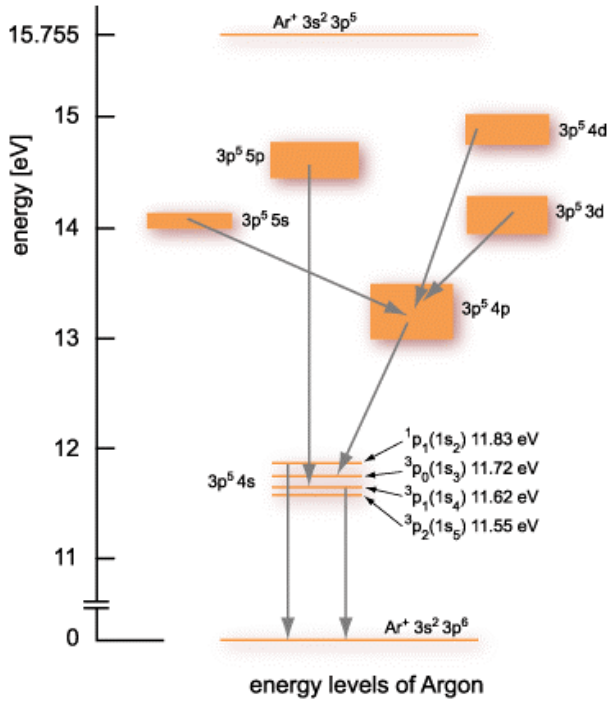

Figure 20: energy level of argon and several transitions [FeLo00]

Following the emission of photons there are also several possible reactions after a primary absorption of a photon. This activation of a singulett (S) or triplett (T) state is followed by vibrational and rotational deactivation. Another possibility is the emission of a photon after the collision with a molecule (M). The next table summarises these effects independently of the process gas.

Physical Processes	
Fluorescence:	$S^* \rightarrow S + h\nu$
Collision Induced Emission:	$S^* + M \rightarrow S + M + h\nu$
Induced Emission:	$S^* + h\nu \rightarrow S + 2h\nu$
Intersystem Crossing (ISC):	$S^* \rightarrow T^*$
Phosphorescence:	$T^* \rightarrow S + h\nu$
Internal Conversion:	$S^* \rightarrow S'$
Electronic Singlet Energy Transfer	$S^* + S \rightarrow S + S^*$
Energy Pooling:	$S^* + S^* \rightarrow S^{**} + S$
Electronic Triplet Energy Transfer	$T^* + S \rightarrow T + S^*$ or $T^* + h\nu \rightarrow T^{**}$

Table 4 : photon effects - several physical processes can occur after an activation of a singulett or triplett state

The spectrum of the discharge also ranges in the visible area and shows specific lines for different gases. Therefore, coarse impurities of the process gases or the ablation of sample material can be easily spotted by examining the colour of the discharge visually.

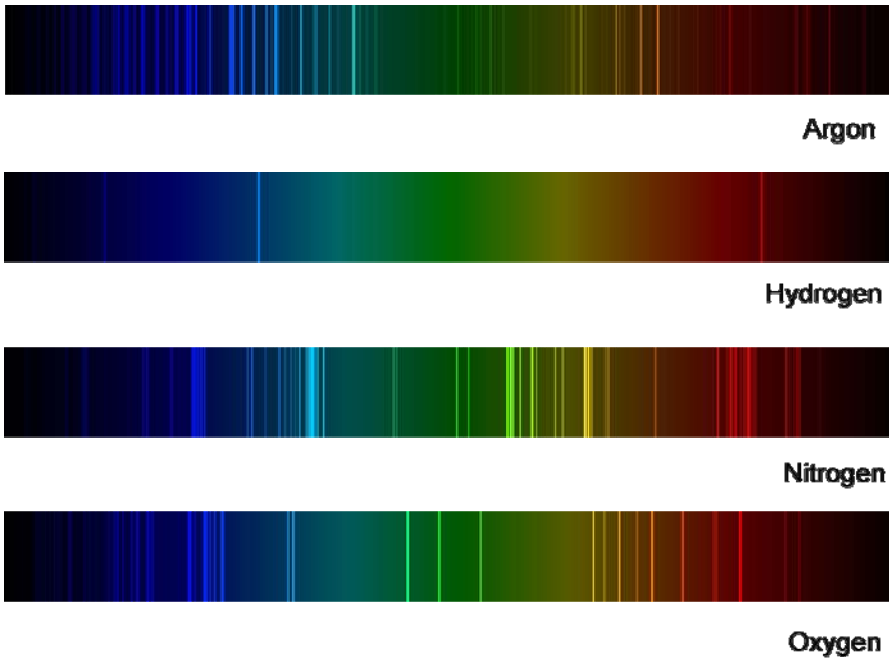

Figure 21: emission lines in the visible range for different process gases [www01]

This examination of the visible spectra is not suitable for the detection of small amounts of contamination. For a more precise examination better instruments are needed (like a UV spectrometer which is capable to detect photon energies above 12eV).

Ions are created when electrons are removed or attached to a neutral. Different from photons, their characteristics relate also to matter and not only to energy. In the gaseous phase they could react with other ions or neutrals in the following ways:

Reaction	Description	Evidence
$A^+ + B \rightarrow B^+ + A$	Charge exchange [5]	Ion energy spectra
$A^+ + B \rightarrow B + A^+$	Elastic scattering	Ion energy spectra
$A^+ + B \rightarrow A^+ + B^* + e^-$	Excitation	Ionisation efficiency
$A^+ + B \rightarrow A^+ + B^+ + e^-$	Ionisation	Ionisation efficiency
$A + B^* \rightarrow A^+ + B + e^-$	Penning ionisation	Ionisation efficiency
$A^+ + BC \rightarrow A^+ + B + C$	Fragmentation / dissociation	Residual gas analysis
$e^- + A^+ + B \rightarrow A + B$	Volume recombination	Plasma decay
$A^{\pm} + B \rightarrow AB^{\pm}$	Oligomerisation	Ion mass spectra
$A+B \rightarrow AB$	Oligomerisation	Residual gas analysis

Table 5: gas phase reaction involving ions and neutrals

They have only a marginal impact on the modification process due to their small gain of energy (table 2 shows their temperature only 0.01eV higher than the temperature of the neutrals), but thereby they do not complicate the surface reactions.

A third group of the plasma species are the electrons. Most of them are elastically scattered in the gas phase, but some can also excite or ionise an atom or molecule. These are summarised with possible detection techniques in the next table.

Reaction	Description	Evidence
$e^- + A \rightarrow A + e^-$	Elastic Scattering	Thermal electrons
$e^- + A \rightarrow A^+ + e^- + e^-$	Penning-Ionisation	Conductivity
$e^- + A^+ \rightarrow A^* + e^-$	Excitation	-
$e^- + A^* \rightarrow e^- + A + h\nu$	De-Excitation	Light emission
$e^- + A^* \rightarrow A + 2\,e^-$	Two-Step Ionisation	Ionisation efficiency
$e^- + AB \rightarrow A + B + e^-$	Fragmentation	Residual gas analysis
$e^- + AB \rightarrow A^+ + B + 2e^-$	Dissociative Ionisation	Residual gas analysis
$e^- + AB \rightarrow A^- + B$	Dissociative Attachment	Residual gas analysis
$e^- + A^+ + B \rightarrow A + B$	Volume Recombination	Plasma decay and steady-state

Table 6: gas phase reactions involving electrons

[5] Called 'resonant' for A=B

2.3.2 Determination of the plasma parameters

For a discussion of the reaction listed above the plasma species need to be analysed with special diagnostics. While for the influence of light spectroscopic methods must be applied (which were not available for a detailed study), the influence of electrons and ions was determined by a LANGMUIR probe [Chap80]. Such a probe consists of a wire made from tungsten. Through immersion in the plasma this wire collects charged particles in function of the potential difference between plasma and probe. The ground plate of the discharge is used as a counter electrode. Because of sign convention, ion currents have a negative and electron currents a positive sign.

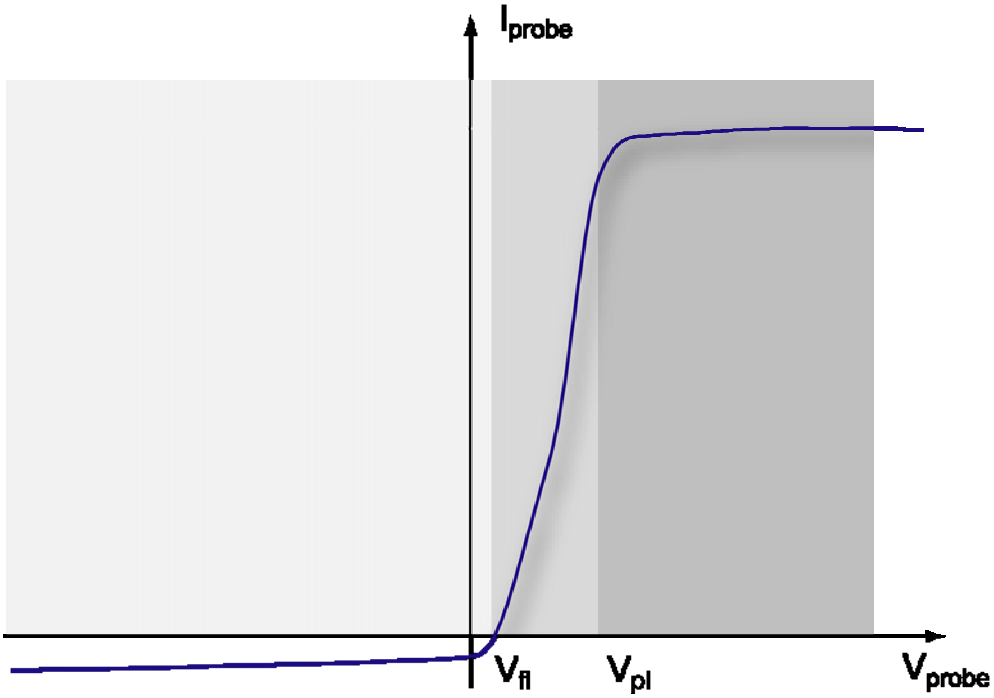

Figure 22: I-V-characteristic for a plasma obtained by a LANGMUIR probe

The characteristic in figure 22 can be divided into three areas by two potentials: the *floating potential* V_{fl} and the *plasma potential* V_{pl}. The floating potential can be recognised directly from the characteristic curve at the point $I(V_{fl})=0$. This means that the same amount of electrons and ions reach the probe and compensate the total current to zero. This potential is self-adjusting for a probe without voltage or with a non-conducting surface. In case of a strongly negative probe voltage (compared to the floating potential), only positively charged ions reach the wire. The corresponding current is called *ion saturation current* of the characteristic. As soon as the probe is sufficiently negative towards the plasma potential, i.e. the electrons are not overcoming the counter field, a peripheral layer with a thickness with up to 10 DEBYE lengths evolves around the probe. If

the size of this peripheral layer is large compared with the radius of the probe r_{probe}, the ions sense this wire with a larger effective radius and when they are crossing the sheath area, the collision parameter determines whether the ions reach the wire or not.

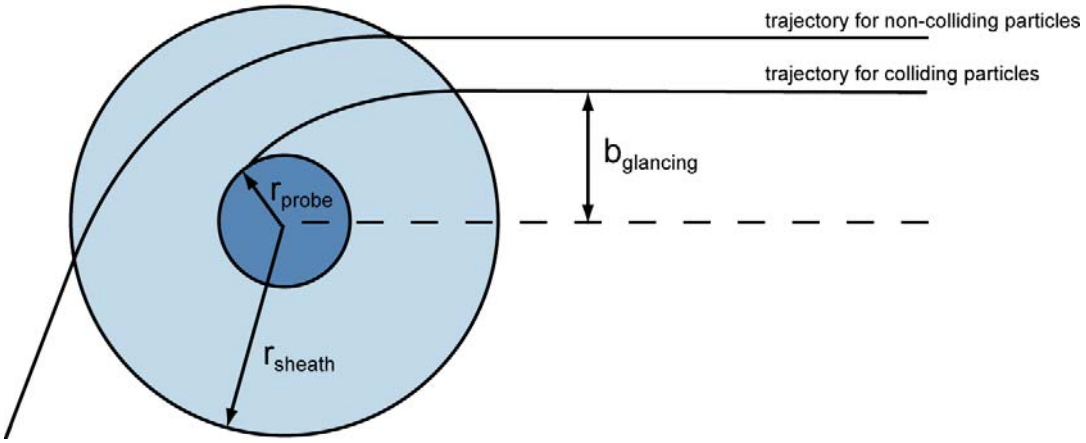

Figure 23 : probe geometry – from right to left trajectories for colliding and non-colliding particles are drawn [Flen93]

The utmost collision parameters $b_{glancing}$ for glancing incidence (see figure 23) can be derived from the energy and momentum conservation law :

$$b_{glancing} = r_{probe}\sqrt{1-\frac{eV_{probe}}{kT_e}}. \tag{26}$$

The limited orbital motion current of ions with BOHM velocity therefore equals with A_{probe} as the product of probe radius and its length:

$$I_{ion} = n_i e \cdot 2\pi A_{probe}\sqrt{\frac{kT_e}{m_{ion}}}\sqrt{1-\frac{eV_{probe}}{kT_e}}. \tag{27}$$

This equation is valid as long as the free path of ions is large compared to r_{sheath} while the collision parameters $b_{glancing}$ must be smaller than this radius. Equation 27 was derived by LANGMUIR and MOTT-SMITH for an infinite layer [LaMS26].

The plasma potential V_{pl} cannot be directly derived from the characteristic curve. It is located near the maximum of the first derivation respectively the passage of zero of the second derivation as long as the characteristic curve is not disturbed by a high frequency plasma modulation. The characteristic curve's area between floating and plasma potential is called *electron residual current*. At this point the probe potential is charged weakly negative based on the plasma potential. Depending on the potential and the energy of the electrons, some of them can overcome this counter field.

When the probe is positively charged against the plasma potential, all electrons are accelerated towards the probe. This leads to the *electron saturation current*. The ions with their small amount of energy cannot overcome the counter field for their positive charge. A space-charge barrier is once again created around the probe, but this time negatively charged. The electron current towards a thin probe is therefore not a real saturation current, rather a current defined by collision parameters. For $V > \frac{2kT_e}{e}$ the formula is given by:

$$I_{electron} = A_{probe} n_e e \cdot \frac{2}{\sqrt{\pi}} \sqrt{\frac{kT_e}{2\pi m_{electron}}} \sqrt{1 - \frac{eV}{kT_e}}. \tag{28}$$

Secondary electron emission can be ignored for this part of the characteristic line because emitted electrons are re-absorbed immediately through the counter field. There are many other processes influencing the electron saturation current like excitation and ionisation by electron impact inside the space-charge barrier. Additionally, for large positive voltages, the electron current can be limited if not enough electrons are supplied through diffusion processes inside the plasma. For these reasons, the equation above frequently fails and the electron saturation current cannot be interpreted.

Electron saturation current also yields information about the distribution in an integral form. The relationship between the second derivative of the characteristic curve and the energy distribution function for the electrons $F_e(E)$ is described by the DRUYVESTEYN formula [Druy30]:

$$\frac{d^2 I}{dV^2} = \sqrt{\frac{2e}{m_{electron}}} \frac{e^2 A_{probe}}{4} \frac{1}{\sqrt{-V}} F_e(E). \tag{29}$$

The velocity distribution function $f_e(v)$ of an isotropic distribution can be normalised

$$\int_0^\infty f_e(v) d^3 v = \int_0^\infty F_e(E) dE = n_e \tag{30}$$

and derived to yield the energy distribution with the following formula

$$f_e(v) = \frac{m_{electron}}{4\pi} \sqrt{\frac{m_{electron}}{2E}} F_e(E). \tag{31}$$

It is obvious from the preceding formulas that the second derivation of the characteristic curve is direct proportional to the velocity distribution of the electrons:

$$\frac{d^2I}{dV^2} = \frac{2\pi e^3}{m_{electron}{}^2} A_{probe} f_e(v)\,. \tag{32}$$

By integration of the velocity distribution, the electron density at the LANGMUIR probe can be calculated as

$$n_e(I'') = \int_0^\infty f_e(v) 4\pi v^2 \cdot dv = \frac{\sqrt{2^3 m_{electron}}}{\sqrt{e^3} A_{probe}} \int_{-\infty}^0 I''(V)\sqrt{-V} \cdot dV\,. \tag{33}$$

The determination of the density is valid for all isotropic distribution functions under the condition of a known plasma potential. Further information about this measurement technique can be found with [Konu92] [Chen65] [CTT75] [SwSc70] [Hutc87] [LoHo68].

Having established a framework for the plasma characterisation and the surface analysis, the experimental characterisation of the plasma will be done in the next chapter. Afterwards the techniques for the surface analysis will be applied.

3. Plasma Analysis

A systematic investigation and description of non-equilibrium plasma physics is difficult to obtain and has not been done so far because particles and fields in a discharge form too complex a system. Trial and error approaches on the other hand have only brought limited insights. Probably the greatest challenge would be to predict the interaction between such a plasma and the surface of a sample.

In this chapter some important preliminary work will be presented. As a plasma itself and the plasma treatment cannot be described in microscopic detail, a new approach has been made to reduce the complexity of the plasma and therefore of the modification. This concept is based on the fact that through the existing microwave discharge mainly photons are created and electrons are excited. If therefore the ions can be neglected, the whole plasma process is simplified without compromising the physics and chemistry behind the treatment. A future goal would be the modification of the sample only through electrons and photons exactly like the plasma treatment does.

To approach this goal, the experimental conditions have also to be idealised in such a way that the plasma process gas and the substrate are as simple in their structure as possible. The experiment itself has to be most accurate to perform changes in the surface region without additional reactions from the impurities. A typical operating procedure in this work takes care of this aspect and is described as follows:

- selection of pure polymer materials;
- cleaning of the surface for polymer foils or spin-coating of solved granular material onto silica wafer or mica;
- plasma, ultraviolet or electron treatment under clean experimental conditions (e.g. residual gas pressure $<10^{-7}$mbar);
- post treatment effects like the reaction with air or substances for chemical labelling like bromine or nitrogen monoxide;
- surface analysis with photoelectron spectroscopy;
- (partly) AFM measurements or other techniques.

The experimental set-up to perform these kinds of experiments can be divided into two main areas: the plasma and the derivatisation chamber. Both are separated by valves (see figure 24) and possess independent vacuum pumping systems, leaving the chambers with residual gas pressures below 10^{-7}mbar.

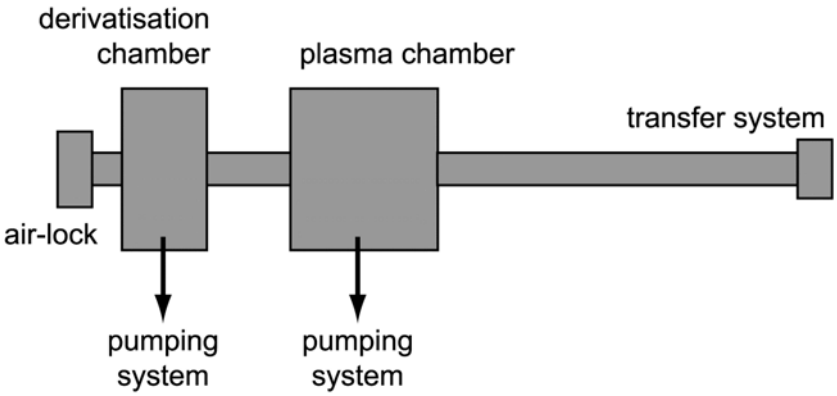

Figure 24: schematic set-up of the measuring apparatus – with the transfer system the sample can be moved between plasma and derivatisation chamber in situ

The sample itself is mounted on a holder which is equipped with threaded bushes and holes for positioning and moving. The holder has to be introduced via an air-lock into the vacuum system and can be transferred afterwards *in-situ* between the two chambers. To change the sample, only a sub-area of the derivation chamber has to be ventilated.
Another aspect relies on the detection of the modification. While earlier research mainly focussed on the macroscopic changes, here the changes on a molecular scale were investigated. This has been made possible on one hand through the application of modern analytical systems and on the other hand through selective labelling reactions according to molecular structures. However, before these techniques are introduced in the second part of this chapter, some theoretical aspects and extensive studies of the inner plasma parameters will be presented in order to understand more about the modification process.

3.1 Characterisation of the Plasma Chamber

From earlier projects supported by the DFG (Deutsche Forschungsgemeinschaft) a microwave (2.45GHz) plasma chamber was able to be used as well as equipment from the University of Osnabrück and the Fraunhofer Institute for Applied Material Science. The plasma chamber was extended by some measuring techniques to analyse the inner parameters of the plasma (LANGMUIR probe and residual gas analysis) and a special chamber for chemical labelling was also available. The 2.45GHz microwave plasma chamber was filled only with high purity gases after the residual gas pressure inside the plasma chamber has reached *ultra high vacuum* (UHV), hindering external reactions. For the surface activation argon (purity > 99.999vol.%, Messer Griesheim) was used as a process gas. Functionalisation experiments of the polymer have been done either with

oxygen (purity > 99.998vol.%, Messer Griesheim) or nitrogen (purity > 99.999vol.%, Messer Griesheim).

The process gas flow was controlled by a dose valve in combination with a gas flow monitor. The pressure in both chambers was examined by two compact FullRange^{TM} gauges (Balzers Instruments). A rough vacuum was obtained by a rotary slide-valve vacuum pump for the plasma chamber and a membrane pump for the derivatisation chamber. As a second step, each unit was equipped with a turbo molecular pump to reach ultra high vacuum.

The plasma chamber consists of a cyclotron, whose microwaves are coupled into a wave-guide. After passing a crystal window, the process gas inside the plasma chamber is excited and forms the discharge. The expansion of the discharge depends on the outer parameters (process gas pressure and power consumption), which can be monitored and controlled separately. The process gas flows from an upper side into the chamber while the LANGMUIR probe is positioned inside the plasma.

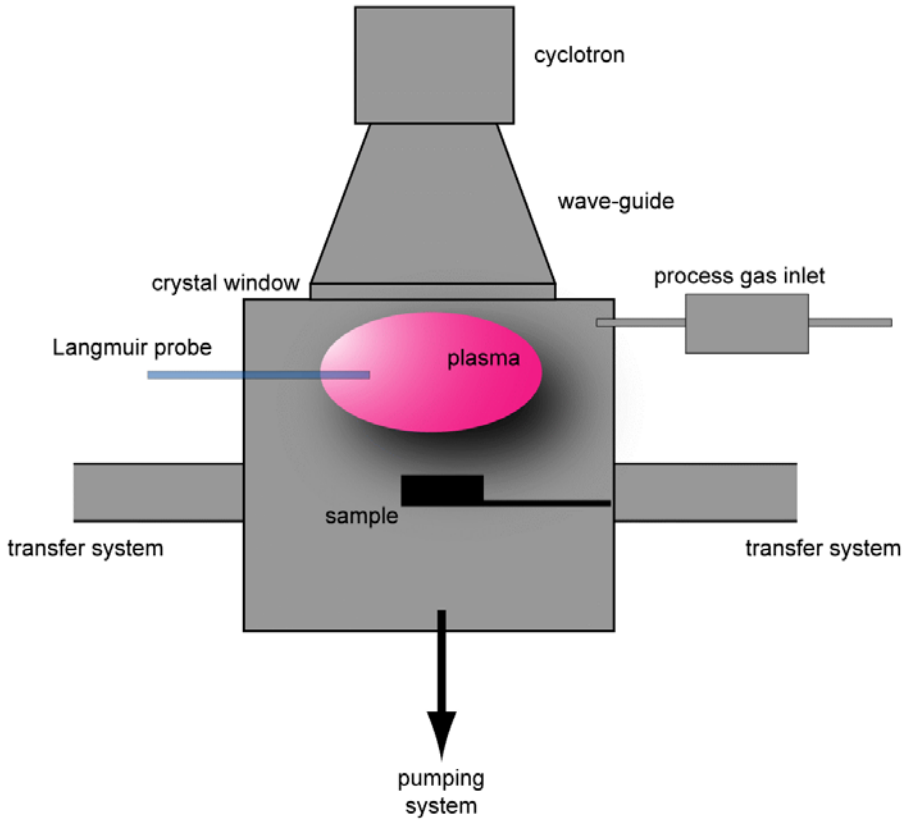

Figure 25: schematic view of the plasma chamber – while the outer plasma parameters were controlled by the process gas inlet and the pumping system, the inner parameters were analysed by a LANGMUIR probe

For the reproducibility of the experimental results, the chambers can be heated so that absorbed particles and molecules would be removed from the chamber walls.

So far surface modifications due to plasma treatment were mainly characterised by the kind of excitation and the process gas (including the values for pressure and flow). While it has been shown that this information is not significant for a reproducible modification (problems with the scaling-up), and even the shape of the reactor and the plasma source influences the modification [KhOv00], a more precise description of the plasma is needed. On the other hand it is impossible to describe photons, electrons, ions, and neutrals in terms of their individual energy and direction of movement, but for example the energy distribution of charges in combination with corporate properties (like electron or ion density) allows a description of the inner parameters of a plasma, which are relevant for the modification and independent from the shape of the reactor. So first of all an overview of these discharge parameters is needed, including a distinction between different regions of plasma parameters which can be created (see figure 22 in *determination of plasma parameters*).
Important factors for the discharge are the initiation and breakdown conditions, which ideally can be calculated by the pressure and the excitation frequency [KoMa70] [Nors79].

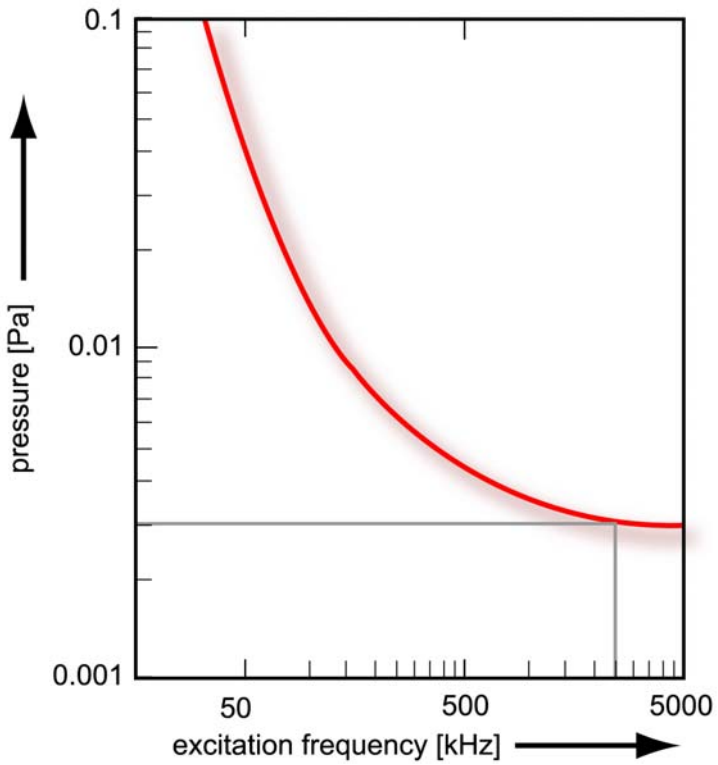

Figure 26: theoretical graph for the ignition of the discharge – the necessary pressure to initiate the plasma decreases with higher excitation frequencies

As the figure above represents theoretical values under ideal conditions, these values have to be determined experimentally for the existing set-up and will be presented later. While in this experiment the excitation frequency is fixed, the pressure can be controlled for different process gas flow rates by the pumping unit. For the 2.45GHz microwave discharge a pressure of at least $3 \cdot 10^{-2}$Pa (corresponding $3 \cdot 10^{-4}$mbar) is needed, while a discharge with a smaller excitation frequency needs a higher process gas pressure.
The pumping capacity reaches a residual gas pressure of below $3 \cdot 10^{-8}$mbar. As soon as a process gas (argon) floods the plasma chamber, this value increases as shown in the pumping capacity characteristic in figure 27.

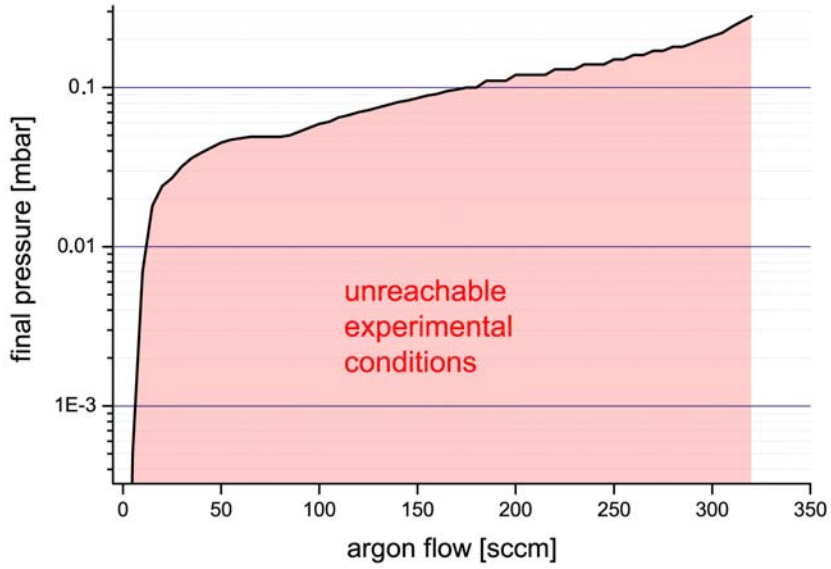

Figure 27: pumping capacity for argon – the pumping system is capable of reaching all pressures above the red coloured area

After a sharp increase of the final pressure for small argon flows up to approx. 30sccm, the graph becomes a light ascending straight line. From an experimental point of view with the set-up, a reasonable lower bound for an argon flow up to 180sccm was a pressure of 0.1mbar, which is defined by the capacity of the pumping unit. Experiments can also be performed with a higher gas flow at a pressure of 10^{-4}bar or higher, but these results will be discounted here because of instabilities in the discharge.
Consequently, the discharge shows very stable behaviour with time for this flow of process gas and pressures between 0.1 and 10mbar. This means that the described conditions were far away from a breakdown and therefore appropriate for the experiments. A problem with the stability of the discharge can be evaluated visually as a flickering light as well as from measurements with the LANGMUIR probe, where the characteristic line is irregular and shows several spikes.

Although the inner parameters naturally respond to changes of pressure, gas flow, power consumption and excitation frequency, they cannot yet be calculated from these values but ought to be measured. The main focus of the comparison between outer and inner parameters lies on the influences of the electrons.

In the following paragraph, the electron energy distribution function (EEDF) will be described in detail. Also the properties of the electrons will be discussed in depth because of two reasons:

- generally electrons have an impact on the surface modification;
- from the precise determination of the inner properties of the discharge one can draw conclusions as to the possible interactions with a wall.

For the determination of the plasma parameters, a LANGMUIR probe by HIDEN Analytics was used. The evaluation of the ***I-V-characteristic*** with the included software was sometimes not precise enough so that some of the parameters had to be calculated "by hand" from the spectra. The following figure shows the probe and the equivalent circuit. The probe mainly consists of a tungsten wire with 0.4mm in diameter and a circuit to adjust the voltage and measure the current.

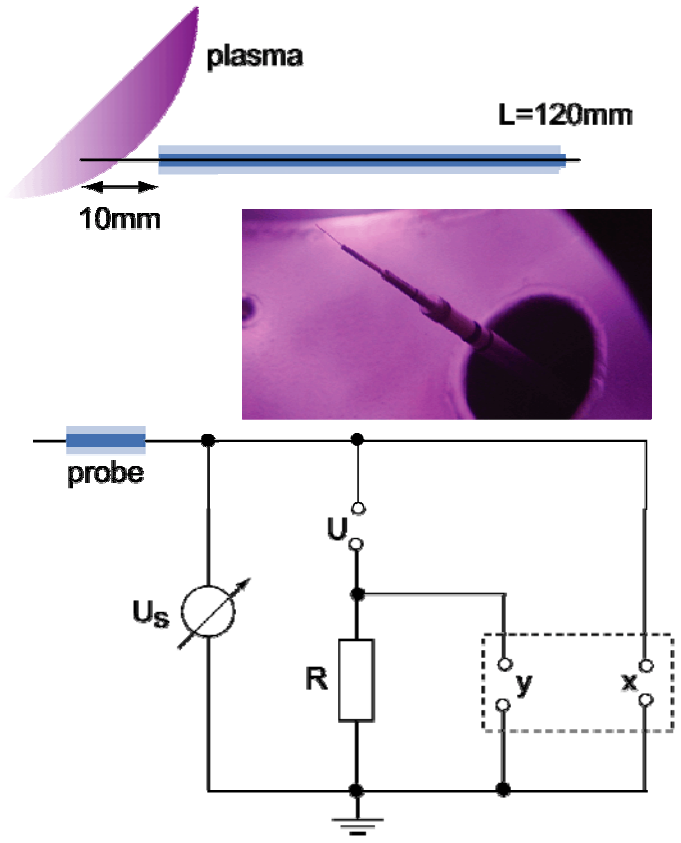

Figure 28: LANGMUIR probe and equivalent circuit [Hide97]

The characteristic curve for the probe varies with the current by several magnitudes. Because of the twofold derivative for the analysis, the curve had to be very smooth but also precise. The numerical smoothing of the data leads to a less accurate energy resolution and therefore the physical structures blur. For obtaining acceptable data, different approaches are possible. FLENDER describes the benefit of a continual up- and down-scanning of a voltage interval, especially sampling with randomly chosen starting voltages [Flen93]. The potential of the probe is selected by chance, so relaxation processes for the current become visible, which can be used to determine contamination. While this sophisticated approach was not possible to realise with the present device, the parameters like measurement time, measuring points and different voltages had to be optimised. Finally, the integration time was set to 0.5s per data point and an incremental width of 10mV. The potential ramp was set from –30V to +30V. For values higher than +50V the wire started to glow because too many electrons from the plasma have been attracted. A normal scan consists of 600 data points. Prior to the measurement, the LANGMUIR probe was pre-charged for cleaning reasons. With these preparations, the I-V-characteristic is smooth enough for calculating the plasma parameters.

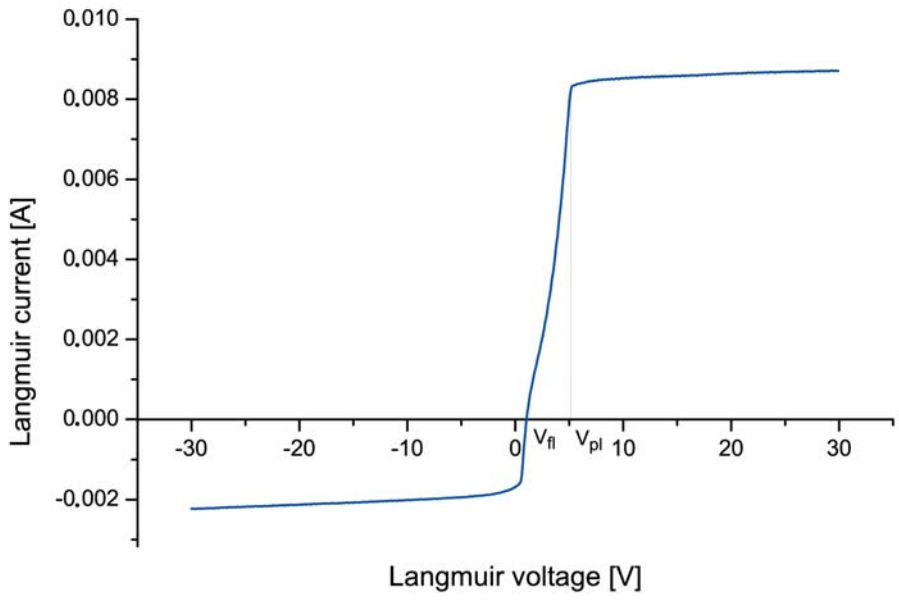

Figure 29: I-V-Graph – a typical profile for a LANGMUIR characteristic

The figure above shows a typical profile for a LANGMUIR characteristic. The three areas of interaction between the wire and the charged particles inside the plasma can be easily made up. The characteristic is also smooth enough so that the following calculations can be performed by the provided software.

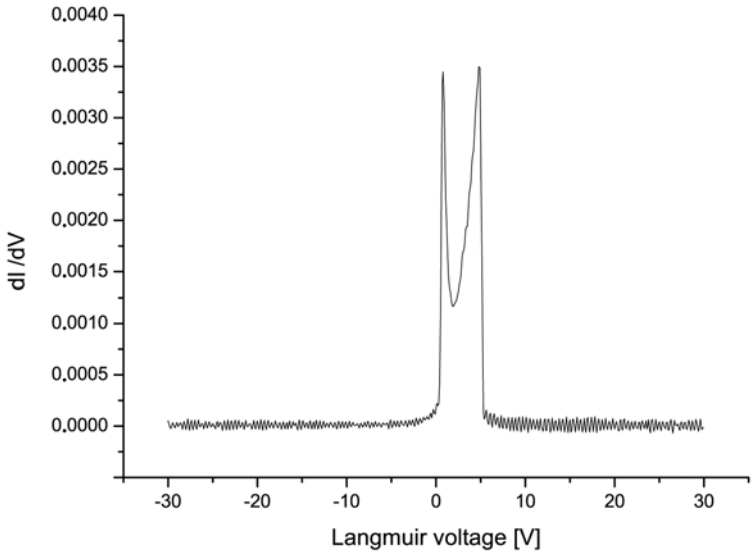

Figure 30: first derivative of the LANGMUIR characteristic

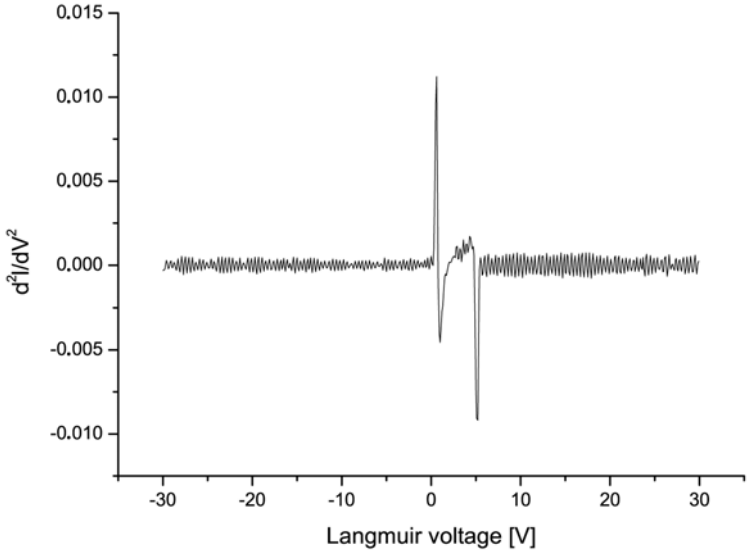

Figure 31: second derivative of the LANGMUIR characteristic

From the graphs, the floating potential with 1.5eV and the plasma potential with 5.5eV can be evaluated. The derivatives are also important for the evaluation of the I-V-correlation, because with them the electron energy distribution function, the densities of the charged particles and other inner plasma parameters can be calculated (see chapter 2.3.2 for theoretical aspects of the calculation).

3.2 Electron energy distribution function

Combined with the electron density, the EEDF can be used to describe the probability of reactions caused by electrons. This includes reactions inside the plasma, with the walls of the experimental set-up and with the polymer surface, which should be modified. Therefore it is also important for a later modelling of the plasma conditions.

From a theoretical point of view it is possible to calculate the electron temperature by using the values for the collision cross sections, electron density and reaction rates in the formula. For an argon microwave discharge this can be evaluated to T_e=2.15eV, but ignoring the non thermal distributed electrons leads also to misinterpretation.
Typical for a MAXWELLIAN (or thermal) distribution is the high proportion of low energy electrons (bulk) and the low proportion of high energy electrons (tail). Two of them are shown on the left of the next figure with different temperatures, while on the right different forms of velocities are compared to which other formulas and literature refer.

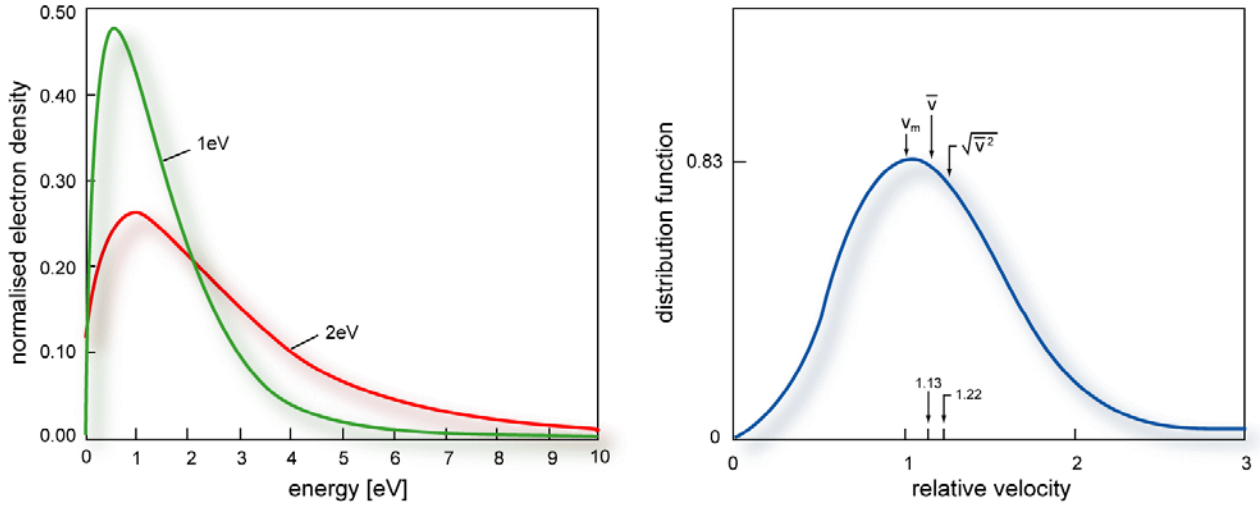

Figure 32: MAXWELL distributions for 1 and 2eV electrons and different definitions of velocity (similar to [Voge97][Greu98])

The reactions taking place inside the plasma refer to collision processes, and those have a threshold of some electron volts. As mentioned before the threshold energy for the excitation of argon for example is about 11.6eV, for the ionisation 15.8eV. The fraction of MAXWELL distributed electrons with T_e=2eV which are capable of such reactions can be calculated as 0.01 for the excitation and 0.001 for the ionisation. However, as there are a lot of electrons inside the plasma such reactions are likely.

When these theoretical values are compared with the obtained data in figure 33, first of all two distinctive shapes of the electron energy distribution functions are drawn to attention. The line-shape does also not look like MAXWELLIAN distributions, but more like DRUGVESTAN or BI-MAXWELLIAN [FLEN93]. The measurements were obtained at different argon gas pressures while the input power was set to 70% of the maximum power and the process gas flow to 18sccm.

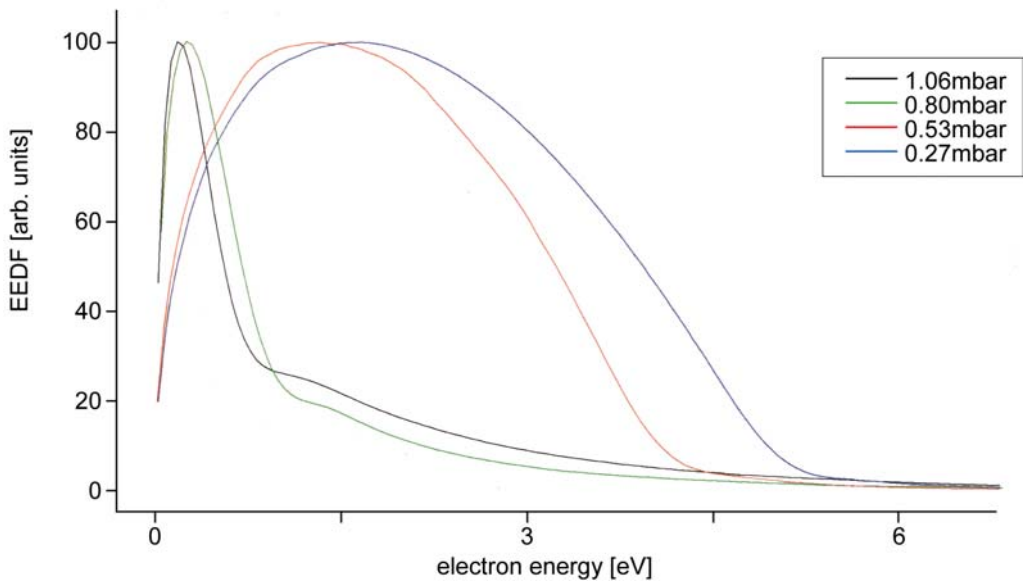

Figure 33: comparison of different EEDF for varying pressure

The graphs with the lower maximum of energy refer to discharges with higher process gas pressure (black: 1.06mbar, green: 0.80mbar) while a lower pressure leads to higher electron energies (red: 0.53mbar and blue: 0.27mbar).

As the characteristic suggests, there are far more electrons with higher energy for lower pressure plasma discharges. This result agrees with theoretical considerations and it is also interesting for the surface treatment, because electrons with higher energies have a higher probability of modifying the polymer.

Not only the pressure can be varied, but also the input power. The small variation of the shape of the EEDF is displayed in the next figure, while the pressure was lowered to 0.13mbar (this value for the pressure leads to the “best” shape of the EEDF in the experiments).

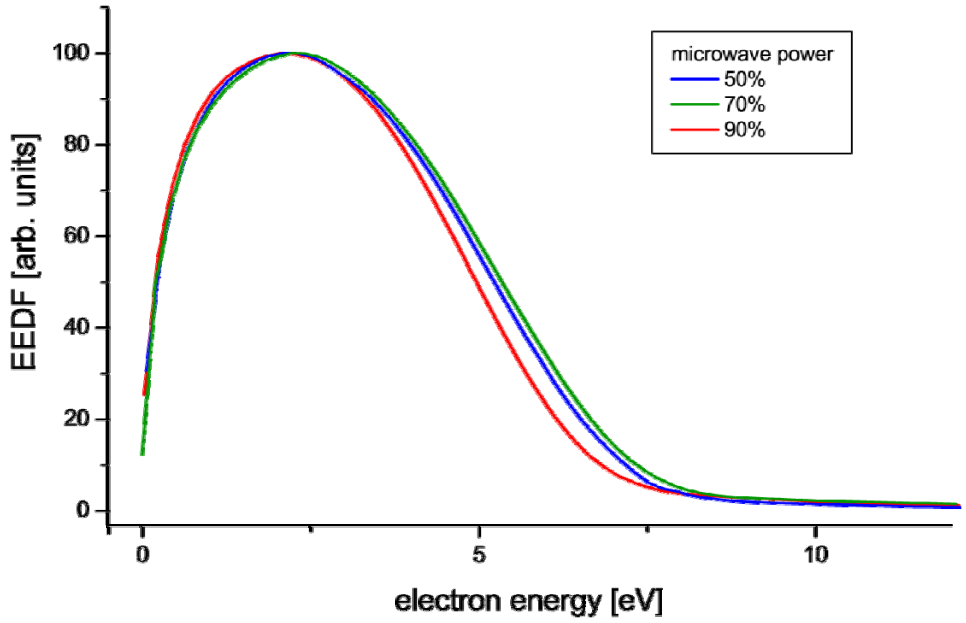

Figure 34 : comparison of different EEDF with varying input power – the energy beyond 12eV are omitted

The green characteristic (corresponding 70% microwave power input) showed the highest proportion of electrons in the tail of the distribution (2.5eV and above). As these electrons are needed for the modification process, the following plasma treatments were mainly performed at these maximised conditions[6] with a process gas pressure of 0.13mbar and a power input of 70%.

The shape of the green line in the figure above can be evaluated in more detail according to higher electron energies. Therefore it is plotted again in figure 35 with the total length of the electron energy axis measured with the LANGMUIR probe. The total area corresponds to the electron density evaluated below.

[6] Trying to minimise the EEDF leads to a distribution with its main peak at about 0.15eV and a tail up to an energy of about 3.5eV. This amount of energy is not sufficient for a modification of the polymer.

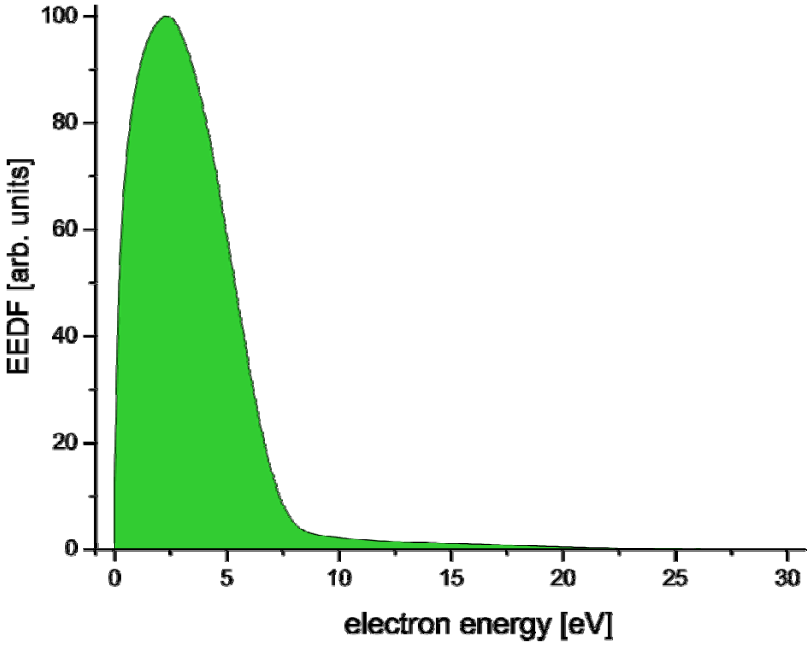

Figure 35: integral display of the optimised electron energy distribution function for a pressure of 0.13mbar, a flow of 18sccm and a power consumption of 70%

The area of the distribution function can roughly be divided into the bulk with low energy electrons (from zero to around 7eV) and the tail with higher energy electrons (7eV and above). In the next table several more energy intervals are displayed.

Area	Percentage
>20eV	0.32
17.5-20eV	0.30
15-17.5eV	0.44
12.5-15eV	0.65
10-12.5eV	0.84
7.5-10eV	1.92
5-7.5eV	14.09
4-5eV	13.61
3-4eV	17.38
2-3eV	19.27
1-2eV	18.50
<1eV	12.68

Table 7: evaluation of electron energy distribution function – for several energy intervals the proportion of plasma electrons are given

It can be concluded that a significant proportion of plasma electrons have enough energy to perform excitation, fragmentation and ionisation reactions and that the obtained characteristic is different from the theoretical MAXWELLIAN shape. As not only the EEDF will influence the modification, but also the electron density (and from an overall point of

view the other plasma species), this and further inner plasma parameters will be the next points of investigation.

3.3 Further plasma parameters

There are more aspects for the description of plasmas than the parameters discussed above. Important for a plasma characterisation is also the density of charge carriers. While negatively charged ions exist as well as multiple charged ions, the densities for ions and electrons need not to be equal. As these incidents are seldom referred to as single positively charged ions, in this work electrons and ions are summarised as charge carriers in consideration of quasi neutrality[7]. The density can be computed out of the I-V characteristic and varies as, for example, for different pressures of the argon process gases shown in figure 36.

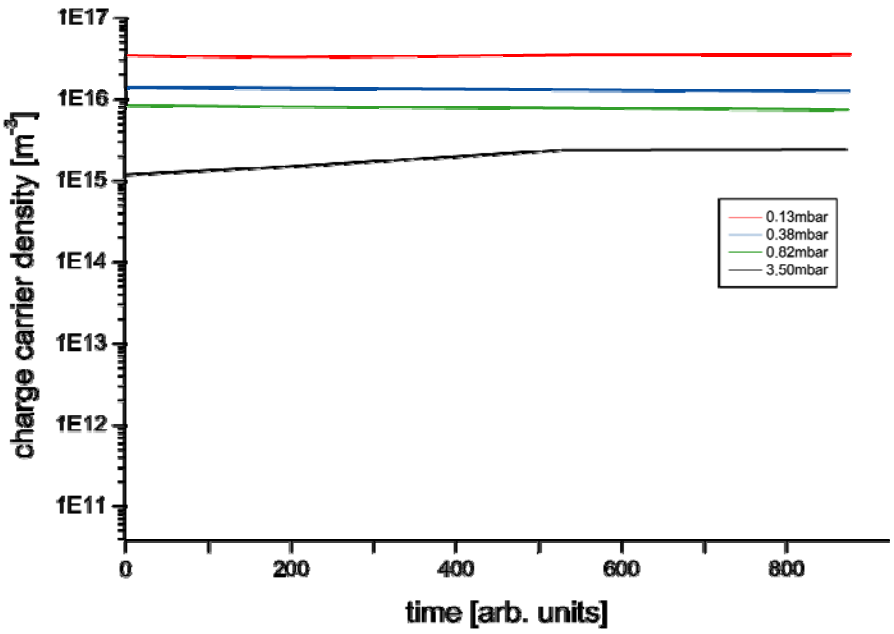

Figure 36: charge carrier density for different pressures – ions and electrons are not distinguished according to quasi neutrality

The charge carrier density increases with decreasing pressures, precisely from $1.8 \cdot 10^{15} m^{-3}$ for a pressure of 3.50mbar to a value of $3.5 \cdot 10^{16} m^{-3}$ for a pressure of 0.13mbar. As the controlling of the pressure leads to smaller mistakes (all pressures can be held by an error of about 2% of their values), a variation with time is visible for the black line (3.5mbar). The highest charge carrier density for the so far maximised EEDF supports the later modification under these plasma conditions. The charge carrier density

[7] this can be defined for multiple charged ions as $|n_e - Z \cdot n_i| << n_e$ after [Frey95]

rises within the first seconds because in the first sweep of the I-V characteristic the control unit of the LANGMUIR probe performs an automatic ranging of the current. This kind of fault can also be observed in the following measurements of plasma parameters.

Also important for a later treatment is the influence of ions. As discussed previously, their energy should be estimated as too small to have an impact on the polymer modification, but through the bombardment of the surface with electrons a sheath region is created, resulting in an electric field [Vale00].

In this field the ions are accelerated toward the surface and this gain of energy exceeds the amount from the microwave field (it was quoted in table 2 to be 0.04eV). So the observed difference between floating potential V_{fl} and plasma potential V_{pl} gives experimentally the energy of the ions.

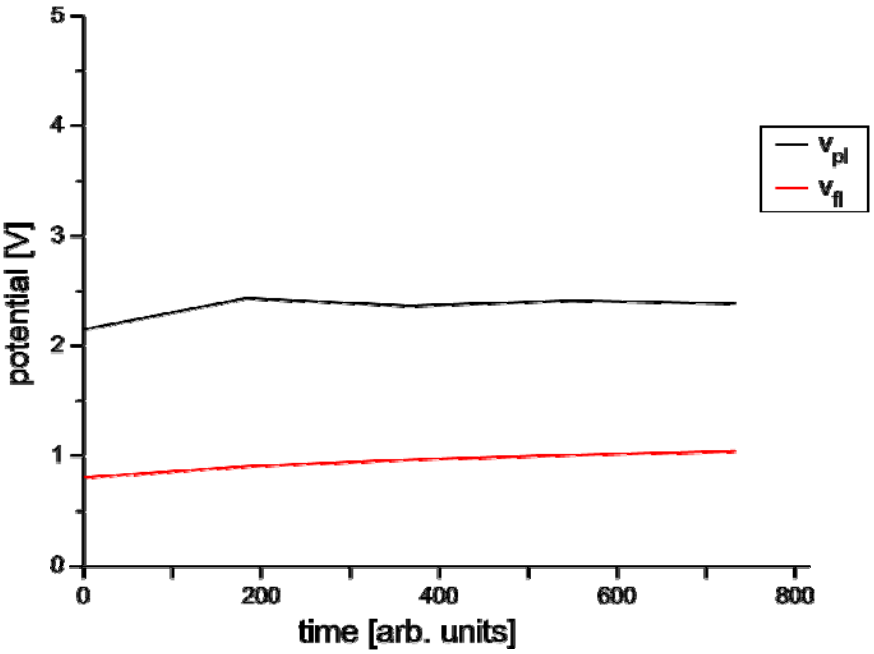

Figure 37: floating potential and plasma potential

The figure above shows the time dependencies of both values for the argon microwave plasma under constant outer conditions. The potentials stay nearly constant with time due to a stable discharge. This difference of 1eV to 1.5eV is typical for the measurements, although the potentials vary in their values. Further measurements have shown that the potentials decrease with increasing pressure which is in agreement to other studies [ChFu00].

The next figure represents the variation of the plasma potential according to the input power for the different outer parameters. The input power was lowered from 100% (green line) over 70% (red line) to 40% (blue line).

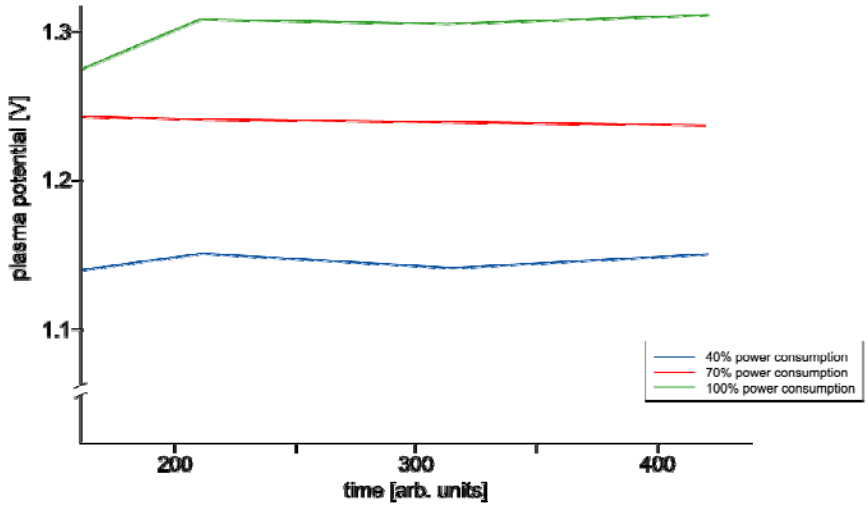

Figure 38: characteristic of the plasma potential for different power consumption

The change in power of the microwave excitation has a greater influence on the charge carrier density (see figure 39) and the potentials than for the shape of the EEDF. The time dependent plasma potential behaviour is displayed there for different power consumption, varying again from 100% (green line) over 70% (red line) to 40% (blue line).

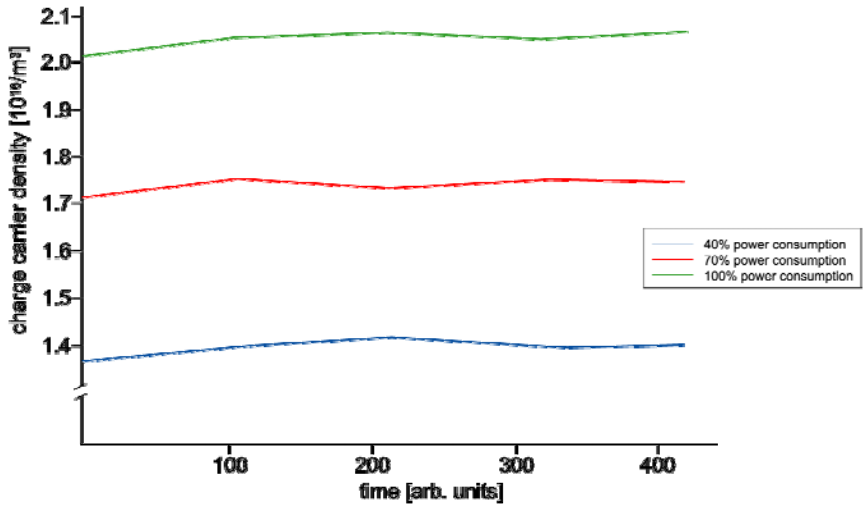

Figure 39: charge carrier density for different power consumption

Figure 39 shows the total charge carrier density according to the microwave excitation power. The total density rises from $1.35 \cdot 10^{16} m^{-3}$ for 40% of the maximum power absorption to $2.03 \cdot 10^{16} m^{-3}$ for 100% of it while the rising seems to be equidistant. Values below 40% of the total injection power lead experimentally to a breakdown of the discharge.

This result conflicts with the previous considerations to optimise the charge carrier density and the shape of the EEDF simultaneously. A higher power consumption leads to a higher density of electrons but the proportion of high kinetic electrons declines. In the same way the next graph (figure 40), displaying the charge carrier density according to the gas flow rate, also conflicts with the previously selected plasma parameters with an argon flow of 18sccm.

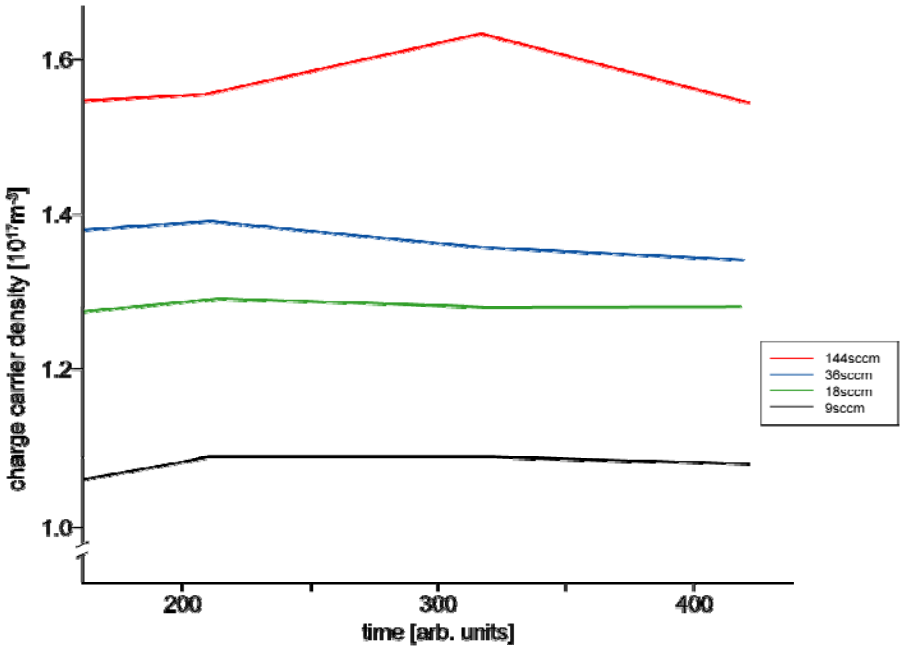

Figure 40: charge carrier density according to the gas flow rate

The implications from the last graphs show that the optimisation of plasma parameters is a question of balancing the importance of the EEDF on one side with the need for a high charge carrier density on the other side. In the further considerations the aspect of the EEDF shape was preferred because the disadvantage of a lower charge carrier density can be compensated by a longer treatment time. For an industrial application this may be vice versa.

As shown in the previous figures the charge carrier density is dependent on the three outer parameter gas flow, pressure and power input. With the previously displayed data

and some further measurements this behaviour can be summarised by three-dimensional plots, displayed in the following graphs. Each graph showing the gas flow and a second parameter.

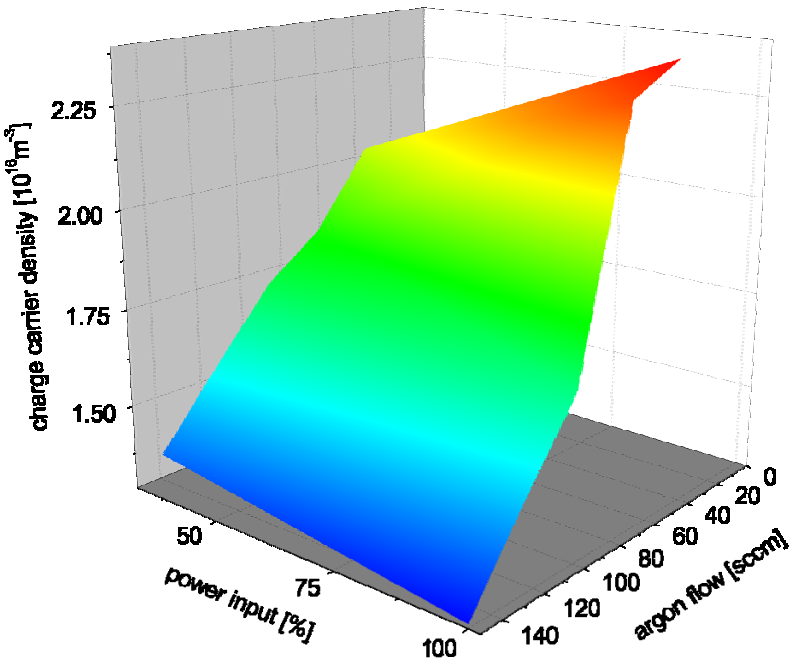

Figure 41 : charge carrier density according to argon flow and power input

Figure 41 shows a small rise of charge carrier density with a higher power consumption, but a stronger effect is obtained for smaller argon flow.

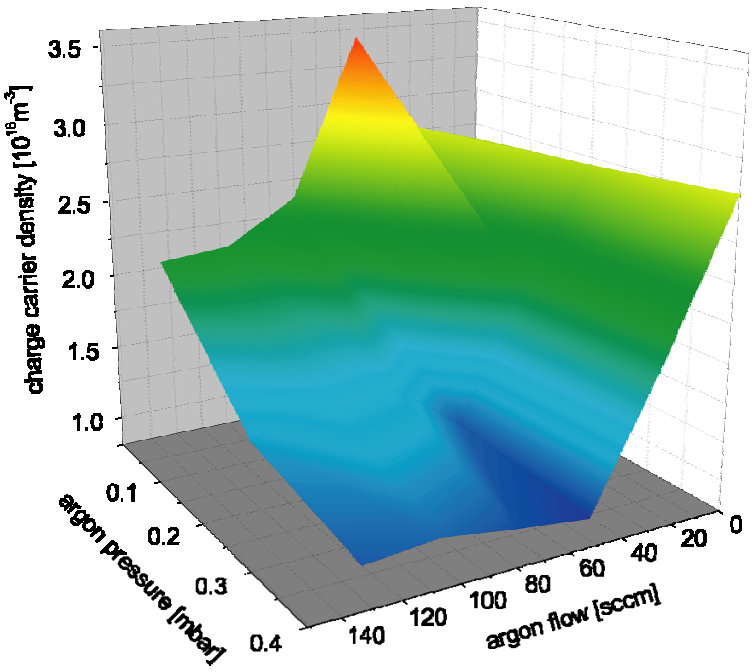

Figure 42: charge carrier density according to argon flow and pressure

Smaller argon pressure leads also to higher densities for charger carries, but the correlation with the argon flow is less distinctive (see figure 42). Both graphs confirm that the parameters are nearly optimised for the discharge concerning the charge carrier density.

One aspect not taken into full consideration so far is how far an electron removed from the ion in the oscillating field of a microwave discharge. The answer gives a parameter called DEBYE length, which can also be computed from the I-V-graph. Figure 43 presents some of these lengths according to the process gas flow.

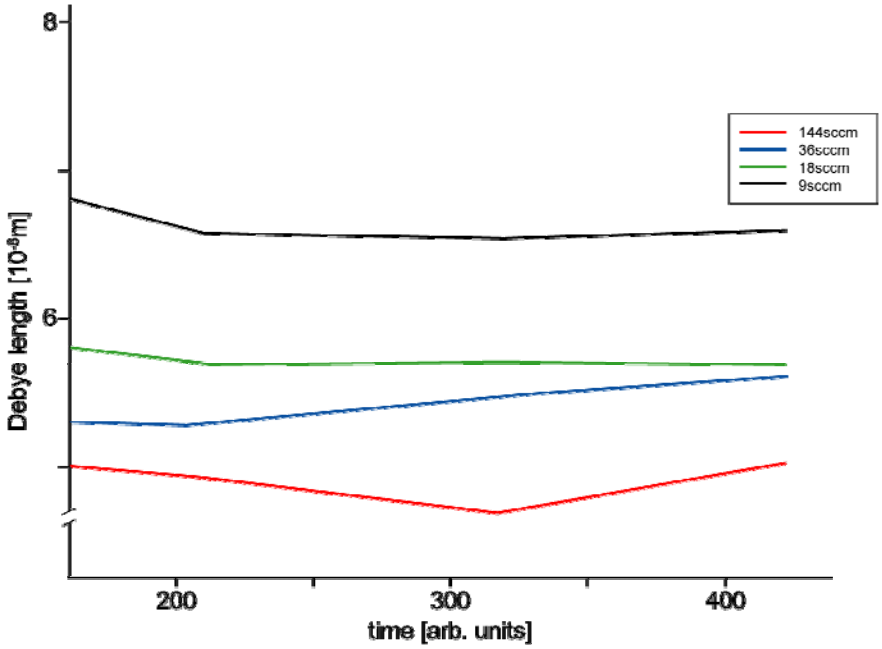

Figure 43: DEBYE length according to the process gas flow

The graph shows that the DEBYE length decreases with rising process gas flow, but varies only slightly around $6 \cdot 10^{-6}$m. For the treatment conditions a rounded DEBYE length of 10^{-5}m should be kept in mind.

Several further measurements concerning these plasma parameters have been performed and fit to the plasma theory [Roos91], but as they are not relevant to the following considerations they will not be displayed.

3.4 Consequences for the treatment

Analysing the measurements of inner plasma parameters leads to some ideas for the following procedure. These include an estimation of the electron bombardment on the surface as well as the construction of a special sample holder.

The information of the inner plasma parameters will now be used to calculate an electron current similar to the influence of plasma electrons. This is necessary because the polymer surface will later be modified with electrons from a charge neutralisation source to simulate the same reactions as in a plasma treatment.

For the electron treatment of the surface a charge neutralisation electron source (LEG41, VG Microtech) was used. The electrons are created by the EDISON effect and were focussed and separated according to their kinetic energy. The main advantage of this device is the treatment of small spots at very low electron energies.

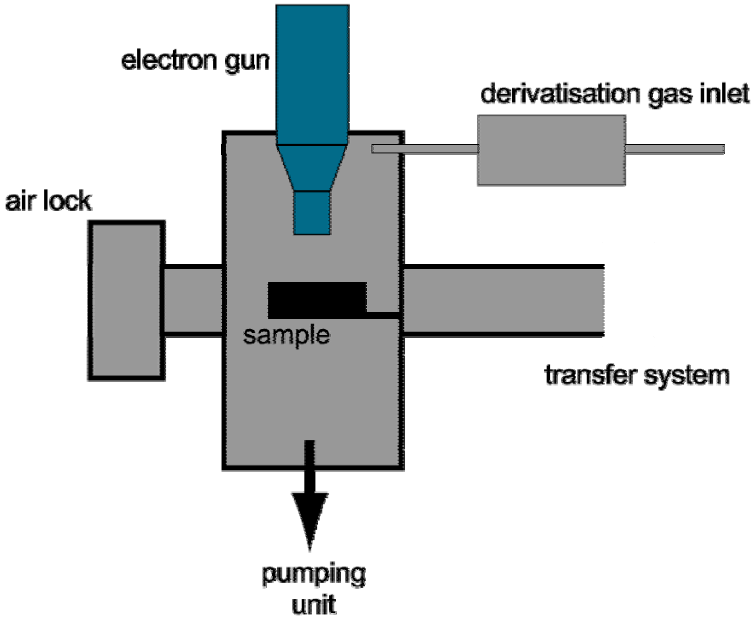

Figure 44: schematic view of the derivatisation chamber – next to the inlet for the gaseous derivatisation substances, the samples can also be treated with electrons in this chamber

Typical values for the optimised plasma were an electron density of 10^{16} electrons per m^3 and a DEBYE length of 10^{-5}m for the default frequency of $2.45 \cdot 10^9$Hz. As the DEBYE length refers to the screening of an electrical field for an ion, it can be seen as a distance in which electrons can interact with the surface. Regarding the electrons as completely free, a stream of 10^{11}electrons passing an area of $1m^2$ per slice with the thickness of a DEBYE length (or in other words $1.2 \cdot 10^{20}$ electrons hitting a surface area of $1m^2$ within one second

for the microwave excitation). This means for a typical treatment area of the charge neutralisation source, $1.2 \cdot 10^{14}$ electrons impinge an area of 1mm² per second.
Balancing out the values for the LEG41, its target current corresponds to $6 \cdot 10^{12}$ electrons per second with a beam focus of 0.5mm in diameter at a distance of 20mm. Figuring out these geometrical factors, the corresponding treated surface amounts to $2 \cdot 10^{-7} m^2$.
Supposing that the electrons are also not trapped by the surface, the stream through the surface can be calculated as $3 \cdot 10^{13}$ electrons hitting an area of 1mm² per second. Under these assumptions a four times longer treatment time with electrons should lead to the same modification.
These values for the electron gun will later be applied in the modification, measured by the x-ray photoelectron spectroscopy and the atomic force microscopy.

From the determined data, an experiment with correlated values for the modelling of the electron influence can be set up. But next to the modification with electrons, the influence of the particles can be prevented. The idea behind this is to cover the sample with a transparent crystal window for the plasma radiation. For the construction of an appropriate sample holder it has to be taken into account that neither the UV-radiation can be measured with the existing set-up nor can the UV-effect be simulated. Therefore the polymer will be treated simultaneously by the radiation and the plasma. These results can be compared with the separate electron modified polymer. Also a combination of UV and electron treatment can be arranged.

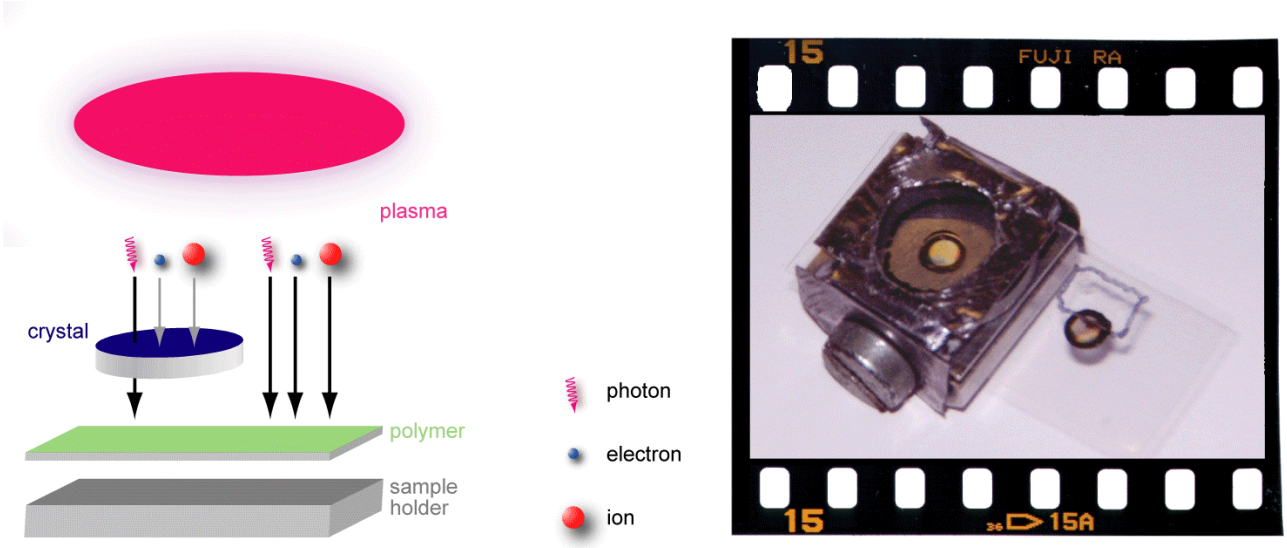

Figure 45: schematic set-up and photo of the constructed sample holder

With the sample holder shown above it is possible to compare the pure plasma treatment with the UV-light modification in one action at the same time under the same conditions. Even when the direct modification of the particles (electrons, ions) is prevented for the covered area of the polymer surface, spacers allow them to penetrate sideways to the radical sites below the window.

For the choice of materials to cover the sample, different kinds of crystals were technically available. The crucial aspect here is the cut-off for the radiation, which is described in the next table for different materials.

Material	Transmission Range [µm]	Photon Energy [eV]
BaF_2	0.152 – 13.200	0.094 – 8.158
CaF_2	0.122 – 10.100	0.123 – 10.164
LiF	0.118 – 7.100	0.175 – 10.508
MgF_2	0.110 – 8.000	0.155 – 11.273
NaF	0.130 – 12.000	0.103 – 9.538
SrF_2	0.120 – 11.200	0.111 – 10.333

Table 8: Transmission range for different materials [Kort00]

Magnesium fluoride was chosen as the crystal in this experiment because of its large transmission to lower wavelength. A more detailed transmission spectra for MgF_2 is shown in figure 46.

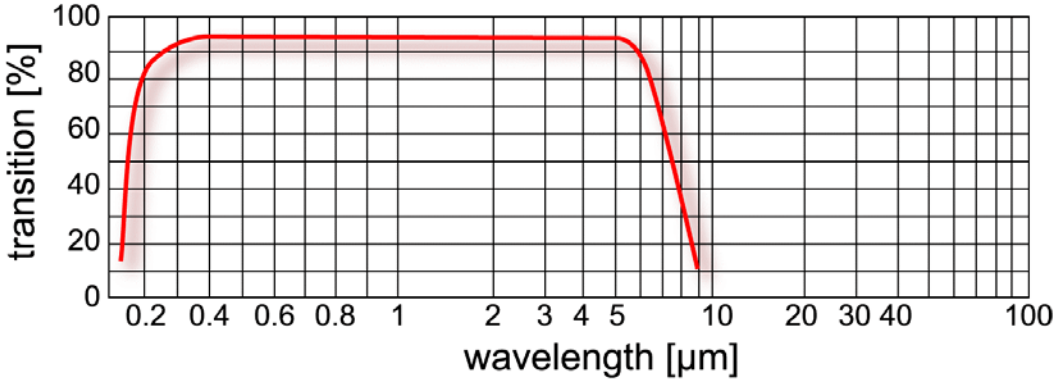

Figure 46: transmission of magnesium fluoride with a thickness of 10mm [www03]

With this transmission range a lot of photochemical reactions are possible and a modification can be expected. The surface reactions are also dependant on the plasma process gas. While here mainly argon is used, other process gases are known to modify and incorporate the polymeric material. Features of the polymer surfaces therefore can be selectively changed under these conditions. Different surface modifications through

plasma influence are collected in the *appendix – surface modifications for different process gases*.

These reactive sites will form new chemical groups after the treatment when they come into contact with air or other substances. All these changes in chemical composition will later be traced by photoelectron spectroscopy.

The handling of the modified samples can be accomplished in two different ways:

- in situ transfer in an activated condition of the modified polymers or
- controlled reaction of the activated sites with chemicals, leading to inert modified surfaces.

Depending on this handling, the obtained data of the modified material varies. The first approach shows information about existing atomic sites of the polymer. This is especially interesting for analysis methods, which can determine radical sites. The information obtained by a XPS analysis is smaller because differences between a radical and an atom in its ground state cannot be figured out. *In-situ* measurements after plasma treatment have been performed e.g. by MÄHL [Mähl96] [MNSB98].

On the other hand, a controlled contamination of the modified sample will help to study the basic processes after an activation of a polymer surface by a plasma, electrons or photons. This includes ventilating the sample with air after different modifications as well as the previously mentioned labelling techniques with miscellaneous chemicals. These kinds of experiments will be presented in the following chapter.

4. Results and Discussion

In this chapter XPS and AFM measurements will be presented. The photoelectron spectra will show the basic composition of the polymer surface and the chemical shifts will illustrate the effects of the different treatments. For a further understanding of the modification processes chemically labelled sites will be included in the discussion.

For XPS measurements the hydrocarbon (CH_x) – line will be the basic adjustment for identifying the chemical groups by chemical shifts. Different carbon groups have previously been examined by BEAMSON and BRIGGS [BeBr92] for various classes of polymers. Together with the work of other authors (adapted from their results) these binding energies were used as a reference for the photoelectron measurements.

When there is only a small shift in the binding energy between two groups, it is sometimes hard to distinguish between chemical groups. As long as the modified polymer is unknown in its composition, these groups cannot be identified anyway.

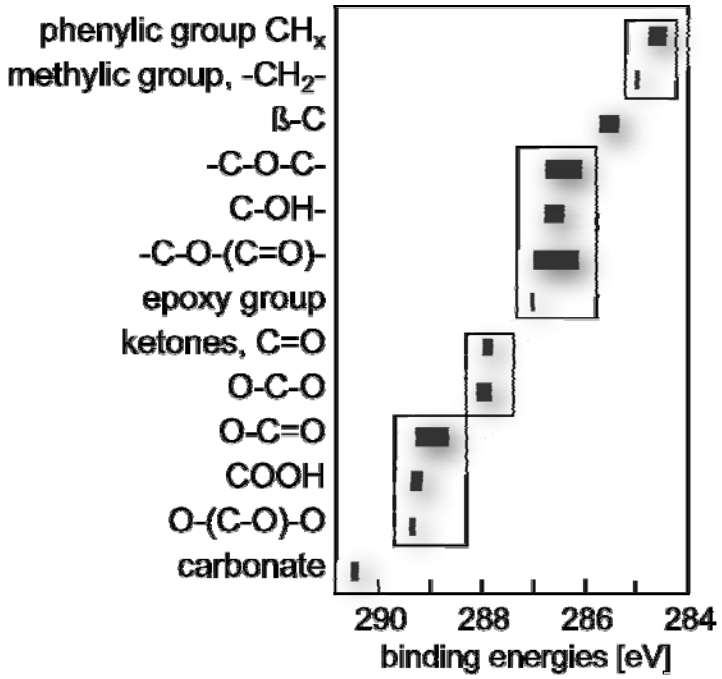

Figure 47: binding energies of different carbon groups - those who are surrounded by a box cannot be distinguished [BeBr92]

To overcome this problem, either the resolution of the spectrometer must be enhanced or the interesting groups must be labelled in a chemical reaction. The first approach requires technical innovation and expenditure, which is not available at the present time. In the future one can think about better analysers, but the half width of the x-ray radiation is still

optimal with the laboratory facility and its monochromator. Other light sources such as a synchrotron can provide radiation with smaller half widths.

Therefore the interesting chemical groups will be modified in this work. In principal, the best results can be achieved if the reaction product consists of atoms other than those from the untreated material. It also has to be considered that the chemical reaction is sensitive to only one chemical surrounding and does not react with a multitude of groups or atoms. Double bonds can be labelled with bromine, which opens the bond and is attached to it.

The change in behaviour of a polymer material can be attributed to chemical modification (the formation of radicals, incorporation of new chemical species, removing of contaminants) or physical changes (electrical and thermal conductivity, surface charging), but also the topography of a modified polymer or other mechanical properties (roughness, elasticity) influences the properties of these materials and therefore these aspects were investigated with an AFM.

4.1 Characterisation of basic modifications

First of all the basic materials must be analysed in order to testify its purity. And it is likewise necessary to compare these pure materials with the resulting spectra or topographies after the treatments. These differences represent a kind of “macroscopic” aspect of the modification.

In this experiments Polyethylene and Polypropylene are used, the analysis with XPS seems adequate. Both polymers are available in form of foils and as granular material. The Polyethylene (Standard Reference Material 1482, linear PE, Mw 13,600) and the Polypropylene (Goodfellow, isotactical PP, LS 139293 N L, PP 306300/2) were dissolved in toluol and then spin-coated on a silicon wafer or on mica. The foils of the polymers were products of a local company without plasticizers and an oxygen concentration at the surface below the detection level (about 0.1 at.%). More about the polymer structures and fabrication can be found in the *appendix – polymers*.

4.1.1 Untreated Polyethylene and Polypropylene

The basic modifications will be studied with the simplest polymer available: Polyethylene (PE). Below also measurements with Polypropylene (PP) will be presented. Other polymers have been also investigated but did not lead to any further information for the basic modification processes than those displayed here.

In order to detect the chemical changes for the different treatments, highly resolved x-ray photoelectron spectra of the unmodified PE were obtained.

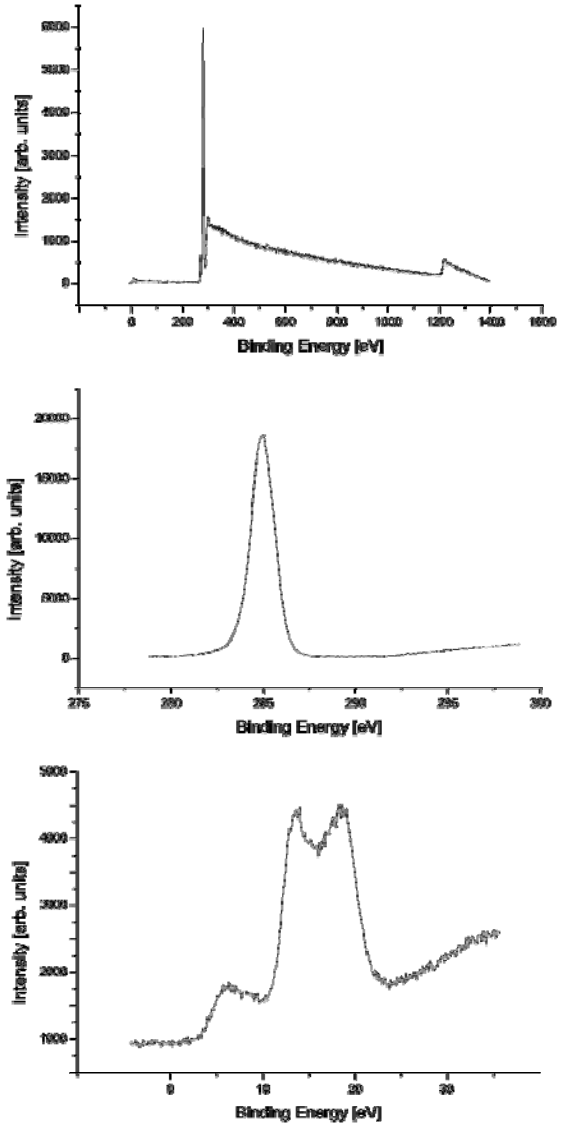

Figure 48 : survey and highly resolved x-ray photoelectron spectra of unmodified Polyethylene foil

From the top to the bottom one can figure out a survey spectrum, the carbon 1s region and valence band area. Hydrogen has a very small photoelectron cross section and therefore it cannot be traced with laboratory equipment. As expected for untreated PE, the survey spectrum only shows the signal from carbon atoms. The shapes can be assigned to the AUGER $KL_{23}L_{23}$ signal at a binding energy of 1223eV, the carbon 1s line at 285eV and the 2s and 2p structures at around 6.5eV, 13.5eV and 19eV. The C1s spectrum displays a single line for the CH_x-groups. When additionally double bonds occur in the polymer structure, a region around a binding energy of 292eV will show a signal according to $\pi \rightarrow \pi^*$ transitions. As these transitions do not occur in the measurement, one can

conclude the exclusion of this type of bond. The valence band region with the 2s and 2p structures is nicely resolved in this measurement and shows the typical shape for this polymer [BeBr92].
As this material shows no impurities, every change in composition later must result from the treatments. Similar spectra were obtained for spin coated polymer films.

A glance at the structural aspects shows a typical structure for polymer foils. The untreated foil shows some coarse grains, some flat areas and regions which look like bubbles (left picture of figure 49). All graphs by the atomic force microscope were analysed by WSxM software [www02]. The height differences after removing the tilt are up to 140nm. The height varies in a GAUSSIAN shaped distribution (on the right top of next figure) while the diameter of the grain size varies between 0.15 and 0.38µm (on the right bottom of the figure).

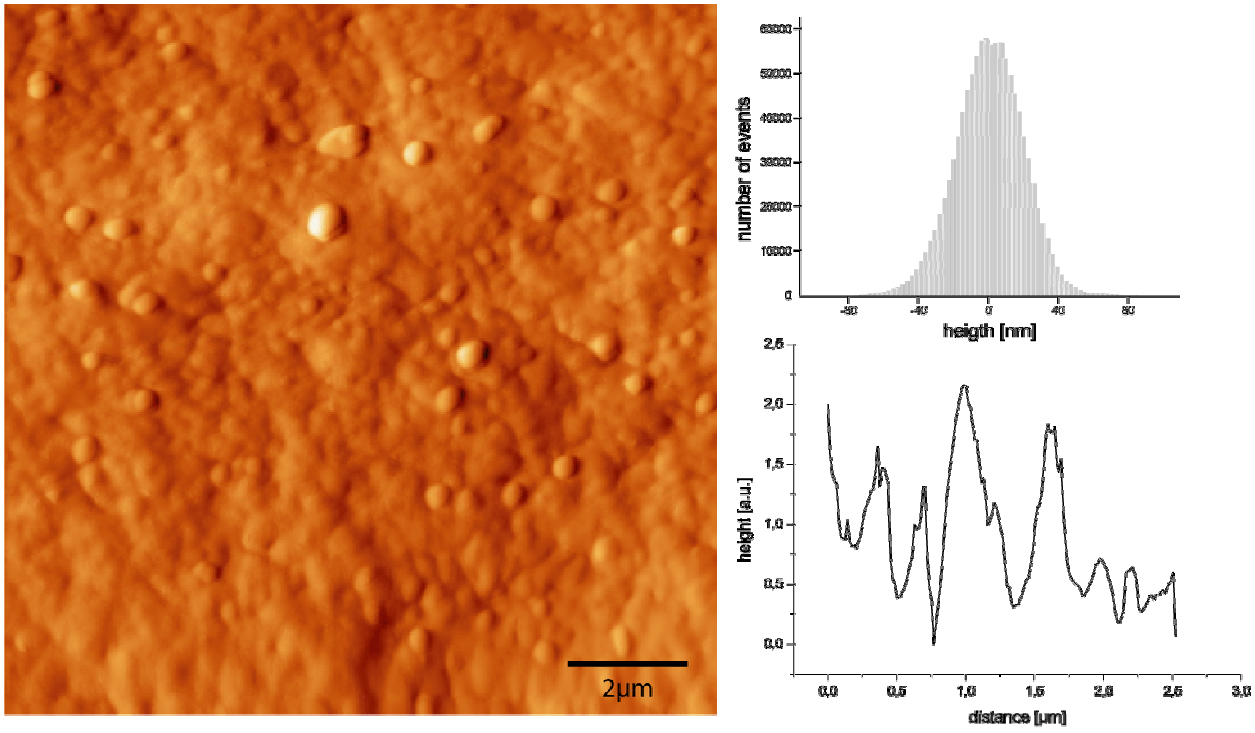

Figure 49 : unmodified PE foil viewed by atomic force microscopy

The image of the untreated PE foil looks similar to other published scanning force images of unmodified Polyethylene like e.g. [ShMö95].

The structure of Polypropylene shows a higher branching of its chemical constitution (see *appendix - polymers*) compared with the PE. This material will be used for the oxygen plasma treatment and for some advanced modification in chapter 4.2.
The XPS survey of the unmodified PP shows the expected carbon 1s line aligned with a binding energy of 285eV and a very small but visible oxygen 1s line.

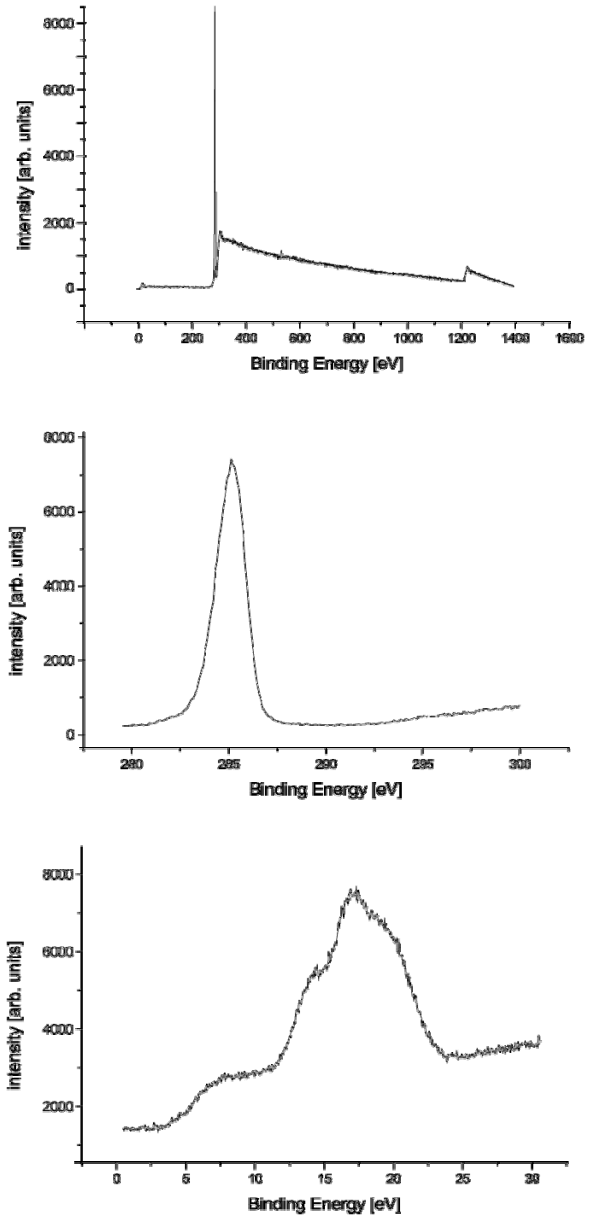

Figure 50: survey and highly resolved x-ray photoelectron spectra of unmodified Polypropylene foil

As the oxygen signal is less than 0.1at.% and this low-level oxidation does not influence the shape of the carbon 1s signal it will be excluded for the following analysis. The valence band area looks similar to the measurements of BEAMSON and BRIGGS [BeBr92] with the carbon 2s region between 5 and 12eV and three lines with binding energies of 13.5, 16.5 and 19.5eV.

The geometrical structure is different from those of PE. Here several furrows can be made out – obviously resulting from the production process. The grooves are irregular in their latitude.

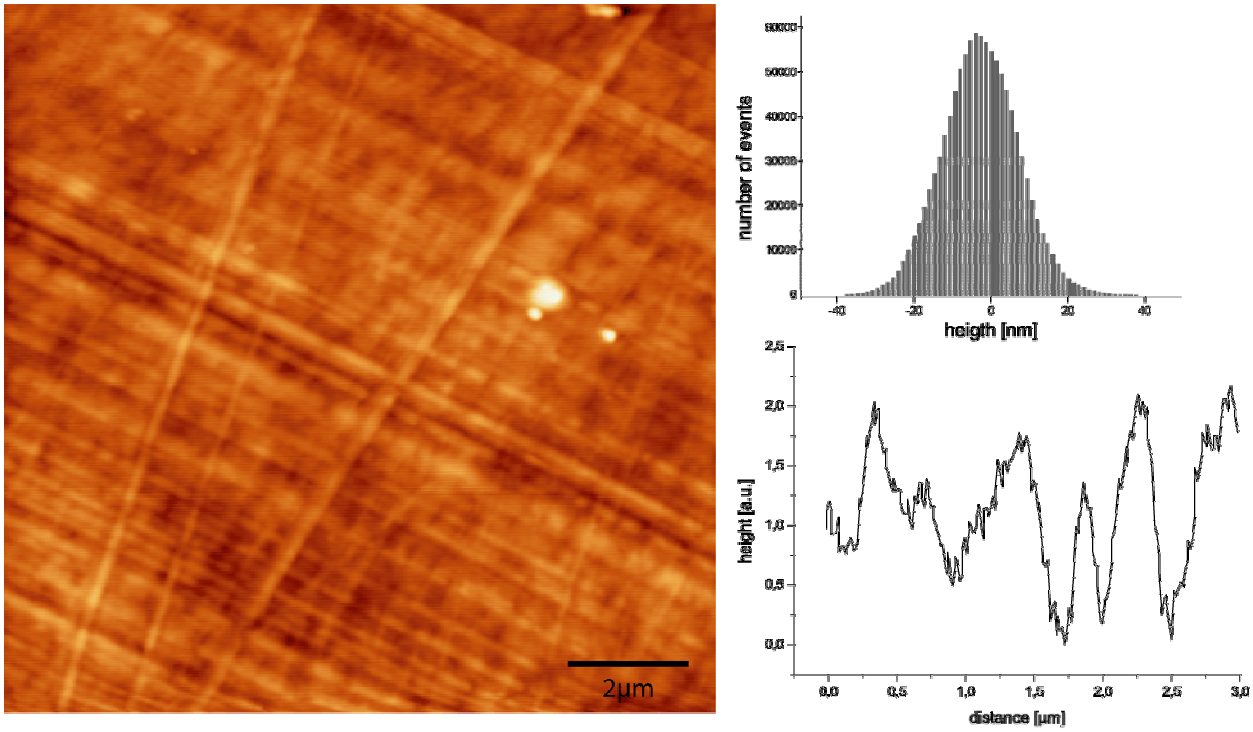

Figure 51: unmodified PP foil viewed by atomic force microscopy

The height differences are up to 80nm and the size of the furrows varies between 0.18 and 0.69µm. There are also smaller splines with sizes less than 50nm.

4.1.2 UV Treatment

The treatment with radiation covers one aspect of a plasma modification. The special features of interaction between UV radiation and polymer materials include deep penetration of several µm into the material and photochemical processes.

The sample was covered with the MgF_2-window on top of the polymer as explained in chapter 3.4, hindering the particle effects, and treated for 60 minutes while next to it the Polyethylene was directly exposed to the plasma influence (these results will be presented in the following). After the treatment, the plasma chamber was flooded with air to allow the passivation of the activated sites of the polymer. As the atmosphere mainly consists of nitrogen and oxygen (other species play only a minor role), the resulting spectra of the

experiment should include some traces of these elements in the form of newly created groups. As the basic material is free from those elements, an occurrence directly confirms these passivation reactions.

The surface reactions are manifold and far more complex than the possible reactions inside an inert gas discharge [Somo94]. These reactions range from the simple reflection on the wall over different kinds of absorption to the formation of bonds with the surface atoms or the etching of the polymer. For the purpose of adsorbing these particles, they can also diffuse along the surface or into the bulk. Furthermore, they can react with already absorbed species or with surface atoms of the solid material in order to form new molecules. Depending on the binding energy of the particles, they may finally desorp back again into the gas phase or stick to the surface by forming a growing film.

Some of the so far enumerated reactions lead to a persistent chemical or structural change of the surface. These effects also depend on a passive or activated surface site and the kinetic energy of the approaching atom or molecule. Raising the kinetic energy of these particles over their thermal ones allows even more reactions to occur, like surface activation, bulk effects like implantation [Öchs97] or damaging or sputtering with several secondary processes (see figure 52).

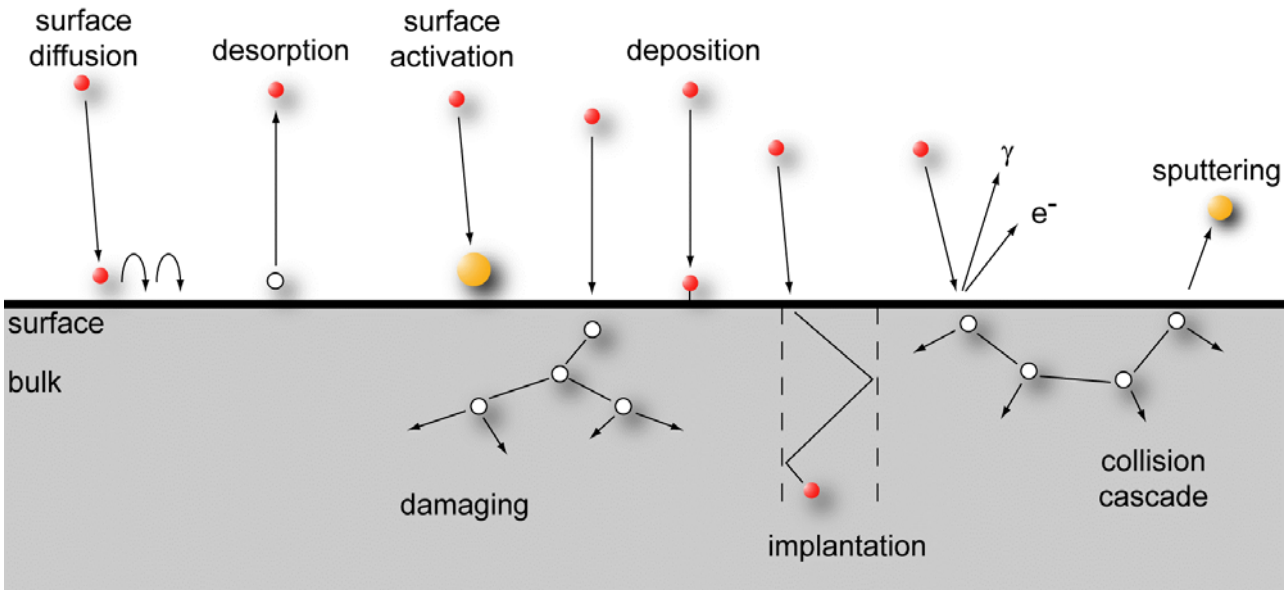

Figure 52: surface reactions and processes enhanced by particle bombardment [Kers01]

Most lasting changes of the polymer surface requires the formation of activated sites or even radical sites. This formation results from the interaction of the polymer with plasma photons or electrons. A free radical is an atom with an odd number of electrons and therefore such radicals are highly reactive. Reactions with radicals contain three stages:

the creation, the change of the electron location and the extinction. In a surface modification, the radicals occur in the main and side chains of the polymer.
If one considers the chemical bond as a pair of electrons, this bond can be broken in two ways:

- both electrons remain on one of the fragments (this leads to ions) A-B $\rightarrow A^+ + B^-$
- the binding electrons distribute on both atoms (this leads to radicals) A-B $\rightarrow A^\bullet + B^\bullet$

The positions for a possible breakage of a bond in Polyethylene are the hydrogen-containing side chains as well as the main chain between two carbon atoms. These are displayed in figure 53. The solid bond symbol points out of the paper towards the reader while the dashed bond symbol points inside the paper. In addition, for Polypropylene the hydrocarbon side chain can break.

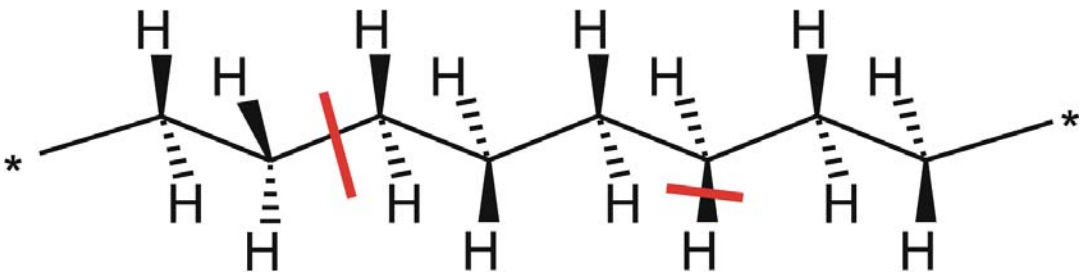

Figure 53: schematic part of a Polyethylene chain – the red lines mark positions for a bondage break resulting in primary radicals (main chain) and secondary radicals (side chain)

While in most cases the bonds are re-established after a breakage, in some cases the chains can be separated from the polymer and are then free to move. Near the surface chains which are especially short will be pumped away or migrate into the discharge and react there. Free groups inside the bulk move more or less quickly through the polymer until they find a suitable reaction partner or reach the surface and leave the polymer. The resulting radical sites at the polymer can be divided into three groups according to the number of rest groups in the vicinity. More information about radicals can be found at [LBP60a] [LBP60b] [SeTa72] while combined reactions like are discussed at [Keud00] [SSKJ00].

The polymer has experienced some of the previously discussed reactions due to the treatment with UV light. As some activated sites should still be present at the polymer surface, they are supposed to interact with the air when coming into contact with it.

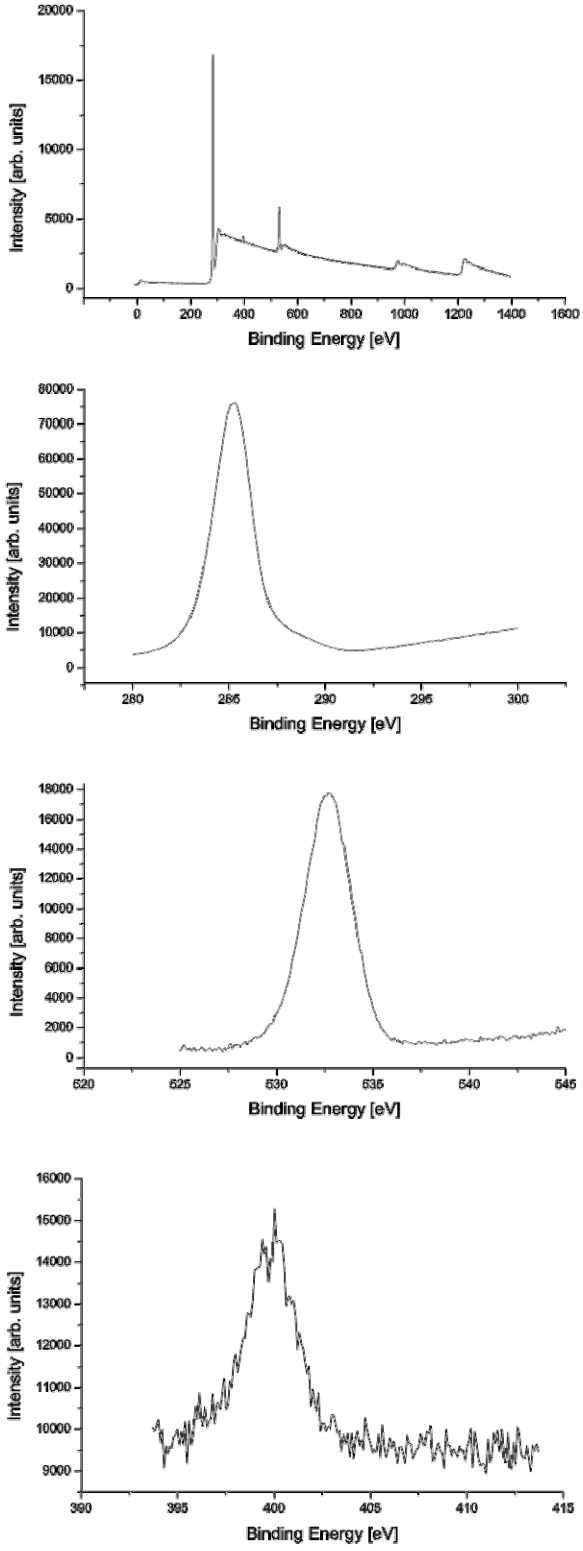

Figure 54: survey and highly resolved x-ray photoelectron spectra of UV modified and with air ventilated Polyethylene foil

As expected for UV treated PE foil, the survey spectrum at the top of figure 54 is extended by signals from oxygen and nitrogen. From the other graphs one can see the high

resolution spectra of carbon 1s, oxygen 1s and nitrogen 1s. The valence band area, which is not displayed in the figure, shows in addition to the carbon 2s and 2p structures, like those of the untreated PE, a small shape around 26eV. This line corresponds to the oxygen 2s signal. The change of the spectrum could be caused by a multitude of reactions, starting from changes in the inner structure of the polymer and leading to various formations of chemical functional molecular groups containing oxygen and nitrogen.

The C1s spectrum displays here not only a single line for the CH_x-groups, but a small tail of photoelectron intensity with higher binding energies. These result from the chemical shift for oxygen containing carbon groups. In the following paragraph we will go into more detail about this feature.

The oxygen 1s signal appears at a binding energy of 532.5eV and shows a relatively broad shape, which possibly contains more than one chemical surrounding. Even the AUGER $KL_{23}L_{23}$ signal of the oxygen can be figured out easily at a binding energy of about 978eV. The less intense KL_1L_{23} and KL_1L_1 lines with binding energies of 999eV and 1013eV vanish within the background noise.

One can consider hydroxyl (in the following abbreviated with CO) and carbonyl (C=O) side chains when allowing a range of 0.3eV around this binding energy as the real source for this signal. As both groups are likely to be formed and the carbon spectra shows a tail to higher binding energies, both kinds of groups will be fitted.

The atomic concentrations are 94.4at.% for the carbon, 5.1at.% for the oxygen and 0.5at.% for the nitrogen. The reason for the higher concentration of oxygen rather than nitrogen after ventilating the treated surface with air could be the higher reactivity of the oxygen according to the electronegativity of this element. Good grounds for this presumption would are comparable diffusion rates of oxygen and nitrogen through the polymer.

Even if the nitrogen concentration is small in comparison to the other element signals, it must be evaluated carefully. First of all its chemical surrounding must be identified. The nitrogen 1s line has a maximum of binding energy at about 399.4eV. Comparing this value with the different nitrogen containing groups displayed in the following graph according to their binding energy[8], this structure can be identified clearly as a nitrile group (C-C≡N), but a fraction of oxime (C=NOH) could not be excluded.

[8] Later in chapter 4.2.2 the sources of these values as well as additional aspects will be given.

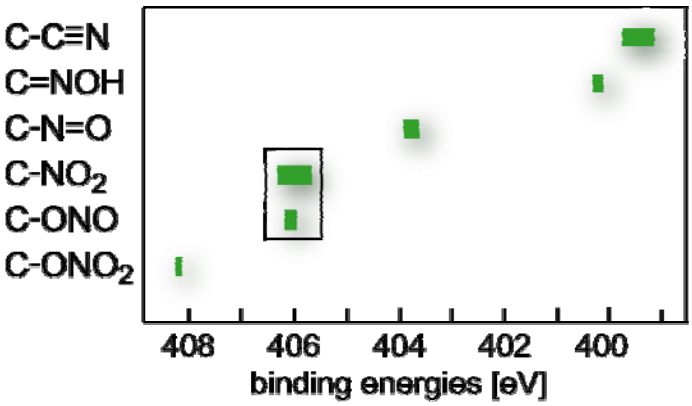

Figure 55 : different nitrogen species according to their binding energies

Due to the intensity of the nitrogen signal being very small, it will not be taken into consideration when fitting different chemical groups to the carbon signal. This fitting was done with Origin and a program called SimPeak, which was developed in our group. For each of the expected groups in the chemical structure a separate peak will be estimated. Next to the background subtraction the full width at half maximum was set for all fits equally while the intensity and the binding energy could be adopted arbitrarily by the program.

According to the considerations made so far (especially as a result of the small shift in binding energy) the carbon 1s signal will be fitted in the following way with three lines corresponding to the hydrocarbons (CH_x), the hydroxyl (CO) and the carbonyl (C=O) groups. Although carboxyl (CO_2) groups might occur after the treatment, their intensity is too small to be traced in the measurements and they get lost in the noise signal. After several theoretical considerations and the results from MÄHL, this fitting procedure seems to be reasonable [MÄHL97].

As the geometry with the angle of incidence for the radiation and the emission angle for the electrons is fixed by the set-up, different information depths can be obtained by tilting the sample holder (see chapter 2.1.2 – *experimental conditions of XPS*). The next figure shows the data of high resolution XPS under several emission angles: at the top a steep angle with 75°, in the middle the normal emission (45°) and below a flat angle with 15°.

Each graph consists of a plot of the measurements (black) and the fit corresponding to the carbon chemical surrounding of CH_x(blue), CO (red) and C=O groups (green).

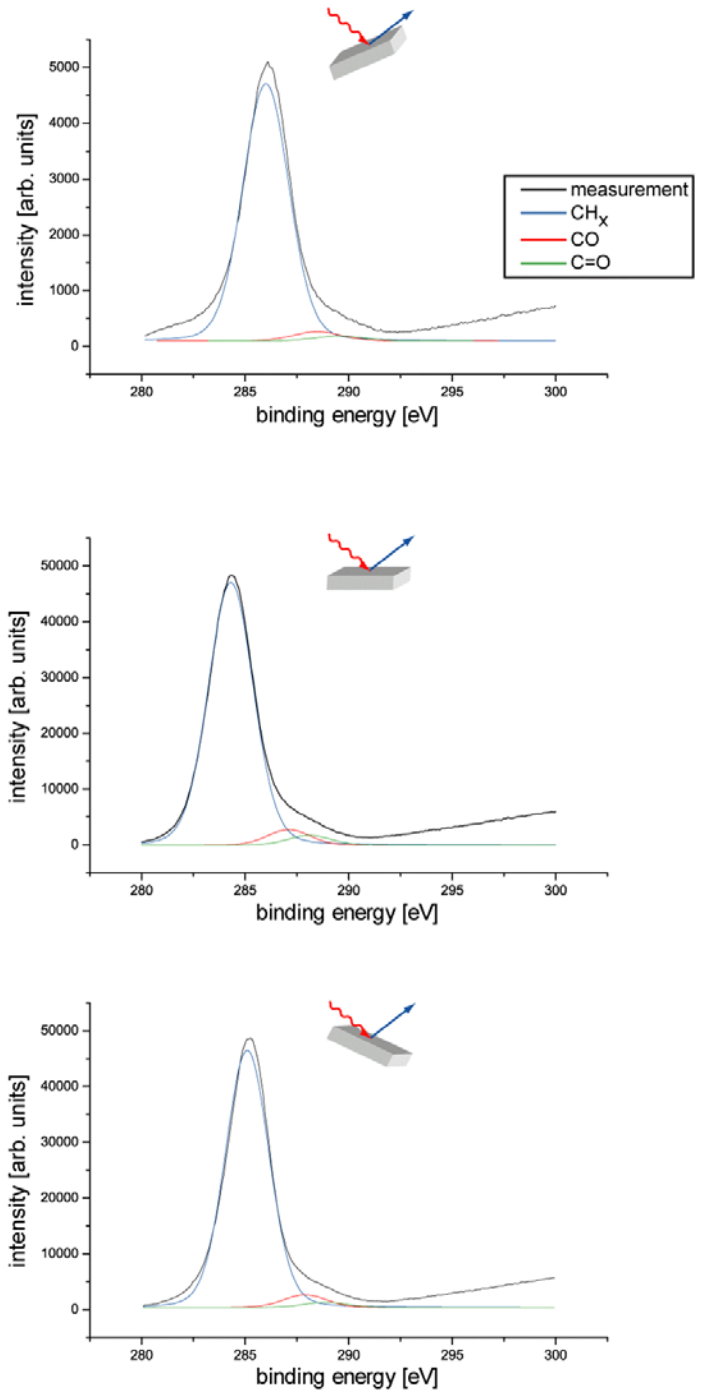

Figure 56 : angle resolved XPS carbon 1s-line of UV modified and with air ventilated Polyethylene foil

There is only a small change in the concentration of the three investigated carbon containing groups. The polymer sample therefore seems to be uniformly modified referred to the analysis depth of the XPS measurements (see figure 1). The next graph will compare these results.

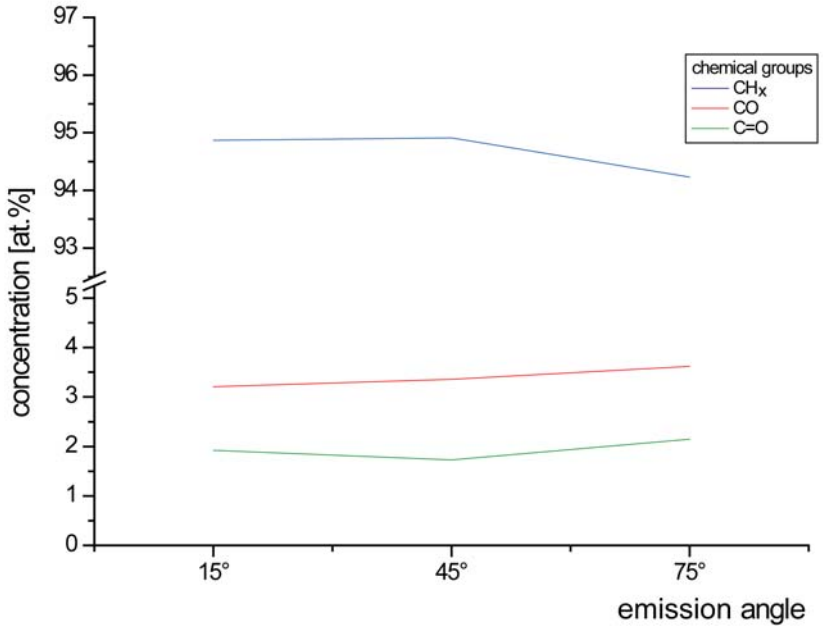

Figure 57: angle resolved XPS of UV modified PE

As the emission angles contain a measure for the depth of the analysed layer, a higher value is connected to a thinner layer. From the figure 57 it can be concluded that the treatment with radiation does not vary very much in the depth distribution of the newly created chemical groups either in quantity or quality. The concentration of the CO and C=O surroundings rise only slightly for higher angles, so that throughout the analysis depth of XPS the sample is modified. As there was no angular dependence for other treatment times, this effect can be attributed to the photolysis effects.

Some further experimental aspects must also be considered. First one can expect some absorption of the UV light by the crystal window, which leads to a smaller modification referred to the direct plasma treatment. As the absorption of the radiation is dependent on the frequencies, this aspect has to be investigated in more detail later.

Secondly, measurements with different treatment durations have been obtained. The results can be summarised by observing that the ratio of oxygen and nitrogen concentrations stay constant with time while the overall concentration of these groups rises (up to 8% oxygen and about 2% nitrogen after 120minutes of treatment time).

Interesting further aspects for UV modifications as well as several references can be found with CHAN et al. [CKH96].

Next some structural changes will be observed by AFM measurements. The grain size varies between 0.23 and 0.48µm. Compared with the untreated material, the foil reveals far smoother grain sizes. This observation is strengthened by narrow height distribution of the histogram.

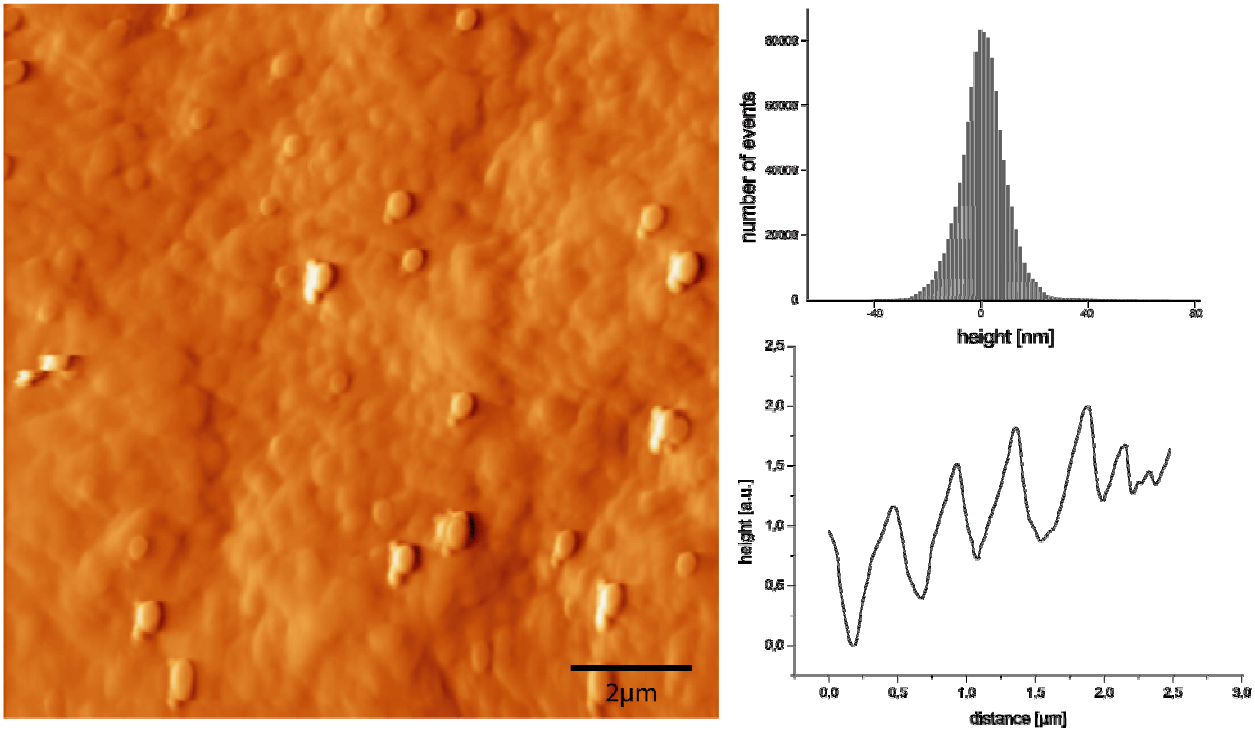

Figure 58 : UV modified PE foil viewed by atomic force microscopy

Further aspects of the modification processes will become clearer by obtaining XPS and AFM measurements for the plasma and electron modification. Especially if the polymer signal shows an angular dependence after plasma treatment, at least a part of it must be caused by particles.

4.1.3 Plasma Treatment

For the plasma treatment mainly argon was used as the process gas. The conditions of the discharge correspond to the optimised values mentioned in the previous chapter. After a detailed discussion of the modifications in an argon plasma, effects with other process gases on a Polyethylene surface will be briefly shown. Examining the survey spectra after 60 minutes of argon plasma treatment and ventilation with air immediately afterwards, the elements - carbon, oxygen and nitrogen - are found with decreasing concentrations at the polymer surface. For these elements high resolution XPS measurements were obtained.

Their formation can be explained by similar arguments to those for the UV modification. Next to the composition of the atmosphere, impurities of the process gas or on the walls of the plasma chamber can be incorporated in chemical groups. These effects have been reported after *in situ* experiments [Mähl97].

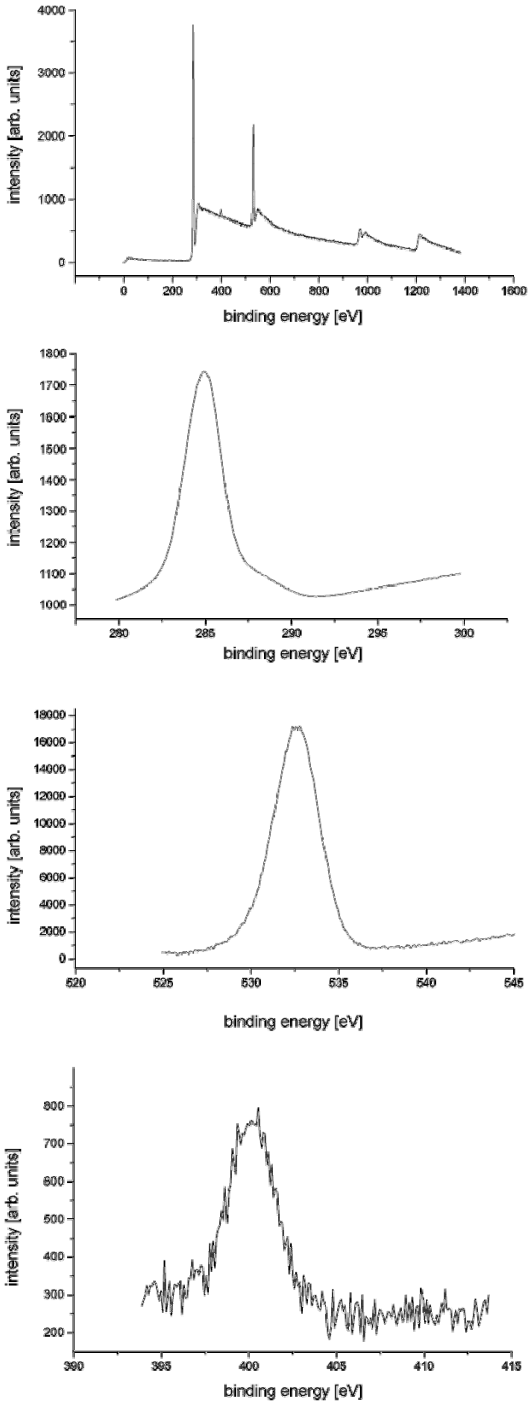

Figure 59 : survey and highly resolved x-ray photoelectron spectra of argon plasma modified and with air ventilated Polyethylene foil

The carbon 1s line in figure 59 shows, next to the main area for hydrocarbon surrounding, a portion for different oxygen and nitrogen containing groups.
Also here the oxygen 1s line directly shows no splitting, but an unsymmetrical shape and a broadening of the half width the same as after radiation. The overall concentration of the oxygen is higher than after the same treatment time with the UV light, so it definitely leads to a different modification. The difference must result from absorption of light in the crystal window or it can be attributed to the particle effects, which are missing in the previously presented results.
Also fitting the spectra with two lines here around the binding energy of 532.6eV gives a more intense peak with 77.6% of the signal intensity at a typical position for the oxygen of a hydroxyl group with 533.3eV binding energy and a less intense one corresponding to a carbonyl group at a binding energy of 532.2eV with 22.4% of the signal.
The nitrogen 1s line with a maximum at the binding energy of 400.3eV corresponds to oxime groups, but as for the shape of the oxygen line, some ratio of nitrile groups can possibly hide in the spectrum.
To compare the argon plasma treatment with the UV (and the later electron) modifications for different layer depths, the carbon main line must also be investigated from different angles which has been done in figure 60.

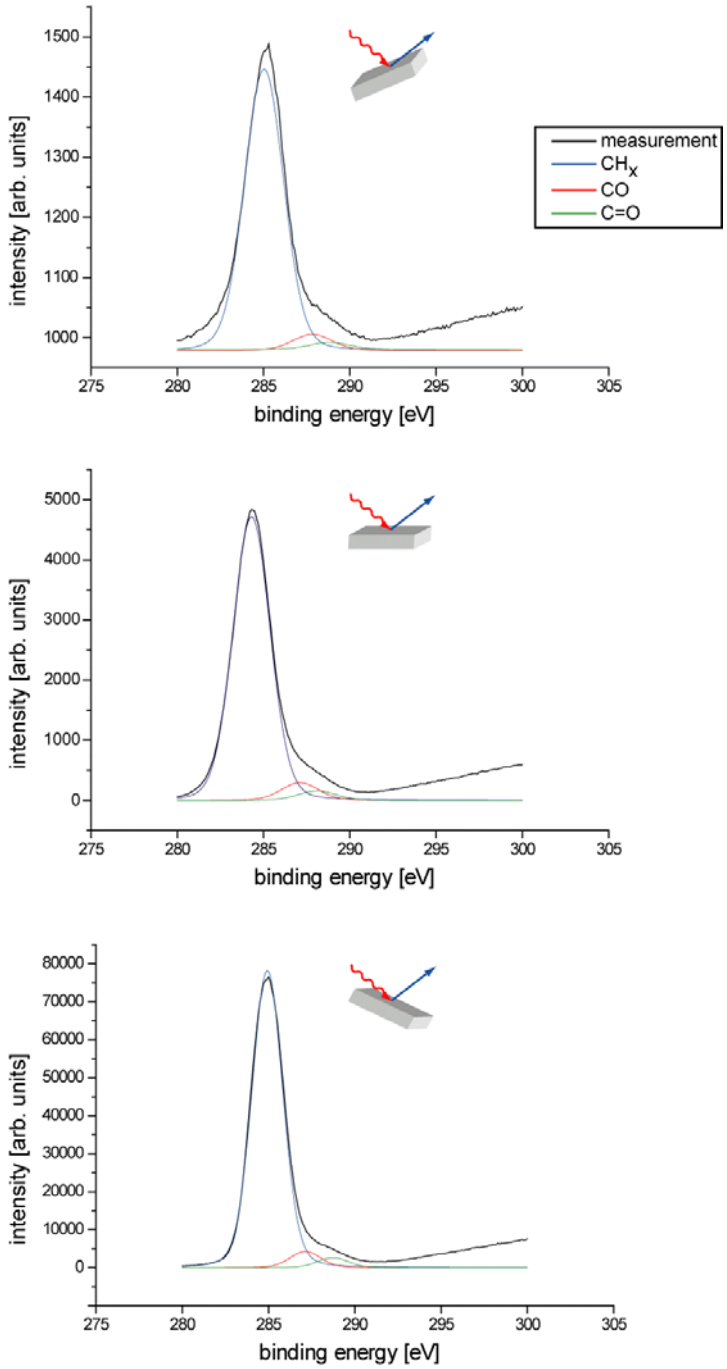

Figure 60: highly resolved x-ray photoelectron carbon 1s-spectra of argon plasma modified and with air ventilated Polyethylene foil under different angles (from top to bottom 75°, 45° and 15°)

The evaluated carbon groups show different distributions for the varying angles of electron emission. When these values are plotted against the angle of emergence, it looks like as displayed in the next graph.

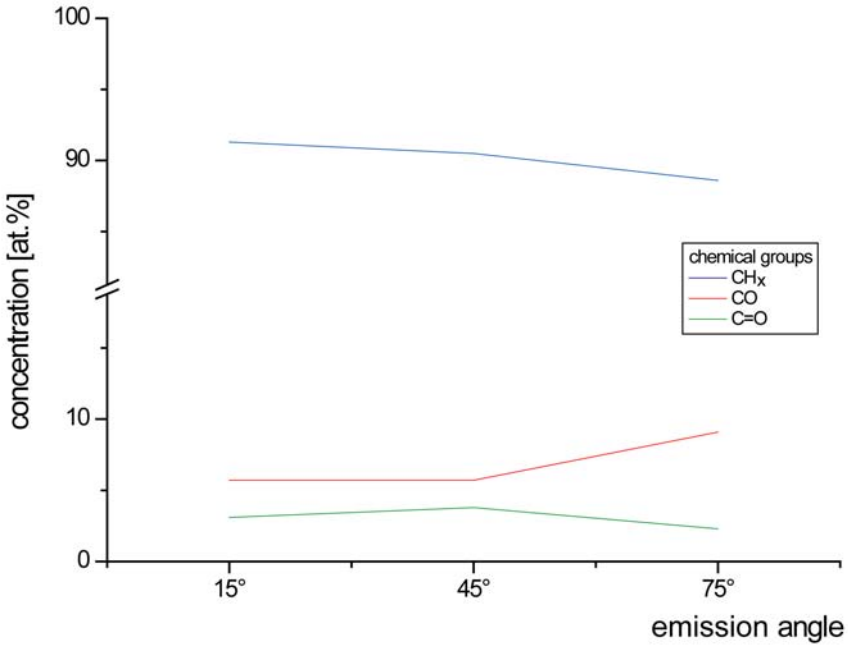

Figure 61 : different carbon groups after plasma treatment according to the incidence angle

The evaluation of figure 61 shows a light angle dependence for the total oxygen signal and the hydroxyl oxygen signal, while the concentration of carbonyl groups is reduced a bit. These values compared with the oxygen 1s line are in good agreement because they give for the more intense CO groups a concentration of 79.8% of the total additional groups while the less intense peak from the C=O groups give 20.2% of it.

Also the different newly attached elements can be listed according to the angle of analysis. For the UV-treatment the nitrogen concentration was too small to do this in an accurate way. The atomic concentration in relation to the angle of emergence shows the following distribution. Also more angles will be displayed to view the permeation of the air compounds.

Angle of analysis	[C1s]	[O1s]	[N1s]
15° (thick layer)	85.19	12.24	2.57
30°	81.64	15.16	3.20
45°	80.84	15.69	3.47
60°	79.74	16.29	3.97
75° (thin layer)	79.79	16.14	4.07

Table 9: different elemental distribution

One can conclude that with thinner layers at the surface the concentration of carbon decreases while those for oxygen and nitrogen rise while in deeper areas of the sample the concentration of these newly created groups diminishes. The percentage rise of the oxygen and nitrogen concentration seems to be identical so two points can be concluded:

- the main effect lies on the after treatment contamination and not on impurities of the process gas and
- none of them shows a preferred permeability through the first layers of the polymer (otherwise an agglomeration of one element should be visible).

The structural analysis displayed in figure 62 reveals a different topography from that of the untreated material as well as from that of the UV modified polymer.

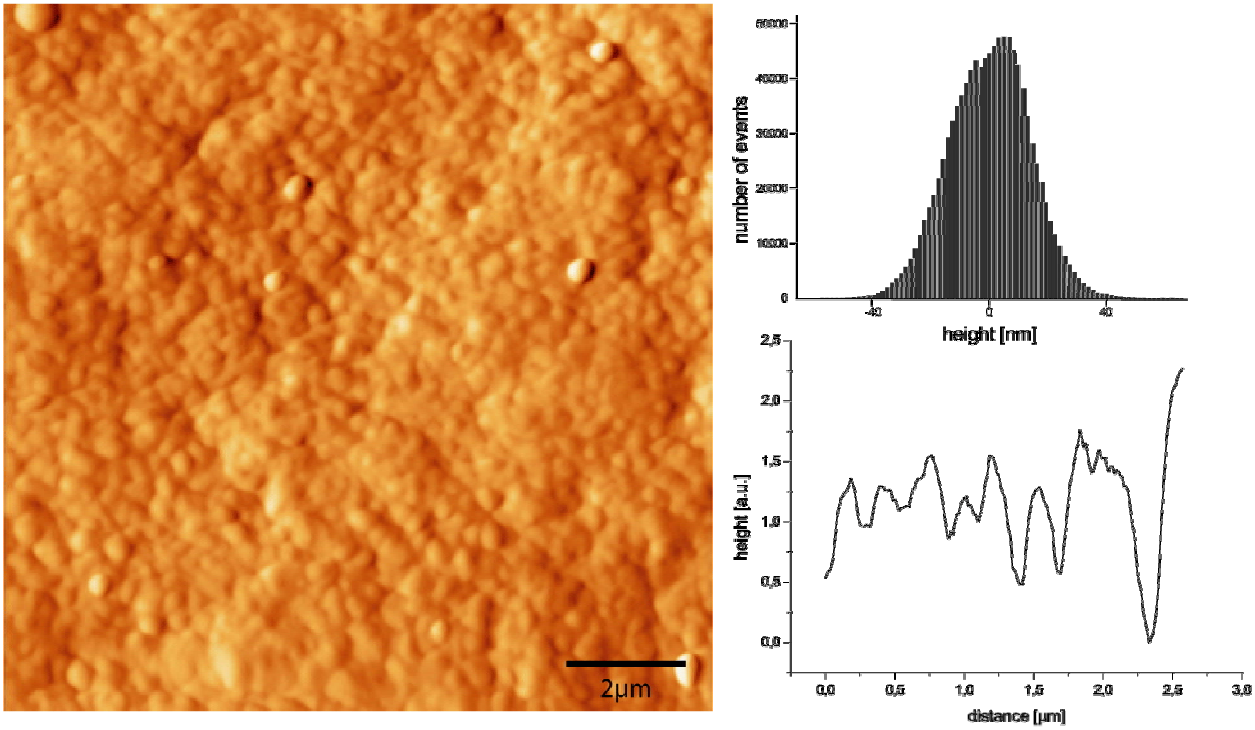

Figure 62 : plasma modified PE foil viewed by atomic force microscopy

Here small grains are visible in a smoothed surrounding with sizes between 0.22 and 0.41µm. It seems in a way that the plasma treatment is a combination of the smoothing UV effects and a kind of keying. In the histogram these effects are both visible by the broadened distribution towards the UV treatment, but still narrower than the untreated material.

Oxygen Plasma Treatment

Next the XPS spectra for two different process gases for the plasma treatment will be presented – oxygen and nitrogen. The plasma conditions are the same as above and the sample is also ventilated with air directly after the treatment, but Polypropylene was used as material for the oxygen plasma treatment and the modification time was reduced to 10 seconds to spare on one hand the pumping system from aggressive oxygen radicals. On the other hand oxygen will functionalise the surface so that only seconds of treatment are sufficient for a clear modification of the surface.

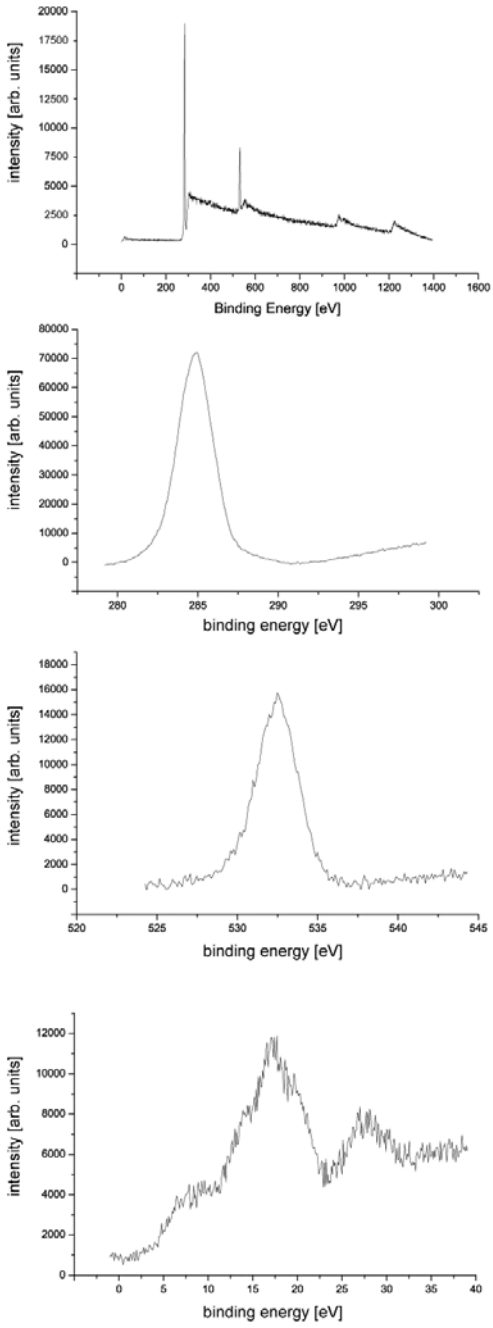

Figure 63: survey and highly resolved x-ray photoelectron spectra of oxygen plasma modified and with air ventilated Polypropylene foil

First a survey spectrum was obtained (see figure 63 above). As only carbon and oxygen lines appear without any nitrogen groups, it seems that species in the oxygen plasma react within a short time with the activated surface sites. The less intense oxygen line compared with the argon plasma treatment can be attributed to the short treatment time. The reason for the absence of the nitrogen must be found in the reaction times of the different occurring processes. So the created radicals on the polymer are long since passivated when the nitrogen from the air appears. The question whether all reactive sites are quenched from the oxygen discharge or if the reaction occurs with the oxygen in the residual gas cannot be answered in this experiment. Such an investigation would be difficult for some aspects, especially because of the oxygen residual gas pressure. Another possibility could be a forced breakdown of the discharge, but this cannot be realised because the plasma particles are too close to the sample.

The high resolution spectra of carbon shows the typical tail towards higher binding energies, caused by the chemical shift through oxygen. Also the oxygen 1s line appears with a typical binding energy of 532.9eV which include signal intensity for single and double bonds with the carbon.

Additionally the valence band area is displayed, but comparing it with other valence band structures is difficult because these are listed in references like [BeBr92] as pure materials while the modified polymer consists of several groups, each of them adding a part to the overall signal. The structure reminds of the smeared out shape of the reference material (see figure 50 for a comparison) with the carbon 2s and 2p structures and an additional signal at a binding energy of around 26eV resulting from the oxygen 2s peak.

Nitrogen Plasma Treatment

Using nitrogen (purity>99.999vol.%, Messer Griesheim) itself as a process gas leads to the following spectra. The conditions of the discharge process are the same as in the previous plasma experiment, except the treatment time was set to 10 minutes.

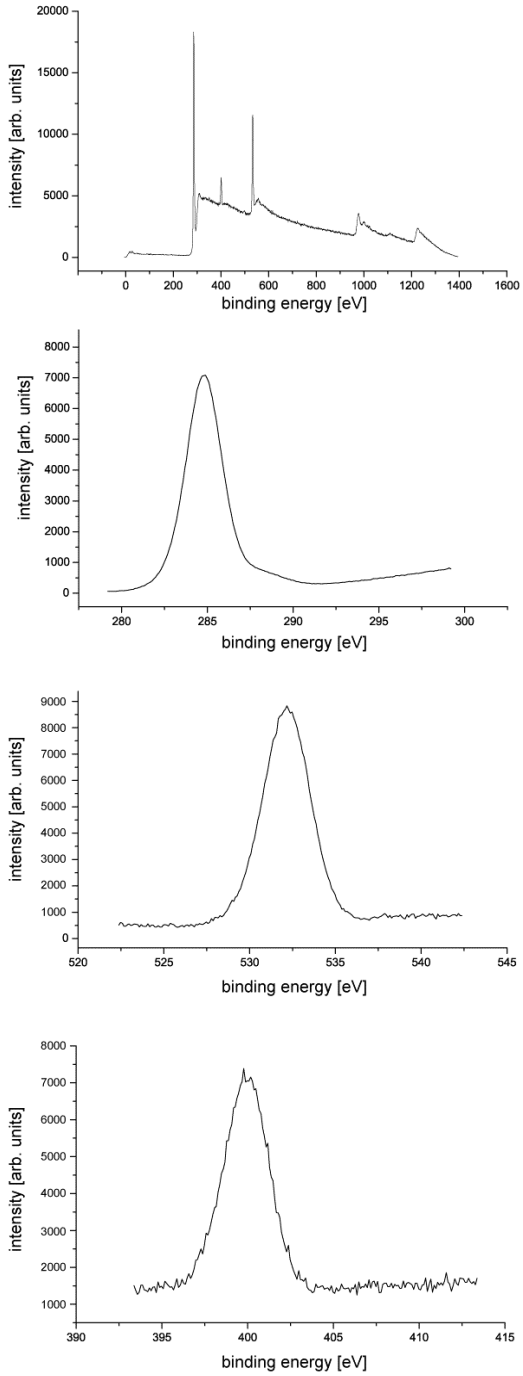

Figure 64: survey and highly resolved x-ray photoelectron spectra of nitrogen plasma modified and with air ventilated Polyethylene foil

Here the highest nitrogen concentrations for all experiments can be found, and also a rather high concentration of oxygen. It seems likely that the nitrogen is placed at the surface near regions while ventilating with air afterwards leads to passivation reactions inside the polymer, in which nitrogen and oxygen are involved. Also here its reactivity leads to several oxygen containing molecular groups. Conclusive results cannot be presented because for this treatment no angular dependence was obtained.

The valence band area will be presented and analysed in chapter 4.1.5. together with the one after electron treatment.

4.1.4 Electron Treatment

The electron treatment is performed with a LEG41 electron gun under UHV conditions. The polymer is placed at a distance of about 50mm away from the device and was treated for 10 minutes with 12eV electrons at a current of 3µA. Immediately after the treatment, the sample was ventilated with air. The next figure plots the recorded x-ray photoelectron measurements.

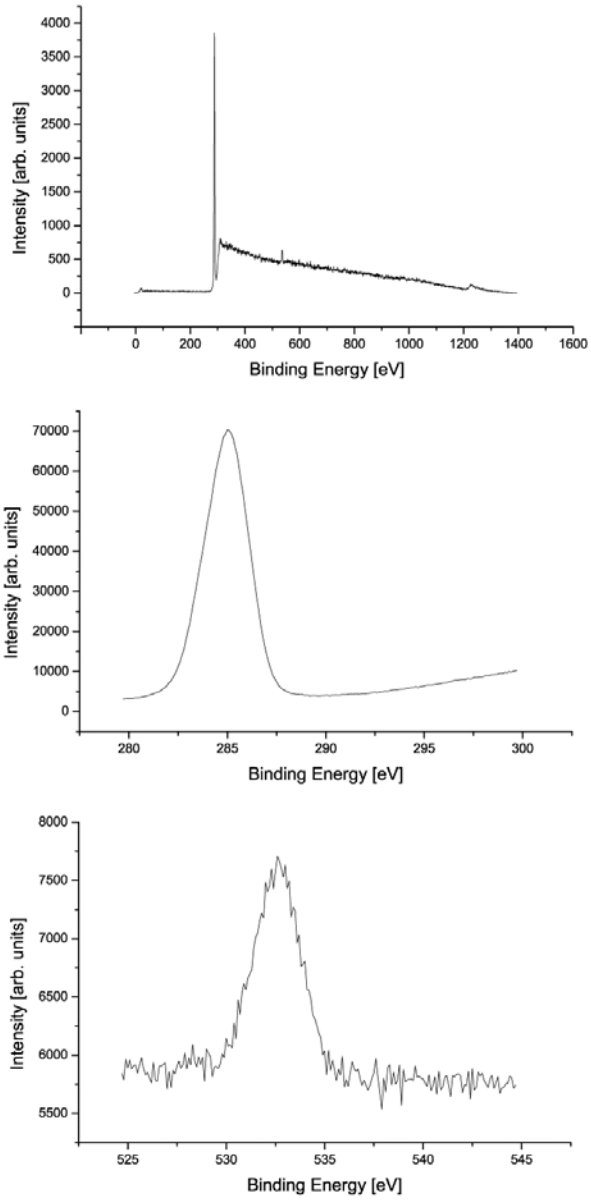

Figure 65: survey and highly resolved x-ray photoelectron spectra of electron modified and with air ventilated Polyethylene foil

Even the electron treatment leads to a small change in the chemical composition of the surface compared with the untreated material. Next to the carbon 1s line a small oxygen 1s line appears, which again can be caused by a multitude of possible reactions.
To examine the change in more detail, first the new composition of the modified material is observed. The concentration of carbon falls from 100at.% of the basic material to a concentration of 99.28at.% carbon and 0.72at.% oxygen after a treatment time of 600 seconds under the conditions described previously in chapter 3.4.
The oxygen 2s line can only be estimated as a bending of the plotted measurements at the binding energy of about 27eV due to the poor concentration of oxygen. The same is valid for the Auger KVV line. As the measurements for the previous modifications show a higher ratio of oxygen concentration towards nitrogen containing groups, it is not surprising that the activated surface reacts mainly with oxygen and therefore no nitrogen signal is observable.
Regarding the carbon, one can again try to fit three chemical surroundings for this carbon line. The predominant one results from the hydrocarbons while the atomic concentrations of the CO and C=O groups with 0.32at.% and 0.40at.% are poor and almost uniform in their values.
To be even more precise when referring to the surface sensitivity, again the carbon 1s line is analysed both under a flat and a steep angle towards the electron analyser, so a relatively thin layer respectively a thick layer of the material is investigated. Two high resolution spectra for the carbon 1s line under 15° and 75° are shown in the next figure.

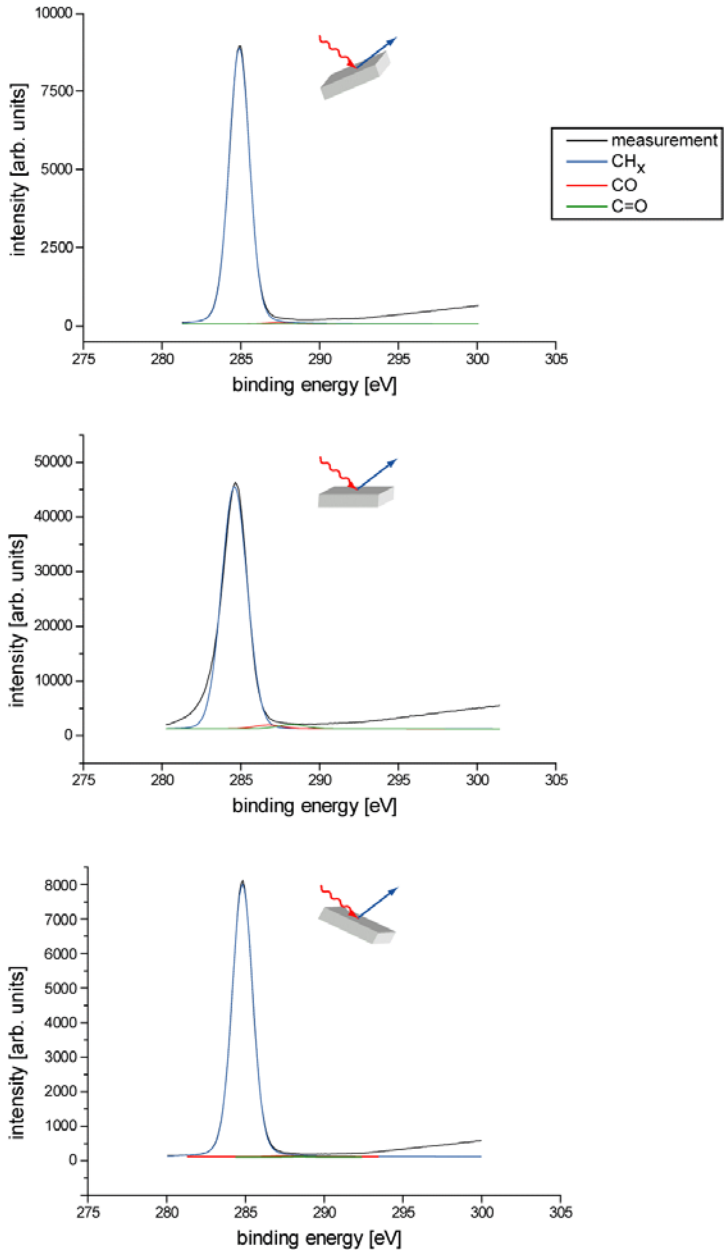

Figure 66: angle resolved XPS carbon 1s-line of electron modified and with air ventilated Polyethylene foil

While the measurements for electron treatment only reveal a small amount of oxygen (about 1% at maximum), nevertheless they are evaluated and displayed in figure 67 for the different chemical groups. Anyhow, they should only be seen as an indication of angle dependent incorporation of oxygen containing groups.

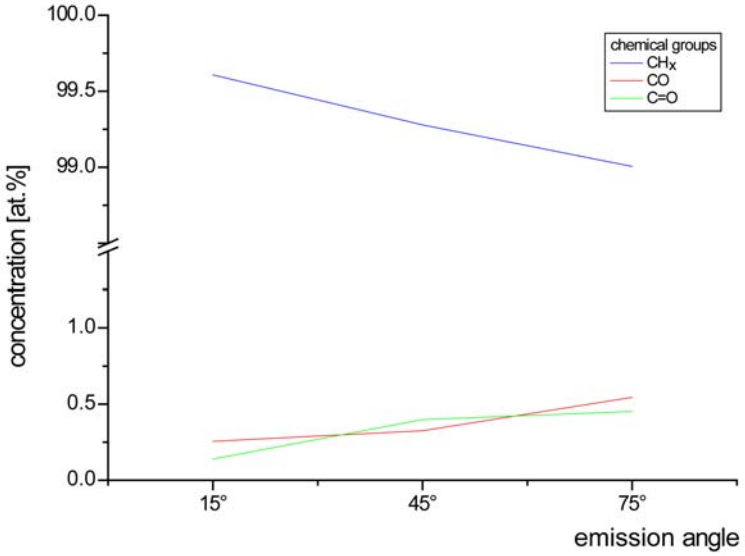

Figure 67 : angle distribution of different carbon groups after electron modification

One can see that chemical groups are created near the surface region of the polymer sample because the relative concentration of oxygen for the thin layer is 2.5 times larger than for the thick layer. The angle resolved measurements for this kind of treatment are therefore completely different from those of the UV treatment, but can explain the light angular dependence of the plasma treatment when this modification is considered as a combination of photon and electron effects.

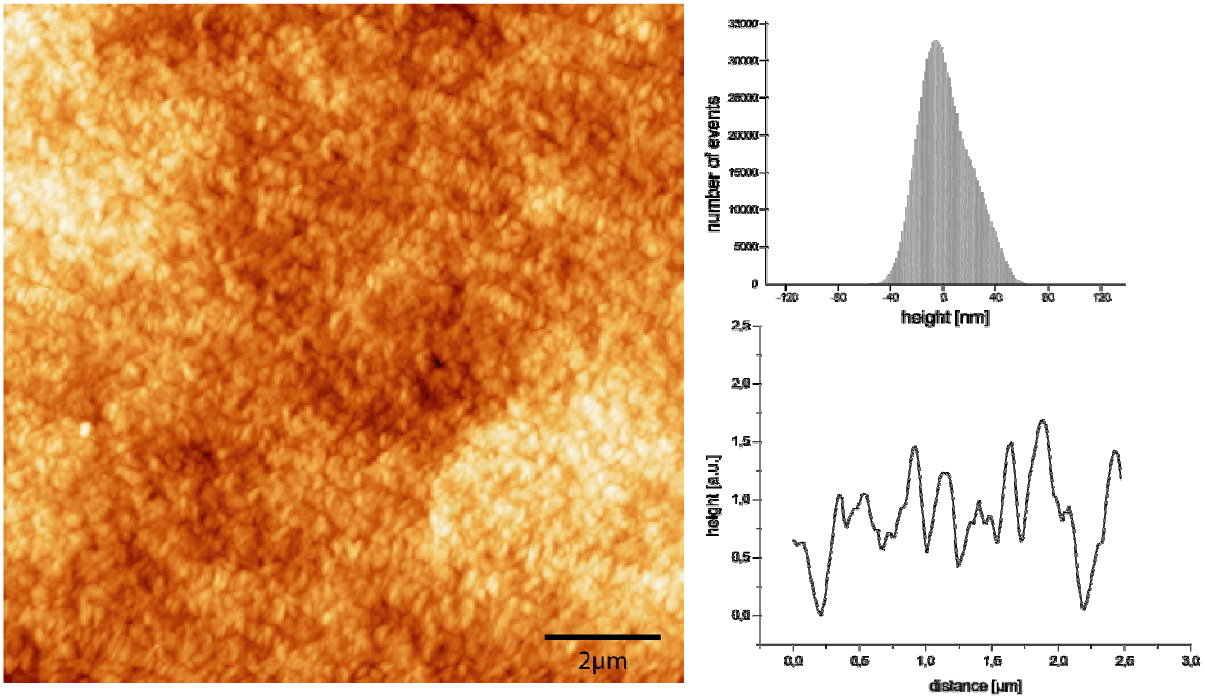

Figure 68 : electron modified PE foil viewed by atomic force microscopy

The structural analysis of the electron modified PE foil in figure 68 is also very informative. Basically it reveals far smaller grains than those of the untreated material with sizes between 0.09 and 0.30µm. It seems that the surface is roughened through these finer structures but in a very uniform manner, as one can see by the histogram data.

These and further structural effects will be compared with each other next, together with some comparisons concerning the chemical change and the elasticity of the modified polymers.

4.1.5 Further Measurements and Comparisons

While all treatments lead to a modification of the polymer surface, the individual changes in the chemical composition and their topography are quite different. So far our knowledge can be summarised that the treatments show different concentrations of newly created groups at the surface, the modification depth varies for the treatments and the topography shows quite different structures. Several other aspects of the modifications are still unanswered, like the influence of treatment time (especially if the plasma process can be modelled by a longer irradiation with UV light) as even for short treatment times changes in the chemical composition are reported [Mähl97]. The changes of the valence band area will be discussed briefly for electron and nitrogen plasma treatment. And concerning the structure of the treated polymers phase images and force distance curves will also be shown.

At first the processing time for the next experiments was reduced to 30 minutes, which leads in the survey spectra to smaller fractions of newly created chemical functional molecular groups next to the dominating carbon 1s line. The typical AUGER signals for carbon and oxygen also appear. The nitrogen peak in the UV treated survey vanishes completely, while a small signal can be made out after the argon plasma treatment.

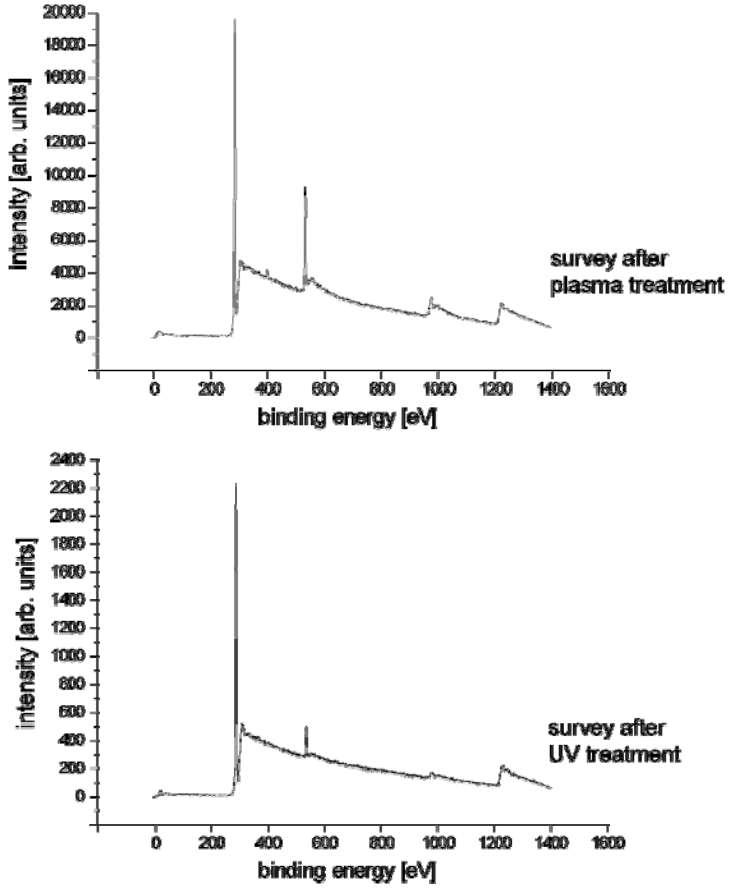

Figure 69: comparison of plasma and UV treatment for 30 minutes

Evaluating the modified polymers in the high resolution mode of the photoelectron spectrometer under a steep angle (according to surface near layers), the two modified Polyethylene foils in figure 69 show the following composition:

Element	UV treatment	Plasma treatment
Cabon	95.3at.%	83.2at.%
Oxygen	4.3at.%	14.7at.%
Nitrogen	0.4at.%	2.1at.%

Table 10: comparison of angle resolved plasma and UV treatment

A short comparison of these relative intensities will answer the question if even for the topmost surface layers a plasma treatment can be achieved with purely radiation effects (maybe with a longer treatment). In the high resolution spectra a small nitrogen signal of 0.4at.% can be found for the UV treatment, while the relative signal after the plasma treatment is more than five times larger. Also the oxygen 1s intensity of the plasma treatment dominates the one for photolysis reactions, but here the corresponding concentration is only three and a half times larger. The hypothesis of a simple blocking of the reaction because of the crystal window can be rejected according to the evaluation of

these measurements. Both kinds of treatment lead in principle to different chemical changes of the surface.

Therefore it can be concluded that the effects of a longer processing with UV treatment cannot be matched with the modification of an argon plasma (like 60 minutes treatment time – see previous measurements). Focusing on the depth of the modification (examined by different emission angles) gives the same picture because the distribution of the chemical functional groups is different for both treatments.

Also here the carbon 1s signal was fitted with three lines, resulting from the CH_x, the CO and the C=O groups. The fraction of relative intensities between the oxygen containing groups [hydroxyl]:[carbonyl] varies between the UV (1.68) and the plasma modification (1.84). This discrepancy was found also for shorter treatments down to 5 seconds treatment time.

To summarise the comparison between UV and plasma modification, two effects show up for: the angle dependencies of plasma and UV treatment are different and the composition of a plasma modification cannot exactly be generated by pure UV treatment (even with a different treatment time).

As the next aspect some valence band areas are regarded in more detail. Figure 70 shows the untreated Polyethylene foil (chapter 4.1.1) together with the ones after electron treatment (chapter 4.1.4) and after nitrogen plasma treatment (chapter 4.1.3)

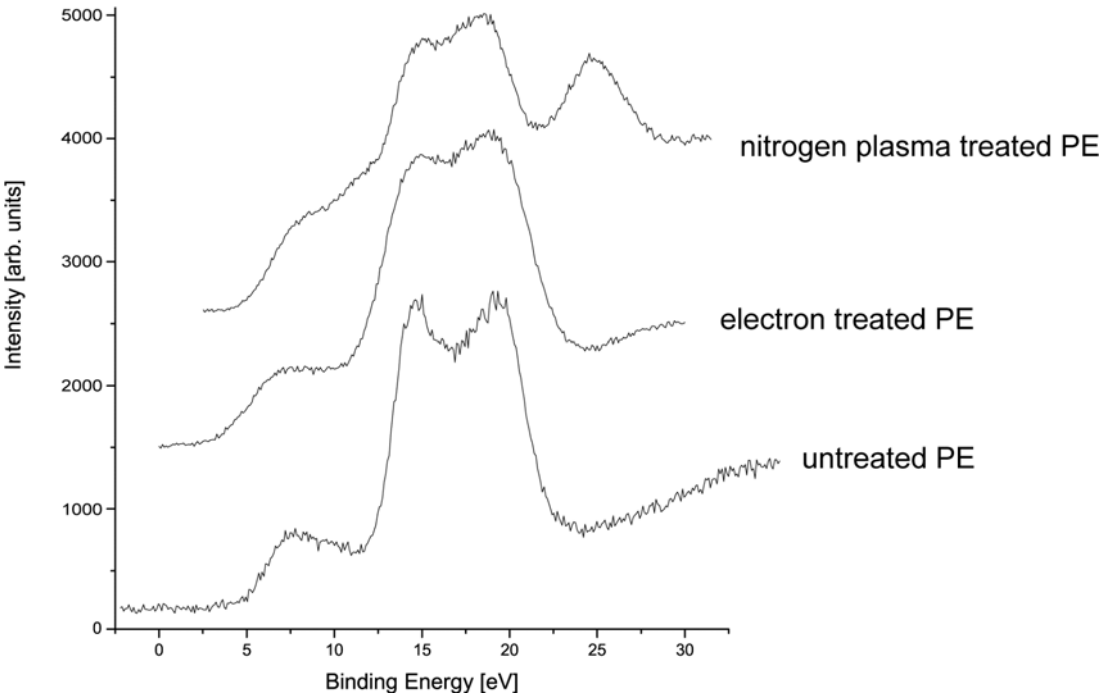

Figure 70: XPS valence band spectra of untreated, electron and nitrogen plasma treated Polyethylene foils

The spectra of the treated PE foils show on one hand all the carbon 2s and 2p structures known by the untreated material. It can be therefore assumed that the newly incorporated groups mainly occur in the side-chains while the polymer main chain stay unchanged (reasons for that will be discussed in chapter 4.2.2).

On the other hand the splitting of the C 2s is not as distinct as without treatment, so several other groups can be incorporated to the previous structure. Adding characteristic valence band lines of other polymers, like a combination of Poly(vinyl methyl ether) and Poly(vinyl alcohol), with the original PE can result in a similar spectrum as the measured ones. Pure hydrocarbons groups are also possible to cause the changes in the structures.

For the nitrogen plasma treatment this is especially relevant as the signal for the oxygen 2s appears at a binding energy of 26eV and possibly the nitrogen 2s signal is hidden in the lower energy edge of the O 2s peak. To explain these lines, further functional groups must be taken into consideration like Polyacrylonitrile (PAN) or Polymethacrylamide (PMAM).

The valence band spectra for these compounds can be looked up at [BeBr92]. A quantitative analysis of the valence band structure is impossible as the concentrations of possible end groups are unknown.

After showing several results for the different treatments, some additional measurements will be presented to confirm the results. The next aspect deals with the question whether sputtering of the material occurred or not. For coating processes the film thickness could be monitored by a crystal micro-balance based on the phenomenon that the resonance frequency v_q of a quartz crystal wafer depends on the thickness x_q and the velocity v_q of the shearing threshold. Therefore the following relation [Lu75] can be applied $\nu_q \cdot x_q = \frac{v_q}{2}$.

When the thickness of the crystal changes (due to the addition or **removal** of material) by an infinitesimal amount of dx_q, the mass also changes about dm_q and therefore also the resonance frequency. After a postulation of SAUERBREY [Saue59] the change in the little mass is independent from the material which is added or removed and causes the same shift in the resonance frequency dv_q $\frac{d\nu_q}{\nu_q} = \frac{dm}{m_q}$.

From the difference of the resonance frequencies between the unmodified and the modified crystal one can obtain the mass of the coating $m_{\mathrm{mod}} = m_{un\,\mathrm{mod}}\left(\frac{\nu_{\mathrm{mod}} - \nu_{un\,\mathrm{mod}}}{\nu_{un\,\mathrm{mod}}}\right)$.

WILKEN measured with this technique the ablation for several polymers under UV and plasma treatment [Wilk98]. In the experiments he found a high ablation for the first seconds, which he attributed to degassing and other effects. After 60 minutes photolysis time Polyethylene shows a mass loss of 0.9µg/cm², corresponding to an ablation of 9.5nm (the measuring error was specified with 0.07µg/cm²). The value was identical after 60 minutes of plasma treatment in a hydrogen microwave discharge. From these values it can be concluded that electrons and ions don't play a significant role in the PE ablation process. With 7.2µg/cm² Polypropylene shows a higher mass loss than the PE after 60 minutes photolysis time (corresponding an ablation of 80nm). Also the value for the plasma treatment using the same measuring conditions was higher with 9.2µg/cm². The difference between these values represents a kind of measure for the sputtering effects for the electrons and ions.

For our experiments the quartz of a micro-balance was coated with Polyethylene by a spin-coating process [Extr94]. The device was then inserted into the plasma chamber at the position where the sample will normally be modified. The measurements, displayed in the next figure, show a high ablation within the first seconds.

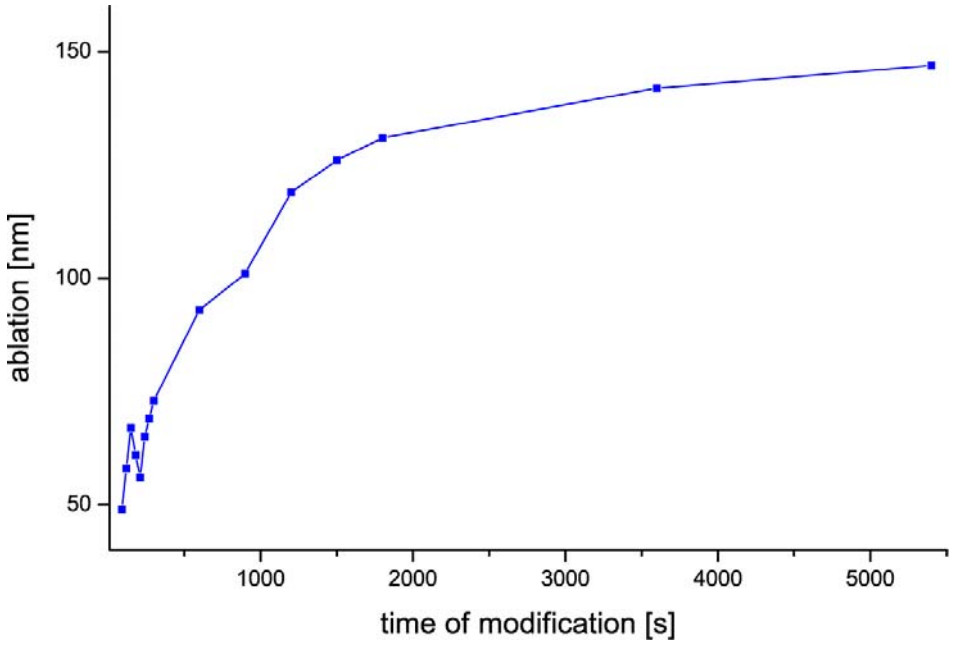

Figure 71: ablation of polymer material by an argon plasma – the measurements of the micro-balance indicate a progression with time of the degradation

The high degradation at the polymer surface is one reason that the treatments must not be described only by chemical changes but also by structural changes. The values for the ablation are ten times higher than those of WILKEN, but they still sound reasonable due to the different reactor geometry, power consumption and process gas. Another hint is the approach to a maximum of ablation, which is not caused by a complete removal of polymer material as this objection was controlled by XPS measurements.
After several hours of plasma treatment the difference between the modified and unmodified areas of the micro-balance became visible.

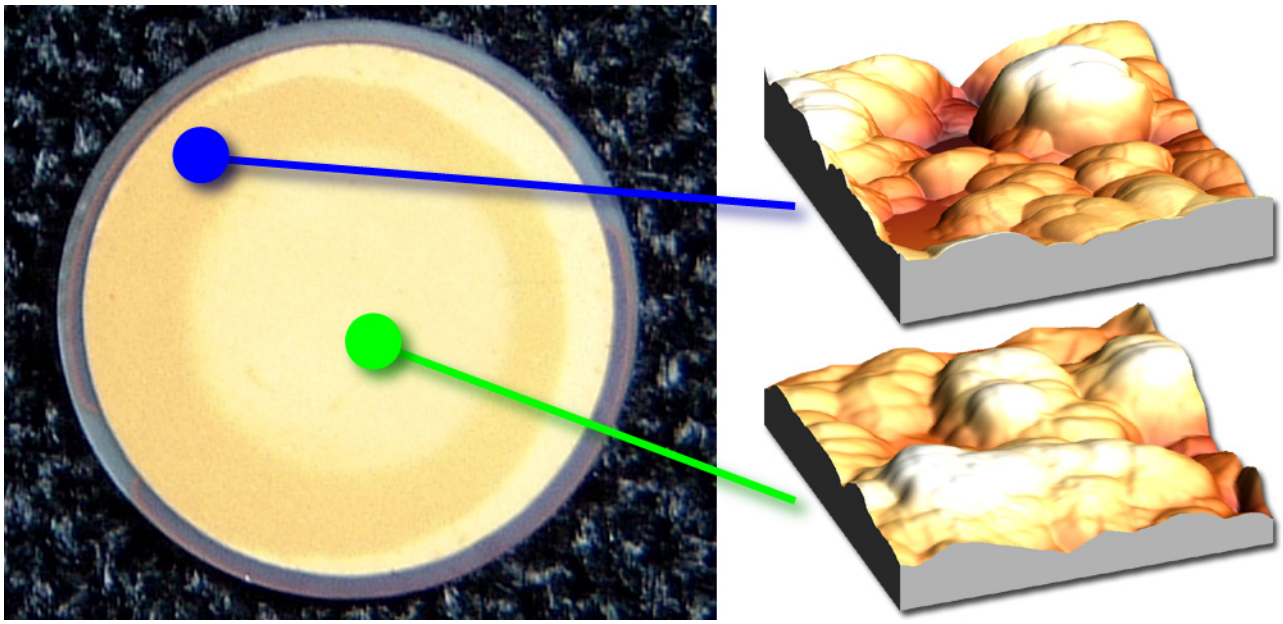

Figure 72 : photo and AFM measurements of the micro-balance quartz after plasma treatment – at the light coloured centre of the quartz the plasma could directly reach and remove the polymer, while towards the edge the polymer was shadowed by the set-up.

One can see by the AFM measurements displayed on the right in figure 72 an overall smoothing of the polymer structure when comparing the results for the shadowed area (blue marker) with the plasma treated area (green marker). The difference in topography can be specified with a height range of 220nm for the untreated Polyethylene, while the treated one shows a difference of 110nm between valleys and hills (the investigated area has an edge length of 2µm).

For structural aspects of a surface modification more information can be obtained. First, by changing the scan widths further details of the structure can be investigated. The scan size was therefore set to 4.811µm (the numbers after the decimal place result from the analogue – digital converter) while the other parameters stay unchanged from the previous ones.

Here are some remarks about the different signals displayed in the next figures: the sum signal adds all the signals of all four photodiode-segments and therefore should give a uniform picture as long as the movement of the tip does not leave the area of the detector. The error signal measures the difference between the set-point voltage and the vibration amplitude (wave mode) or cantilever flexure (contact mode). The phase signal, which was described in chapter 2.2.1, can differentiate between materials of the sample surface under ideal experimental conditions.

Regarding the following images, the four different aspects of the AFM measurements were compared. First of all, it can be seen that all measurements show a reasonable sum signal (respectively the second picture from the top), so the laser beam does not leave the photo-detector area and therefore a systematic error for the device can be excluded.

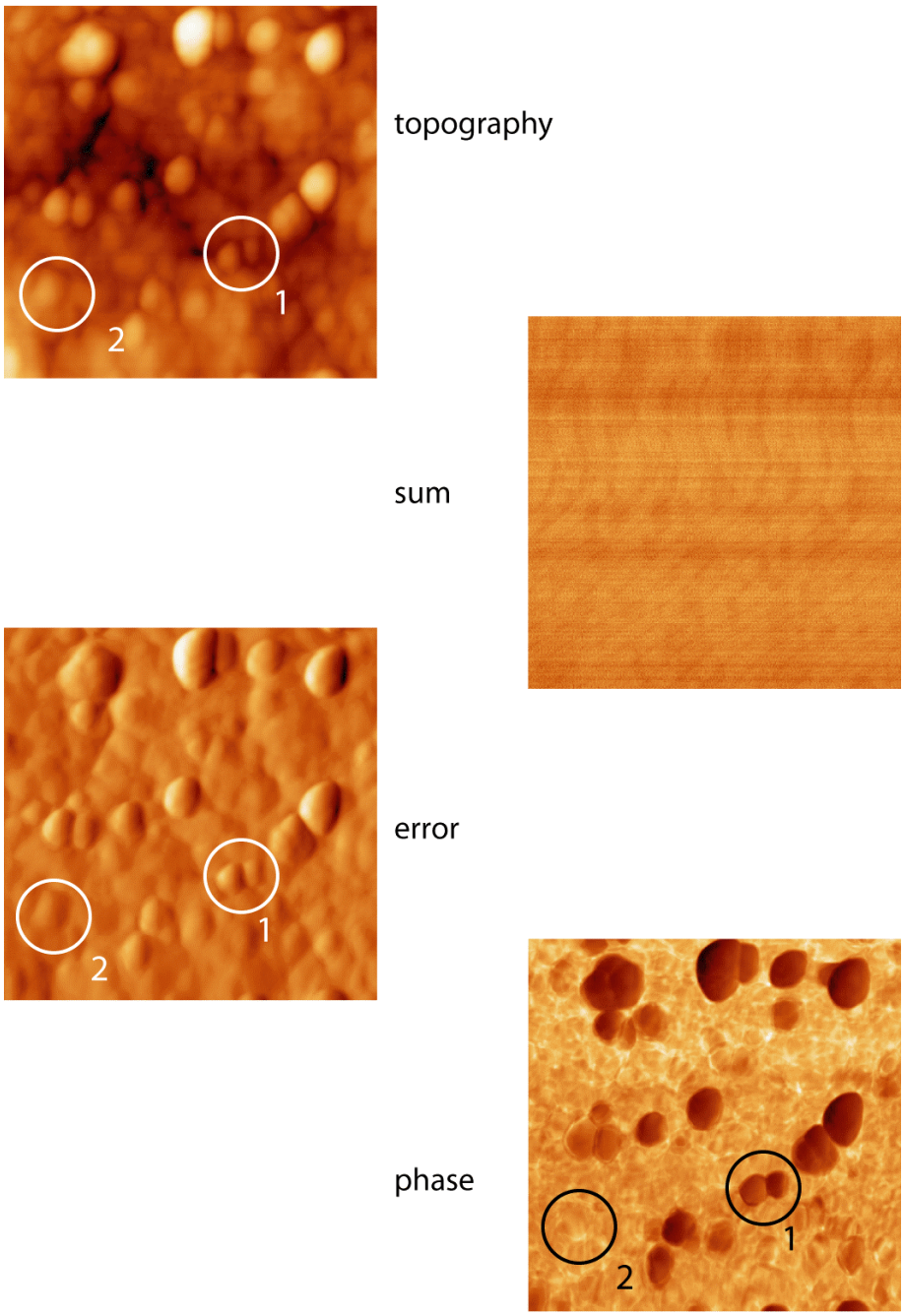

Figure 73: topography, sum, error and phase measurements of untreated Polyethylene foil with atomic force microscopy

The AFM measurements of untreated PE give a value for the fractal dimension[9] of 2.16. In the phase image one can see that the bigger grains have a different phase than the smaller ones. The signal detects also structures which can hardly be seen in the other images (1), while structures in those graphs vanish in the phase picture (2). The height differences in the topography were between hills and valleys is 140nm.

[9] The fractal dimension of a surface gives a kind of roughness and will often be used as parameter for wettability experiments [Hazl90]. A fractal dimension of 2 describes an ideal plane while a value of 3 would represent a volume.

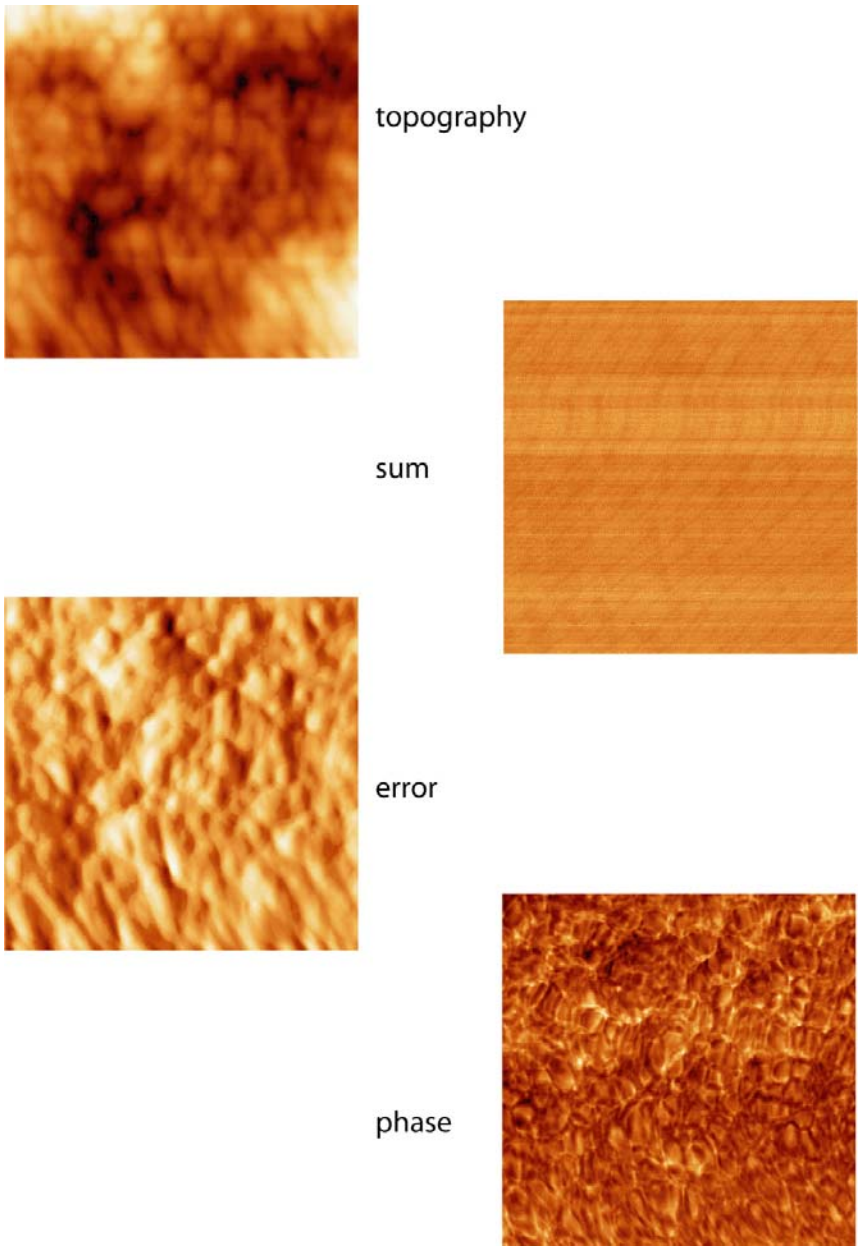

Figure 74: topography, sum, error and phase measurements of UV treated Polyethylene foil with atomic force microscopy

Compared with the topography figure of the untreated material, the bigger grains have disappeared, but the figure is blurred out a bit. Nevertheless the phase contrast is sharp, the larger grains have disappeared and a substructure, which is different from the topography and error signal, is revealed by the measurements. The fractal dimension reaches with 2.14 a lower value than the untreated material (it is also the lowest value for all measurements). This corresponds to a smoothest surface and is in good agreement with the height differences of 80nm for the topography.

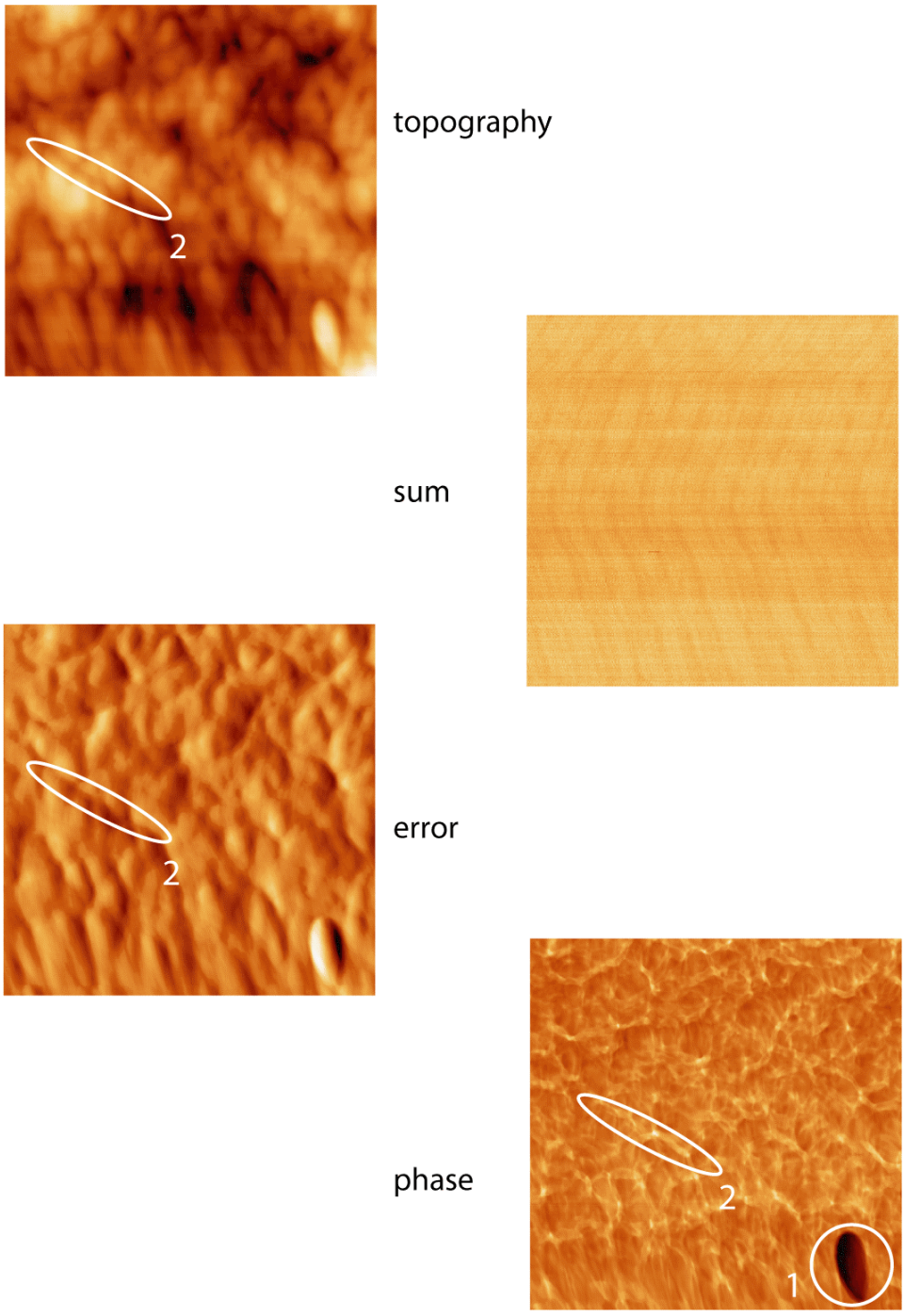

Figure 75: topography, sum, error and phase measurements of plasma treated Polyethylene foil with atomic force microscopy

The AFM measurements here shows only one big grain with a different phase (1), known by the untreated foil. The fractal dimension is with a value of 2.21 much higher than the previous results and also here a substructure can be made out. Different from the phase image of the UV treatment, this texture corresponds to the topography (2). The difference in the topography between hills and valleys is 90nm and therefore a bit higher than for the UV-treatment.

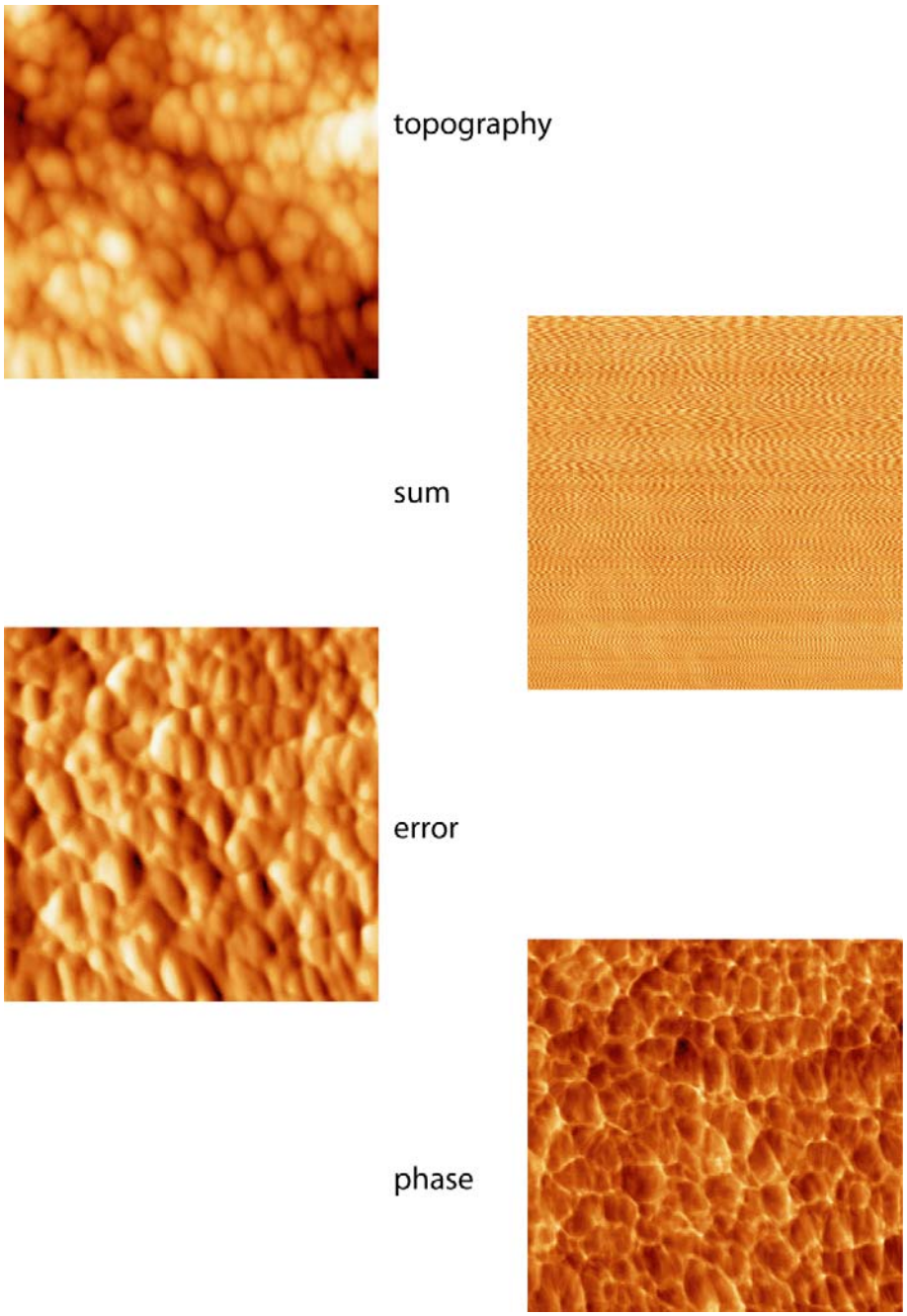

Figure 76 : topography, sum, error and phase measurements of electron treated Polyethylene foil with atomic force microscopy

Compared with the topography figure of the untreated material, also here the bigger grains have disappeared. This time the substructure looks different than those of the UV treatment as it is like for the plasma treated polymer mainly induced by geometrical aspects. The fractal dimension of 2.23 is the highest value for all measurements and indicates a kind of “rough” surface. The difference in the topography between hills and valleys lays with 120nm a bit below the value for the untreated material.

The different treatments of polymer materials show quite different pictures of their topography and phase signal. From the topography and the fractal dimension, the values for the plasma modification range between the ones for the UV and the electron treatment.

The last aspect of the structural analysis is the behaviour of a foil under stress. This value can be measured by force distance curves, obtained under UHV conditions with the Omicron STM/AFM. For the electron treatment this device could not be used so a force distance curve was measured in air with the Quesant Qscope 250. For the UHV measurements the Snap In and Snap Off points are displayed and also the adhesion energies were estimated by integrating the area of the dip with the corresponding force.

Depending on the kind of force interaction, both the approach and retraction characteristic show a typical behaviour. The next figure lists some of these different characteristics to help in analysing the acting forces.

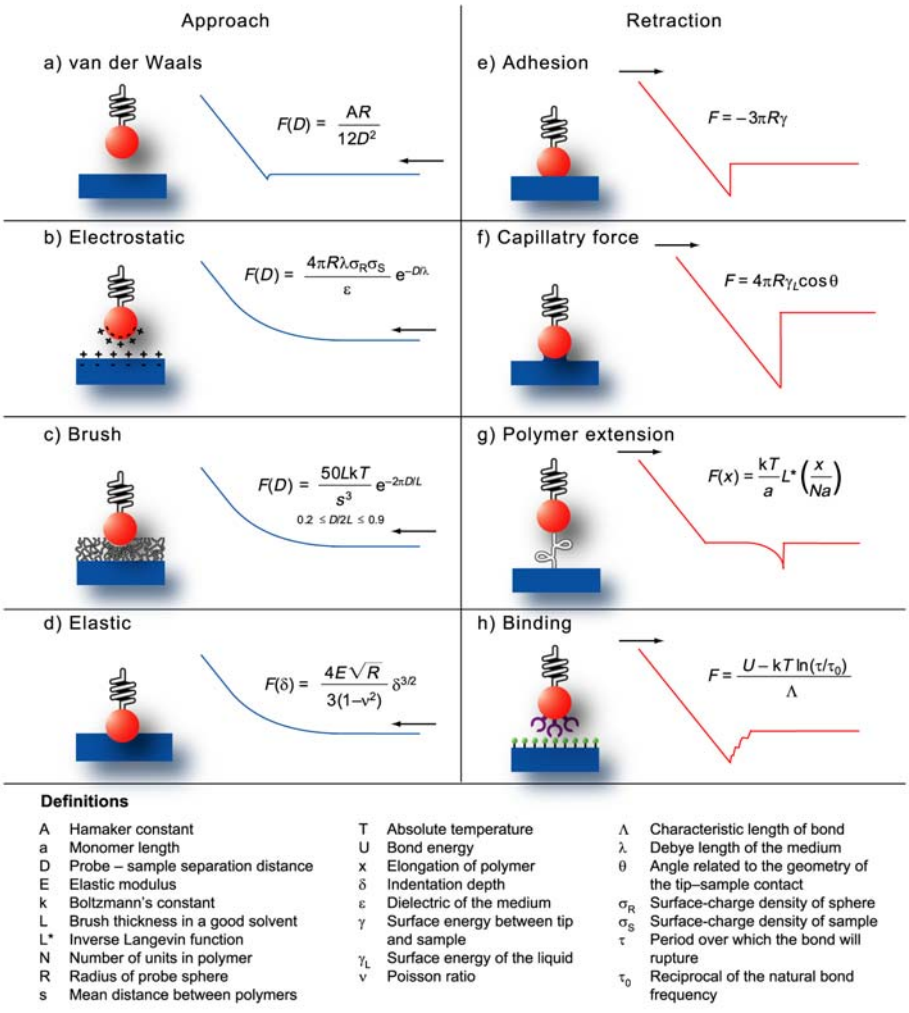

Figure 77: approaching and retracting curves for different kinds of force interactions [HeHo99]

When the force distance measurements are applied to the polymer foils, the characteristic looks like the following for untreated Polyethylene:

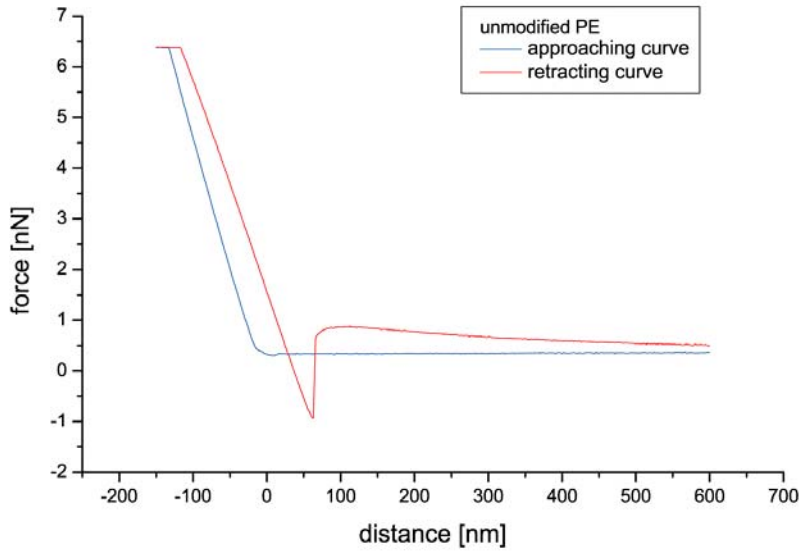

Figure 78: force distance curve for an unmodified PE foil

When the tip advances towards the untreated PE foil there is no clear Snap In point but a small dent in the graph 78. Such behaviour is typical for soft materials because the VAN DER WAALS forces (figure 77.a) are overshadowed by the elastic behaviour (figure 77.d). Brush effects can be discounted because the sample does not show brush-like structures in the AFM images. Electrostatic effects can also be excluded for the shape of the force distance curve according to the material.

When the tip is removed from the sample, firstly it sticks to the surface until the retraction force became higher than the attracting forces. The position of the Snap Off therefore is more distant from the sample than the Snap In and it can be recognised quite clearly. The values for the distance and the forces are displayed in the following table.

Position	Distance [nm]	Force [nN]
Snap In	10.05	0.30
Snap Off	62.27	-0.93

Table 11: Values for Snap In and Snap Off of untreated PE

For the approaching and retracting curves a kind of adhesion energy can be excluded by the shape of the measured line. Taking the areas of the force distance curves into calculation, an area of A_a=0.059nN·nm is covered during the approach (corresponding a "tiny" work of 5.87x10^{-20}J) while the retracting line covered an area of A_r=50.38nN·nm

(corresponding a work of 5.04×10^{-17}J). The distance between Snap In and snap off results to 52.22nm.

The behaviour of the plasma modified PE foil is quite different from the untreated foil. The most obvious difference is the clear Snap In point in the force distance curve.

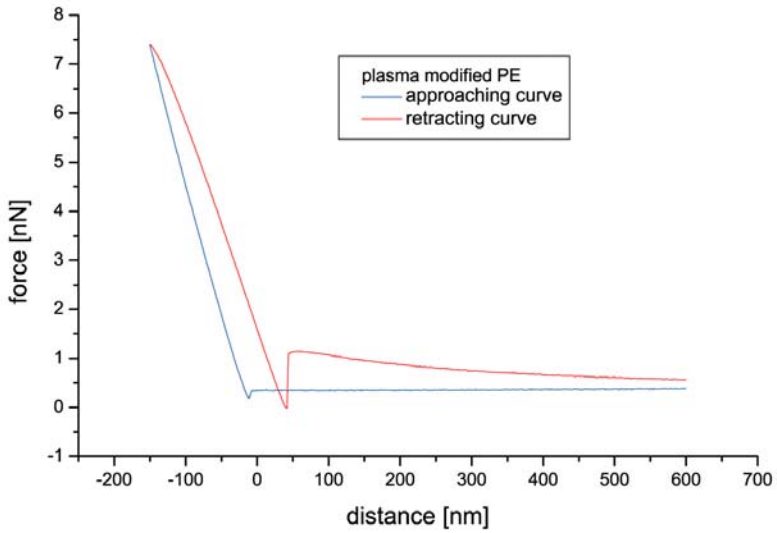

Figure 79: force distance curve for a plasma modified PE foil

This behaviour results from the VAN DER WAALS force, which seems to dominate the shape of the curve. When the tip is removed, it also sticks to the surface, but differently from the previous measurement the sticking is softer due to smaller force values respectively a smaller difference between both forces.
Only the distance of 53.87nm between Snap In and Snap Off is similar to the one of the untreated material. The detailed values are given again in the next table for Snap In and Snap Off points.

Position	Distance [nm]	Force [nN]
Snap In	-11.80	0.19
Snap Off	42.07	-0.02

Table 12: Values for Snap In and Snap Off of plasma modified PE

Taking the areas of tip movement caused by forces into calculation, an area of A_a=0.93nN·nm (corresponding a work of 9.27×10^{-19}J) is covered during approach while the retracting line covered an area of A_r=21.73nN·nm (corresponding a work of 2.17×10^{-17}J). Especially the second value is remarkable because it is less than for the untreated material which means that retracting the tip is easier for the plasma modified polymer than

for the original PE foil. On the other hand measurements have been presented showing a chemical modification of the surface with a high concentration of oxygen containing functional groups. As such a modification is often seen as an evidence for a better adhesion, this proposition is questionable due to the measurements. A possible explanation could be that polymer surface contains weak bounded fragments, which create the hydrophilic behaviour (as it can be concluded from the oxygen signal of the angle resolved XPS measurements). When the cantilever is retracted from the polymer, these fragments stick more easily to the tip than to the polymeric ground material.

A third kind of force distance curve was obtained for the UV treated polymer foil. The graph 80 displays this behaviour.

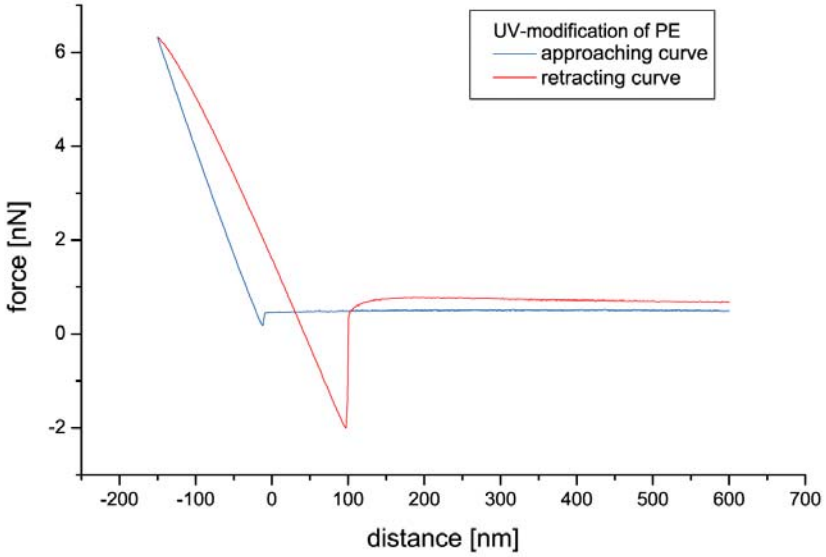

Figure 80: force distance curve for a UV modified PE foil

The Snap In is clearly visible as for the plasma modified PE, so also here the VAN DER WAALS force has the main impact on the approaching curve. Removing the tip from the sample requires a force of 2nN and therefore the distance between Snap In and Snap Off reaches 109.5nm, indication a strong adhesion (see figure 77.e). The occurrence of capillary forces (figure 77.f) can be excluded as the measurements were obtained in the UHV. Their values are displayed in the next table:

Position	Distance [nm]	Force [nN]
Snap In	-12.01	0.16
Snap Off	97.49	-2.00

Table 13: Values for Snap In and Snap Off of UV modified PE

Integrating the movement towards the forces, an area of A_a=1.77nN·nm (or 1.77x10^{-18}J) is spread when approaching the tip while retracting covers an area of A_r=120.01nN·nm (corresponding a work of 1.20x10^{-16}J).
A possible explanation for the different behaviour of plasma and UV treatment may be the structural changes of the surface displayed in figure 74 and figure 75. The substructure of the UV indicates a change of the material properties while the plasma treatment shows only structural changes. The failure of lasting surface treatments for polymer materials under stress has been discussed on several conferences and still is a problem for finishing processes. For a final conclusion if these problems rely solely on weakly bonded fragments further studies are necessary.

The force distance curve for an electron treated foil was only measured in air. Therefore the corresponding graph is not as precisely examined as the others and only some of the previously analysed aspects could be evaluated. To do that also so far presented materials were investigated again in air, from which the force distance curve by UV treatment looks similar to the electron treated one (upper right of figure 81).

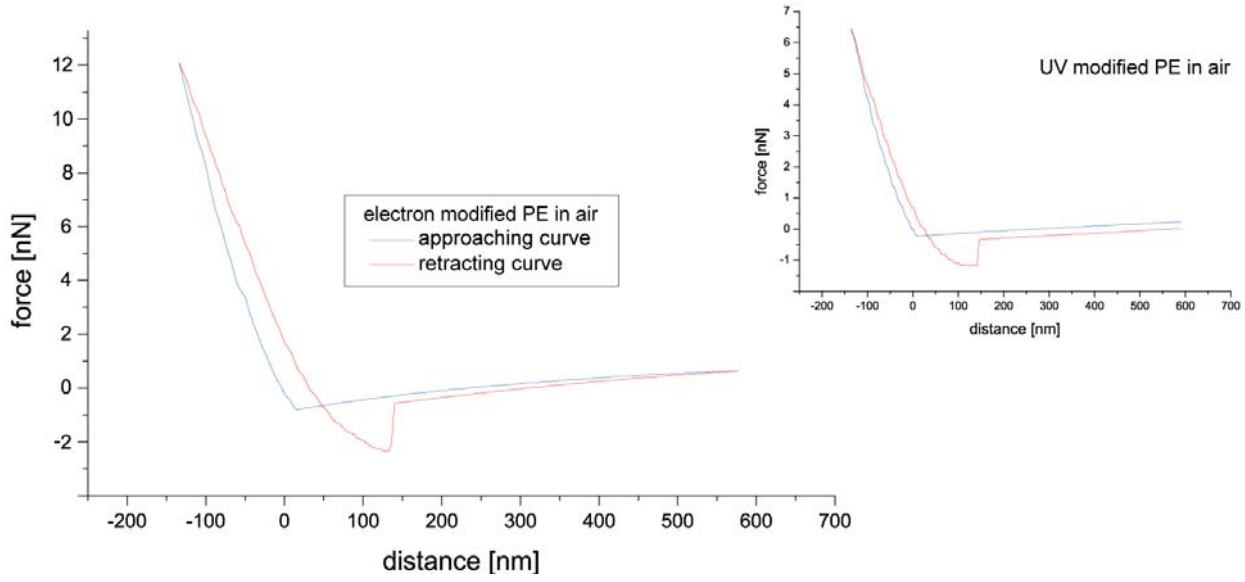

Figure 81: force distance curve for an electron modified PE foil measured in air (additionally the corresponding graph for the UV treatment is displayed in the upper left corner)

Nevertheless, its shape suggests similar behaviour to the UV treated material. The distance amounts to 112.77nm between Snap In and Snap Off (for the UV treatment it is about 130nm compared with 109.5nm obtained by ultra high vacuum conditions).
All obtained values for the electron treatment are displayed in the table 14.

Position	Distance [nm]	Force [nN]
Snap In	16.14	-0.85
Snap Off	128.91	-2.36

Table 14: Values for Snap In and Snap Off of electron modified PE

The force distance measurements show different aspects of tip–surface interactions for the polymer modifications. So far the results can supplement the phase measurements at difficult areas and for further investigations a point by point analysis of the surface with force distance curves would be desirable, even if it cannot be accomplished with the existing set-up.

4.2 Characterisation of selective reactions

The chemical bonding information available from XPS analysis of polymer surfaces is often insufficient to distinguish between some of the functional groups which are expected to be created by the different treatments. Although such groups can be identified by ATR-IR (attenuated total internal reflection infrared spectroscopy), the surface sensitivity of this technique is insufficient for our surface analysis experiments. To overcome this problem, specific functional group reactions are interesting which lead to distinguishable products for the XPS analysis. The primary objective is the labelling of the functional group with an element, which is not present in the material. ANDRADE lists several chemicals with a high cross section for XPS detection for such a derivatisation [Andr85].

Next to the advantages of such a labelling of interesting chemical groups, a major problem is that the reactions at a surface are often different from the ones in a homogeneous solution. Therefore one has to study the behaviour of such reaction with time and concentration of the reactants. Especially gas phase reactions seem to be adequate because there are no solvent or swelling problems and the chemicals can easily penetrate into the material.

Further analysis of the labelled polymer with atomic force microscopy was not performed because the reaction sites of the polymer may have reoriented themselves during the derivatisation process [EvRe81] which may lead to wrong structural results.

Knowledge of the chemical composition of a surface alone does not necessarily help to understand the basic processes of the modification – it merely gives an impression of the overall alteration when being compared with the untreated material. These labelled groups were traced by XPS and their concentration contains information about the incidences of

these microscopic reactions. By this technique, also different kinds of radicals can be distinguished after flooding with nitrogen monoxide. Each type of radical shows a different passivation reaction with a different chemical end product.

The whole derivatisation chamber, including the inlet for the chemicals to label the sample, was illustrated in a previous paragraph (see figure 44). A fine dosing valve was used as a controlled inlet for derivatisation substances, while the pressure was steadily measured. As chemicals for the labelling nitrogen-monoxide (purity > 99.5 vol.%, Messer Griesheim) and bromine (purity > 99.99 vol.%, Aldrich Chemical Company Ltd.) were used. The effects on modified polymers will be presented in the following paragraphs.

4.2.1 Double bonds after different treatments

The formation of double bonds and cross-linkage are common in plasma treatment processes. In the easiest case these new structure result when two carbon radicals are created in their direct vicinity of another chain. For PE this would mean that hydrogen atoms are removed, for PP or other polymers this could also be functional groups. If these radicals are located in the same chain, they can create a double bond, otherwise they can build a cross-linkage between two polymer chains[10] as shown in figure 82.

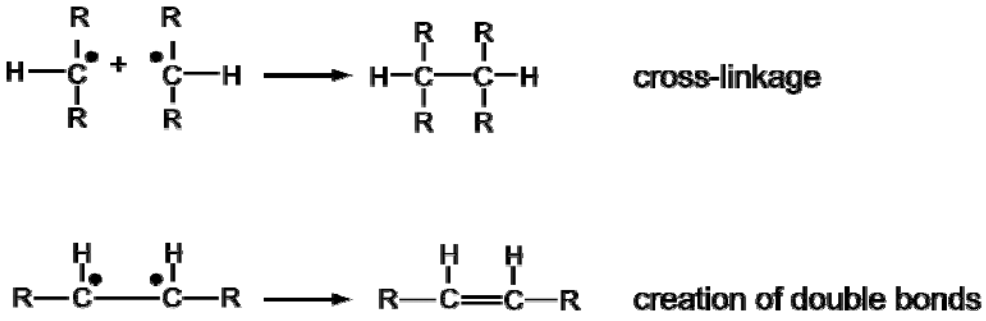

Figure 82: cross-linking and double bonds

Double bonds vary in their binding energy only slightly from the single bonds in a hydrocarbon surrounding and therefore cannot be directly separated by XPS measurements. They can be identified in wet chemical processes [SpCh78] [PGE86] [BBK77] [RiDw74], but there unwanted reactions between the solvents and the polymers can take place. Another possibility is a gaseous phase reaction of a reactive gas or a liquid with a low vapour pressure. An electrophilic addition at the double bonds seems to

[10] loop-like structures can also be created when the polymer chain crosses itself where the radicals interact

be especially suitable and the used substance should become an exclusive label with an unique chemical group for a polymer surface modification.

Two chemicals fulfil this idealistic condition for the labelling: iodine and bromine. As iodine treated polymers are unstable under vacuum XPS treatment [Basc91] and this substance does not penetrate very deeply into polymeric materials (less than 12nm into polyphenylacetylene), bromine was used as the chemical label for detecting double bonds.

According to the electrophilic addition the concentration of the bromine therefore relates directly to the concentration of double bonds. This substitution is displayed in figure 83 where two electrons of the double bond are used to split the bromine molecule and substitute these atoms.

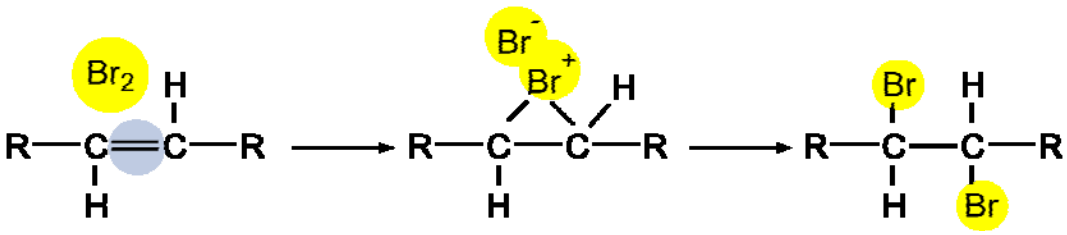

Figure 83: chemical labelling of double bonds with bromine

The bromine (purity>99.99%, Aldrich) was transferred under a protective atmosphere into a glass vessel. With a special dosing valve this vessel was then mounted onto the derivatisation chamber, allowing a controlled inlet of bromine.

The bromine penetrates into the polymer from the surface at least to the investigation depth of XPS. The influence of unsaturated radicals prior to the bromine reaction has been minimised by storing the samples for two hours in the UHV after treatment. These treatment parameters (exposure for 15min with a bromine gaseous pressure of 200mbar) were known from literature and confirmed by additional measurements. The reaction of long chains of unsaturated hydrocarbons in an atmosphere of bromine has been examined by POVSTUGAR et al. [Povs94]. After 5 minutes at a pressure of 160mbar it was found that all double bonds were converted with some stoichiometric errors for oxygen containing groups.

First the concentration of bromine after a Polyethylene argon plasma treatment was measured. The following graph displays the temporal increase of bromine respectively of double bonds.

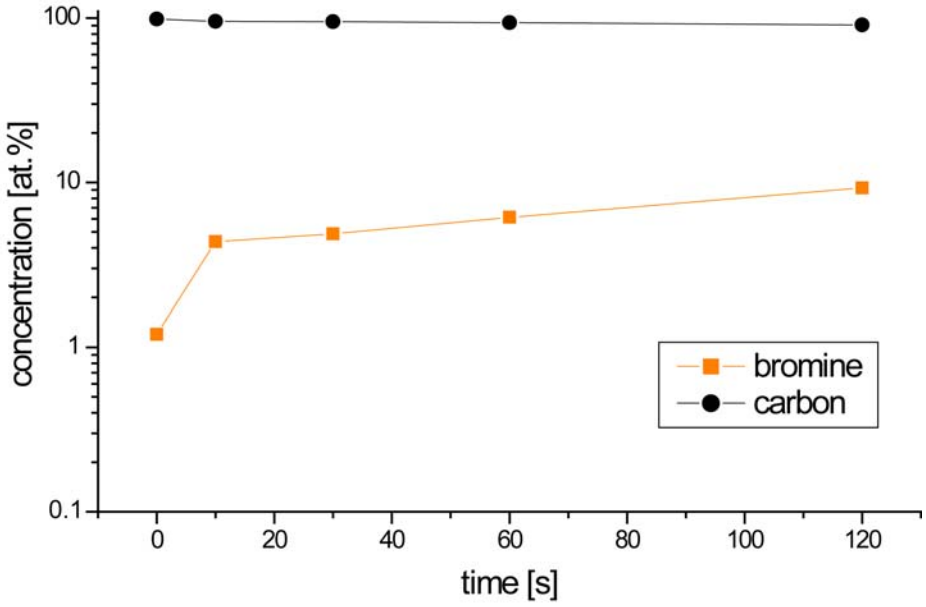

Figure 84: chemical composition of PE after argon plasma treatment and subsequent bromine reaction – even without a treatment (t=0s) a bromine concentration of about 1at.% can be found

Within 120 seconds of treatment time, the concentration of bromine grows steadily. But a control experiment, which was set up to identify the concentration of double bonds of the untreated material, shows a bromine signal of 1.2at.%[11], disqualifying the Polyethylene for the following experiments (see figure 84). This structural aspect was not detected before as the amount of double bonds was too small to cause a significant $\pi \rightarrow \pi^*$ shake-up structure in the spectrum of untreated Polyethylene (shown in chapter 4.1.1).
After the treatment of unmodified PP no bromine signal could be found. Assuming a detection limit of 0.1at.% for the XPS set-up and a similar error, the structure of the Polypropylene seems to be well enough defined for the experiments.

The measurements were performed with the parameters obtained in chapter 3 – *Plasma Analysis*. After the treatment of 15minutes in the plasma respectively 60minutes electron treatment, the Polypropylene samples were stored for one hour in the UHV and then for 15minutes exposed to a bromine atmosphere with a pressure of 200mbar in the derivatisation chamber. For all three different modifications a survey spectra as well as

[11] The concentration of near surface double bonds in chemical terms can be calculated by the formula:
$[C=C] \approx \frac{1}{2}\frac{[Br]_{at\%}}{100}\frac{\rho_{polymer}}{M_c} = [Br]_{at\%} \cdot 0.33 \text{ mol/l.}$
In this formula the polymer density is set to 0.9g/cm^3 according to the value for Polypropylene. A more accurate value for high density Polyethylene (HD-PE) would be $[Br]_{at\%} \cdot 0.35$ mol/l due to its density of ρ=0.95 g/cm^3.

high resolution spectra were obtained by XPS. The surveys of the modified polymers (see the next figure for the example of the UV treatment) only show the expected species carbon and bromine.

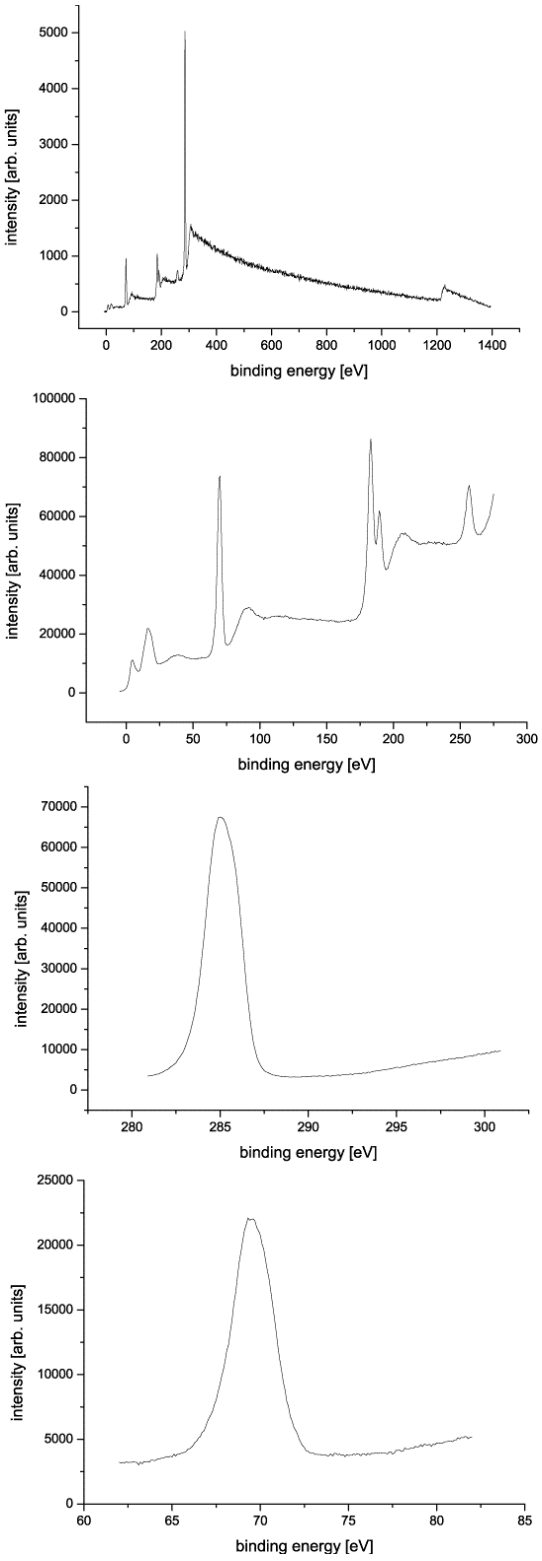

Figure 85: XPS measurements after UV treatment and derivatisation with bromine – from above the survey spectrum, the carbon 1s line, structures with a binding energy between 0 and 280eV and the bromine $3d_{3/2}/_{5/2}$ line

The absence of oxygen in the survey of figure 85 indicates the clean modification conditions for the residual gas pressure of $3 \cdot 10^{-8}$mbar as well as the high purity of the argon gas. The carbon 1s peak is set to a binding energy of 285.0eV using an electron gun to neutralise the charging of the sample. The three main bromine lines are found at 69/70eV, 182/189eV and 256eV corresponding the Br $3d_{3/2}/_{5/2}$ line, the Br $3p_{3/2}/_{1/2}$ line and the Br 3s line. For the evaluation of the bromine concentration, the Br $3d_{3/2}/_{5/2}$ line was examined and the intensities were compared then.

The measurements were again obtained in the angle resolved x-ray photoelectron spectroscopy (ARXPS) mode, where the atomic concentrations according to different angles of emergence for the electrons are recorded. Although the experimental set-up allows the analysis of angles from about 15° to a maximum of about 85°, mainly the outer layers with the corresponding angles from 45° to 85° were investigated. The intensities were evaluated from high resolution spectra and were afterwards plotted against the angles of emergence. The ARXPS results for the plasma treatment, the UV modification and the electron bombardment are presented in the following sections.

UV treatment

A pure foil of PP was mounted on the sample-holder, covered by the MgF_2-window and modified for 15minutes inside the plasma. The MgF_2 crystal window is transparent for wavelengths between 0.11 and 8µm, corresponding to photon energies between 11.3 and 0.2eV (see chapter 3.4 – *consequences for the treatment*). This energy is sufficient to create radical sites at and inside the polymer which be passivated by forming double bonds or cross-linkage as mentioned before.

The conversion of C=C double bonds seems to be complete according to the precision of measuring (otherwise a $\pi \rightarrow \pi^*$ shake-up structure at a binding energy of 291.4eV can be expected, which vanished after the chemical labelling [Dilk77]).

When the XPS signal of the bromine is examined one gets the impression of a clear angular dependence (see figure 86).

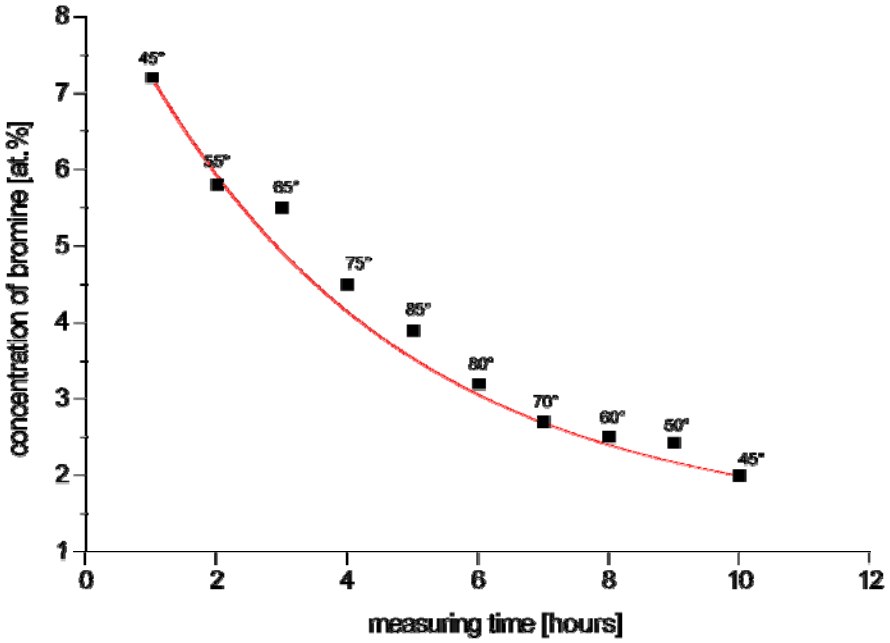

Figure 86: concentration of bromine after UV treatment under different angles of electron emission

Figure 86 shows the obtained data for the bromine concentration with the corresponding angle of electron emission and apparently a decay (red line) of bromine concentration. The first and last data points were obtained under the same measuring conditions (normal emission), therefore they are supposed to show the same total amount of bromine, but its signal decreases with the measuring time, respectively x-ray irradiation. To have the smallest possible decomposition, only short measurements were made but taking into account a reasonable signal to background ratio for the different species. The correction with the exponential loss leads to depth profiles of the bromine concentration namely the concentration of double bonds.

Every measurement took here 60minutes exposure time to the x-rays, while the positioning of the sample afterwards to a new angle was not included (the x-ray tube was off then). The numbers for the concentration were calculated then as the difference of the measurement and the exponential decay of the bromine signal.

The bromine concentration was corrected in the way that the decay curve was subtracted by the values for the bromine concentrations of the different emission angles. Those corrected values varies only a little for the different analysis angles, namely the different analysed depths. They will be compared with figure 87, where additionally a linear fit is displayed according to the angle under which the data points were obtained. Later in this chapter the values for the different treatments will be compared with each other.

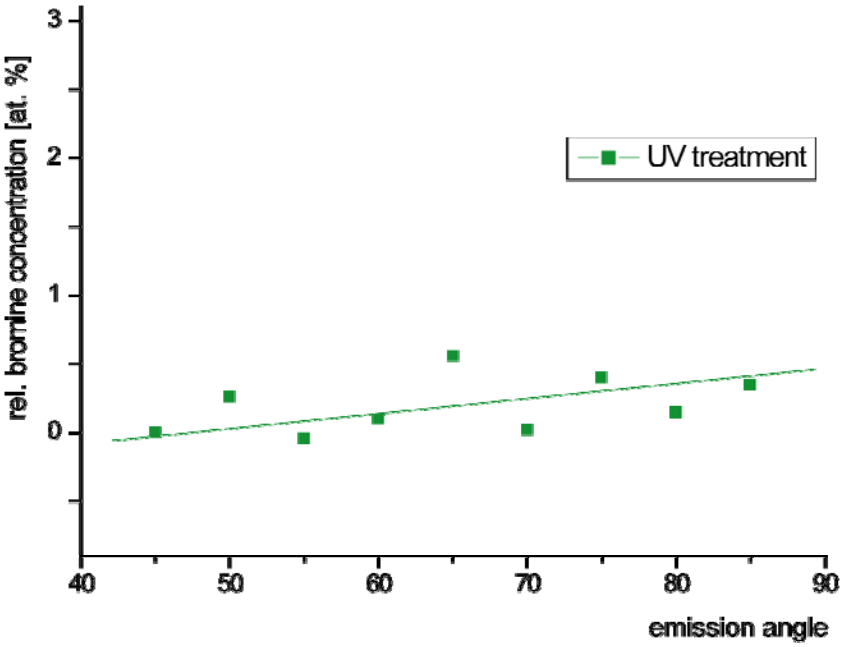

Figure 87: corrected bromine concentration of UV treated PP

The total decay of bromine while measuring must be discussed in more detail. As it was mentioned before the measuring time was kept short and the bromine spectra were calibrated in the way, that some measurements were performed under the same experimental conditions (an angle of emergence of 45° referred to the surface normal) and were plotted as an exponential decay with equidistant steps in time according to the number of obtained data points.

In the previously discussed derivatisation process a bromine molecule opens a double bond and creates two bromine groups. Such bromine groups can be destroyed when irradiated with high energy photons like the x-rays from the photoelectron spectrometer. The bromine then escapes into the vacuum where it is pumped away.

The decay of the bromine can be explained quite easily by the breaking of the still existent bromine groups. While the intensity of the radiation (number of x-ray photons) is constant with time, the number of bromine groups is decreasing. This process can be described as exponential decay $\frac{dN}{dt} = N_0 \cdot e^{-\alpha t}$, where N is the actual number of bromine groups, N_0 is the initial number of bromine groups, t is the time and α is a decay parameter.

Back to the UV modified Polyethylene. In the depth area under consideration the distribution of double bonds is nearly uniform, i.e. this modification shows nearly no angular dependence. To understand this effect, the penetration depth of the radiation into the polymer must be considered. The high penetration depth of the UV light into the

substrate leads only to a poor modification of the surface region, because a small amount of the radiation is absorbed at this region. In this case the structure of the polymer can be modified resulting, for example, in the formation of double bonds. How deep the radiation penetrates into the polymer depends on the absorption coefficient. The LAMBERT BEER law for monochromatic radiation shows how the radiation is absorbed as a function of photon penetration depth for a known absorption coefficient. Not only radiation, but also the mobility of polymer chains and the diffusion coefficients inside the polymer film influence the depth of modification and the photoelectrons are only detected down to a depth of 2-3nm (see chapter 2.1.1 – *theory of XPS*). The differences in concentration for the measurements referred to the normal emission are positive as well as negative at a maximum of 0.5at.%, but there is no correlation between the angle of electron emission and the bromine concentration.

Together with those described, measurements on the obscured areas were also performed (due to the construction of the sample holder). These showed no change on the polymer surface in comparison with the unmodified samples. Therefore it can be concluded that thermal effects through heating up the sample holder do not influence the modification.

Plasma treatment

The modification after the plasma treatment under the same experimental conditions as the UV treatment shows the following bromine concentrations.

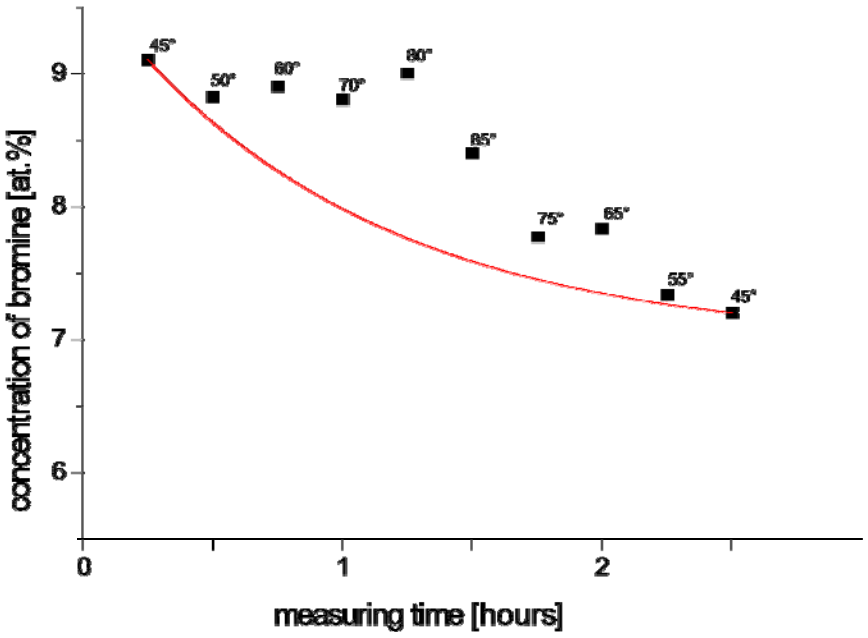

Figure 88: concentration of bromine after plasma treatment

Two important aspects can directly be observed in figure 88 – a higher overall concentration of bromine and an angular dependence where the concentration of bromine rises with higher angles. The higher concentration of bromine corresponds to a higher concentration of double bonds at the polymer surface.

The higher basic concentration of bromine compared with the pure UV treatment can not be explained solemnly with absorption effects inside the crystal window. When WILKEN measured the influence of the UV spectra on a polymer surface with and without an MgF_2 window he found for a hydrogen plasma a loss of about 20% of its intensity [Wilk98]. A plasma modification shows also an interaction of the substrate and the other plasma components: ions and electrons. The effect of ions can be discounted because of their small amount of kinetic energy. This energy was measured with a LANGMUIR probe and found to be at a maximum of less than 3eV while electrons exist in the tail of the distribution which posses a kinetic energy of 12eV or more. The collisions of ions with the surface are therefore eliminated as a source of modification and even if a higher kinetic energy is considered, due to the sheath region of the plasma the ions are below the energy to modify the surface [GrKü95]. The influence of electrons is discussed below in greater detail.

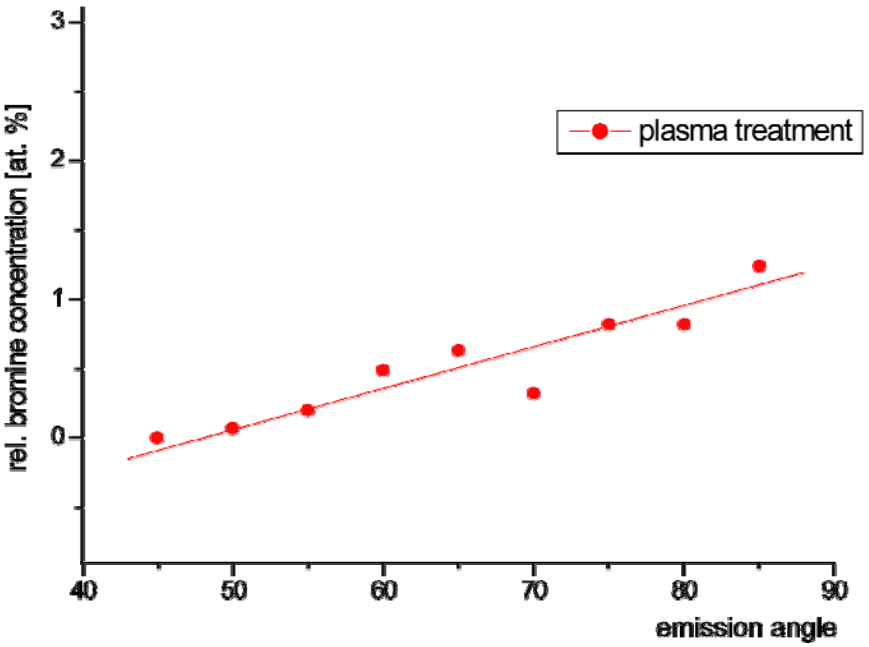

Figure 89: corrected bromine concentration of argon plasma treated PP

The differences in bromine concentration between the highest and smallest penetration depths displayed in figure 89 is about 1at.% and therefore far higher than with the pure

UV-treatment. In this case, effects other than radiation must take place in order to cause this higher concentration of double bonds at the polymer surface.
Again the plasma treatment must be seen as a combination of UV effects and something else. This additional modification is surface sensitive and as particles cannot penetrate as deeply as radiation into the bulk and therefore transferring their energy to the outer layer of the surface, mainly electrons and ions are taken into consideration. The ions seem to play a minor role in microwave generated plasmas (theoretically and experimentally by the previously presented results), so the electrons are supposed to modify the polymer at the surface.

Electron treatment

In the third kind of modification the polymer surface was flooded under UHV conditions for one hour by electrons. The electron energy was set to E_{kin}=12eV and the base pressure of the residual gas was 10^{-7}mbar in the experiment. The value of the kinetic energy is correlated with the electron energy distribution function obtained by LANGMUIR probe measurements in a previous chapter. The electron energy distribution function gives a part of about 2% electrons with a kinetic energy of 12eV or above (see table 7).
Also here the polymer was stored for one hour afterwards in the UHV to allow passivation processes. The following graph shows the uncorrected data points with the characteristic of the exponential loss. The decay here was softer than after UV treatment because of the measurement time could was again reduced.

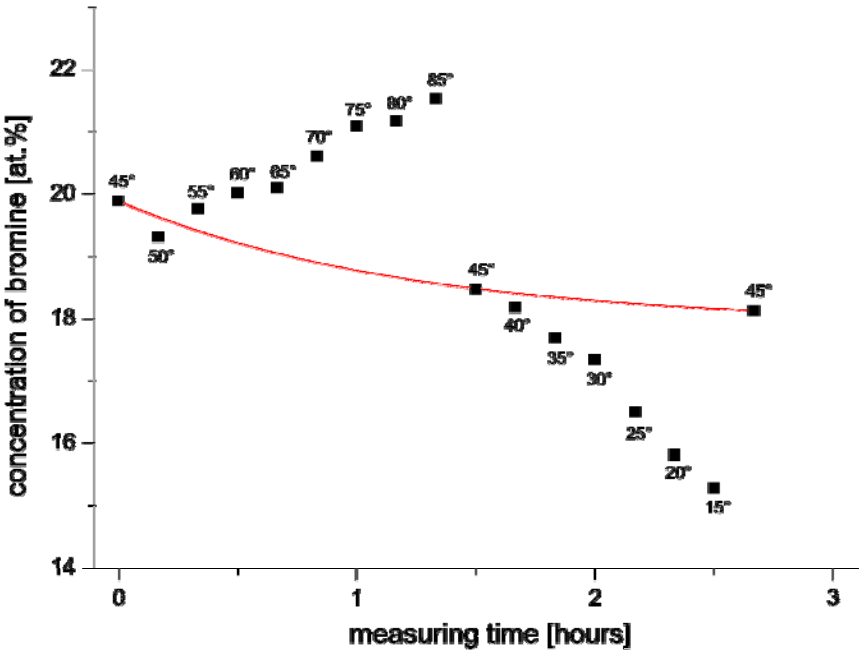

Figure 90: concentration of bromine after electron treatment

The treatment with electrons leads to a clear modification of the polymer surface. Also extended spectra for detection angles below 45° are displayed, which show decreasing concentrations of bromine for decreasing emission angles. The high overall concentration may have two causes: first the obtained plasma parameters are wrong or secondly sputtering reactions inside the argon plasma counteract the effects of the electrons to the polymer surface. The second reason seems to be more likely because the sputtering has been measured for the investigated system, but this argument does not necessarily debilitate the first aspect completely.
Due to the resulting concentration of bromine under normal emission, a penetration of this derivatisation substance into the material can be seen, but still is much smaller than those for the photons.

From these measurements one can conclude that electrons with kinetic energy above the excitation energies for modifying the surface lose their energy in the outer layers of the polymer. The electrons, which are initiators for chemical reactions at the substrate material, therefore have small penetration depths.
For this aspect of the electron modification, figure 91 is also enlightening. It shows an escape depth of only some monolayers with typical kinetic energies of argon microwave plasma electrons.

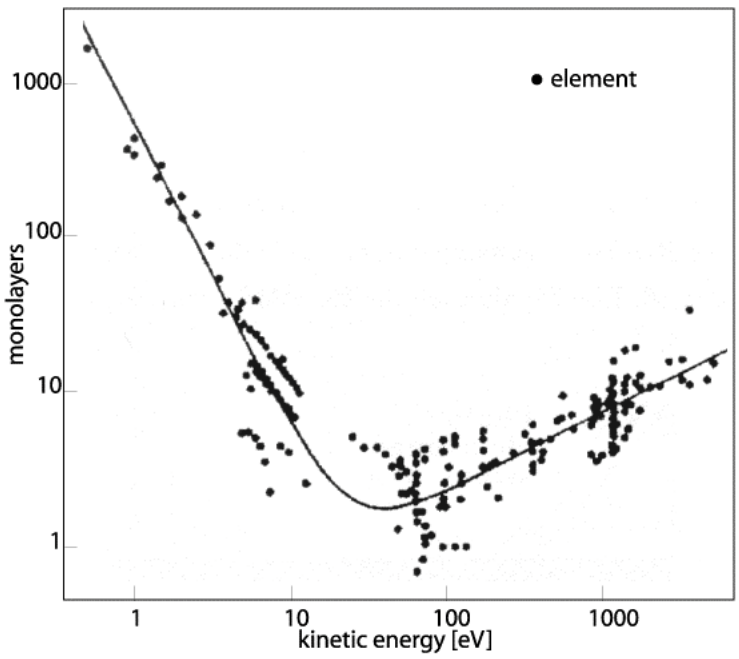

Figure 91: compilation of experimental attenuation length values for different compounds and fitted universal curve [Albe94]

This escape depth is defined as the distance in with the probability of detecting an electron dropped to e^{-1} (which equals 36.8%) of its original value without significant energy loss due to inelastic scattering [Brig98]. Although the energy range is displayed in figure 91 up to several thousand eV, the effects of the electron treatment can be associated kinetic energies up to 30eV (see the EEDF in chapter 3.2) and therefore this theoretical model can explain why the modification depth for electrons is relatively small.

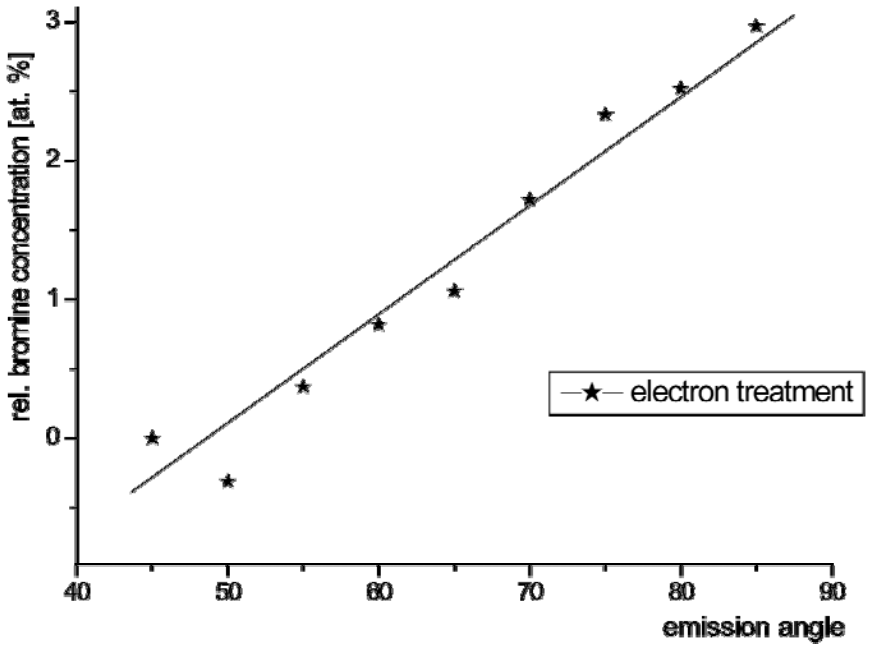

Figure 92: corrected bromine concentration of electron treated PP

Differently from UV photons the electrons penetrate only some atomic layers into the substrate and lose their energy. The difference in concentration covers a range of 6at.% (see figure 91) which is significantly higher than the values for the other treatments.

The results can be summarised in the way that the UV treatment leads to a uniform distribution of bromine at the polymer surface, while the electron treatment create double bonds in the first layer of the sample. With these two species the effect of plasma treatment can also be explained.

But why is the value for the double bonds after the electron modification so much higher than the calculated one from the plasma experiments? One explanation could be the sputtered polymeric material by plasma and UV treatment as discussed for Polyethylene in chapter 4.1.5. As mainly the UV destroys the material, these outer layers go into the gaseous phase and are pumped away. The pure electron treatment leads to an

agglomeration of double bonds because they are not sputtered away as in the plasma treatment.

Linear fits of the angular distribution of the bromine have been displayed in figure 87, 89 and 92. When the relative intensities for electron and UV treatment will be combined, the plasma treatment will be approximated. Regarding a loss of UV-intensity of 20% through the MgF_2-window, a quarter of the detected relative bromine intensity results from the electron treatment to obtain a similar concentration profile as the plasma treatment[12]. This result is shown in the next figure. Experimentally such a modification cannot be easily achieved but needs an adapted electron treatment after the UV irradiation.

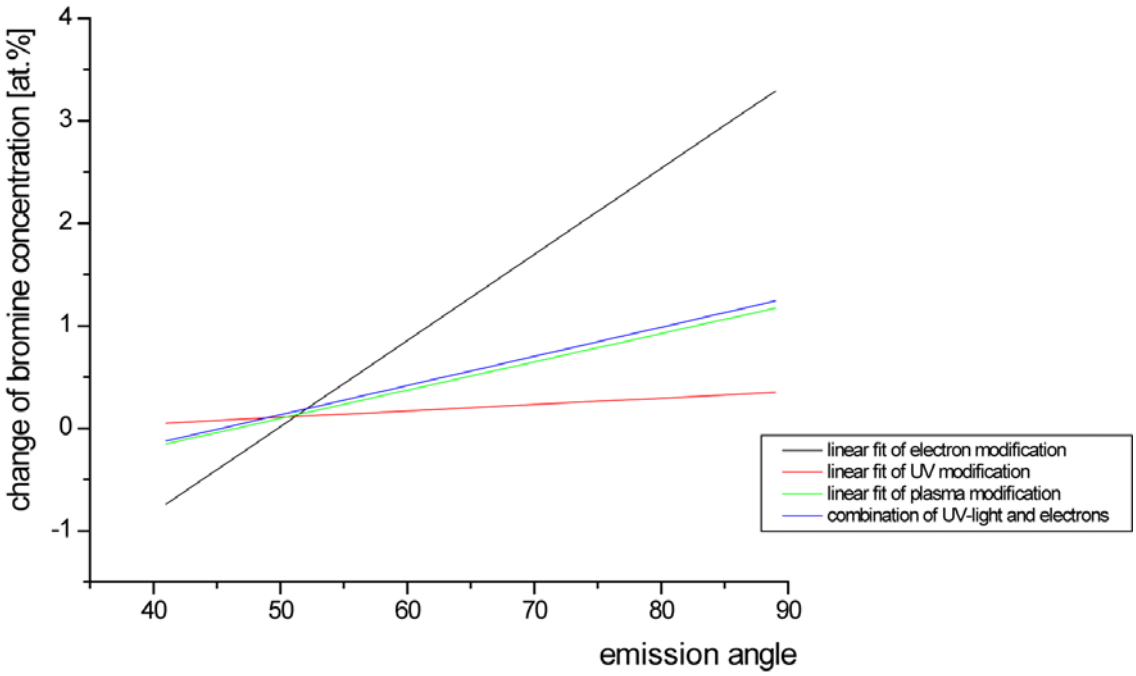

Figure 93: comparison of modifications through plasma, UV and electron treatment – the weighted combination of electron and UV treatment leads to a similar relative modification as the plasma treatment

4.2.2 Radicals after electron treatment

Radicals are more elementary than double bonds and practical even more complicated to be identified. After absorbing energy from an electron or photon, some primary processes take place within the polymer chains, including the formation of radicals. Therefore to understand the modification correctly, their preliminary stages must be investigated.

During and after a polymer modification, the reactive sites play an important role. Radicals are the primary product of the relaxation of an electronically excited C-C or C-H-bond. It is important to get information about the kind of radicals and their concentration created on the topmost surface layers. One possibility is the *Electron Spin Resonance* (ESR)-Spectroscopy. This method is not only sensitive for the topmost layer but also for the bulk properties. Therefore it could not be used for this experimental purpose.

A wet chemical method for the determination of radical concentration was developed by PONCIN-EPAILLARD et al. [PECB94a] [PECB94b]. This method is not appropriate because of the disadvantage of possible interactions of the solvent and the surface.

Another way is the derivatisation of radical sites with nitrogen monoxide and afterwards an examination with photoelectron spectroscopy, similar to the detection of double bonds. After the reaction of the radicals with nitrogen monoxide, three different kinds of radicals (see figure 94) can be distinguished, which finally lead to different chemical groups. These groups show varieties in their binding energy leading to a separation of their photoelectron spectra.

It is possible to convert the three distinguishable types of radicals into different nitrogen containing chemical groups (see figure 94), which can easily be detected by means of x-ray photoelectron spectroscopy.

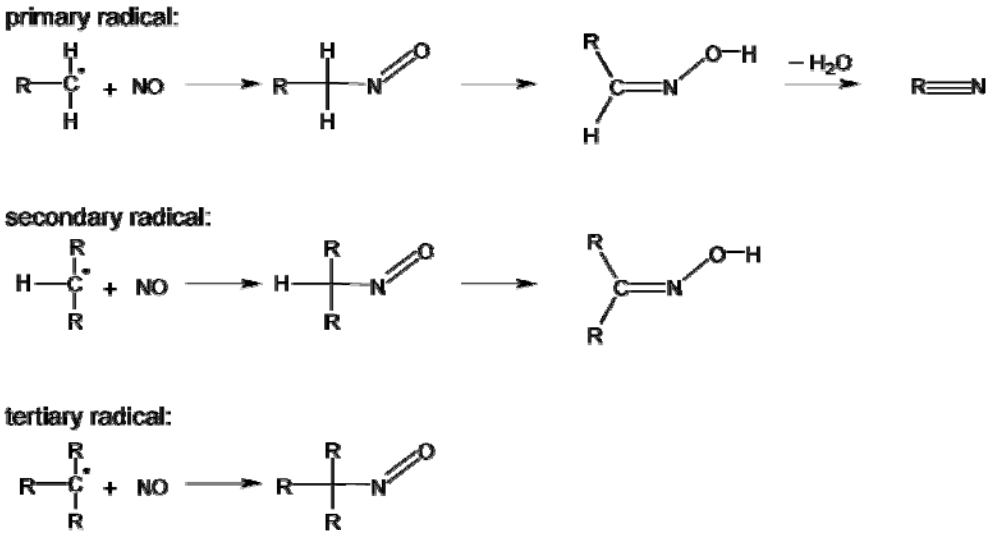

Figure 94: different reaction paths to radical extinction

As the time between treatment and chemical labelling must be very short and influence of other substances must be prevented from the polymer, only electron effects will be

[12] Not to be mixed up with only a quarter of treatment time

presented here (the transfer of the other samples from the plasma to the derivatisation chamber would take too long so that self quenching occurs).
In a first step of the reaction path, the nitrogen monoxide combines with the radicals of the hydrocarbon under the formation of a nitroso group (C-N=O). If a hydrogen atom is attached to the carbon (this is the case for primary and secondary radicals), this nitroso group reacts by tautomerism into an oxime group. On the other hand the nitroso groups seem to be the end of the reaction path for tertiary radicals.
Oxime groups from a reaction of nitrogen monoxide with a primary radical have another hydrogen atom. Therefore a reaction resulting in the creation of a nitrile group should be possible. So each end product is expected to differ for the three types of radicals.
As these nitrogen containing chemical groups posses different binding energies, it is possible to distinguish them in a photoelectron spectrum. The next table compares the binding energies of the nitrogen 1s line in different chemical surroundings.

Functional group	Structure	Binding energy (N 1s)	Reference
Nitrile	C-C≡N	399,1 eV ... 399,5 eV	[BeBr92]
Oxime	C=NOH	400,5 eV	[Wilk98]
Nitroso	C-N=O	403,7 eV	[Bear90]
Nitro	C-NO_2	405,5 eV ... 406,3 eV	[Bear90]
Nitrite	C-ONO	≈ 406 eV	[Wilk98]
Nitrate	C-ONO_2	408,1 eV	[BeBr92]

Table 15: binding energies of nitrogen containing polymers

Again Polyethylene is used in the experiments due to its simple structure. The results will be discussed along with the Polypropylene structure because cross-linkage will occur and the structure of PP has an additional side chain.
The purity of the nitrogen monoxide is crucial for the experiments. Especially the absence of oxygen is necessary because otherwise the nitrogen monoxide reacts to carbon dioxide, leading to unwanted side reactions like the abstraction of a hydrogen from the saturated hydrocarbon [Yoff53] or its addition to a C=C double bond [Burk54].
A control experiment was set up to identify if any form of nitrogen species can be found for untreated polymers. After the polymer was treated in an atmosphere of nitrogen monoxide for 15min with a pressure of 200mbar, no nitrogen could be found at the surface with XPS. Therefore the material has a sufficient purity for these experiments.
The resulting groups should be dependant on several parameters. One of these aspects is the electron energy. The electron energy distribution function showed fractions of

electrons with an energy of 12eV and more. Therefore the first experiments were performed according to different electron energies.

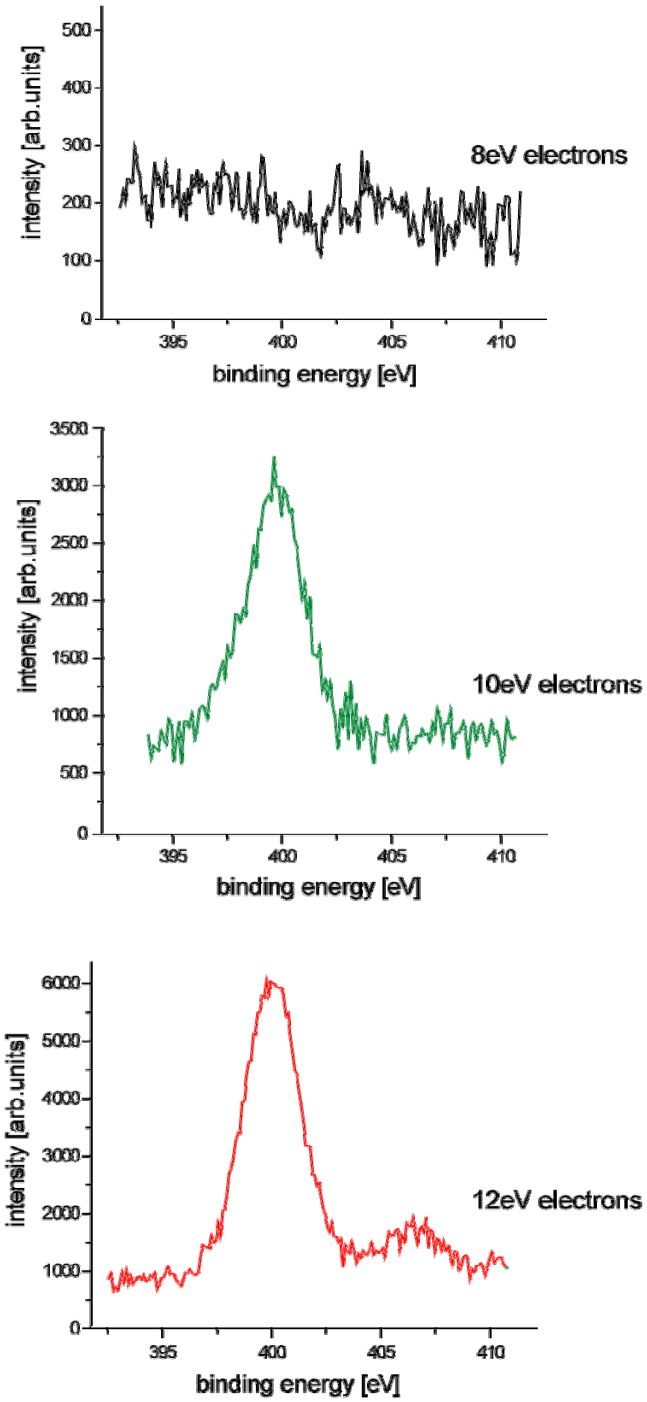

Figure 95 : nitrogen monoxide after electron treatment

For the electron treatment the emergence of the nitrogen groups can be observed when the kinetic energy of the electrons exceeds different values. While a treatment of 15minutes (under the previously mentioned conditions) with an electron energy of 8eV (black line) leads to no nitrogen signal of the photoelectron spectrum in the range between

395 and 410eV binding energy, while the same measurements under the same treatment conditions except a kinetic energy of 10eV (green line) of the electrons shows a peak at the binding energy of 400.5eV. This signal corresponds to an oxime group (C=NOH), which results from a secondary type of a radical (see figure 94).
With an even higher electron energy of 12eV (red line) a second peak appears at a binding energy of 406.5eV. This line corresponds to a nitro (C-NO_2) or nitrite group (C-ONO), but cannot be explained with the previous considerations.

Five reactions can be figured out to discuss the primary processes which occur after the encounter of the polymer with a photon or electron:

- ***Abstraction of a hydrogen molecule under formation of a double bond***
  For Polypropylene there are two possibilities to abstract a hydrogen molecule under formation of a double bond: along the main chain (left) and at a terminal group (right).

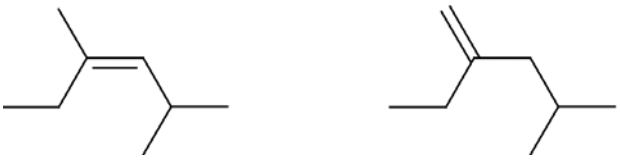

Figure 96: abstraction of a hydrogen molecule and formation of a double bond for Polypropylene

  The second possibility is not given for Polyethylene, and as the terminal double bond is less stable for the PP, the formation along the main chain is preferred.

- **Splitting of a C-H-bond under the formation of a radical and a hydrogen atom**
  This reaction is the most likely one and was displayed in figure 53. For Polypropylene there are even three possible sites for such a splitting, displayed in the next figure.

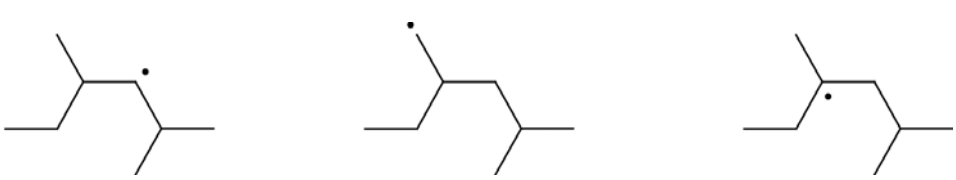

Figure 97: three sites where a splitting of a C-H-bond can occur for Polypropylene

  After the splitting of a C-H-bond, the very mobile hydrogen atom can easily disappear while the immobile carbon, if it is still bonded in the main chain (see figure 97 above on the left), becomes a separated secondary radical. While it is unlikely for the hydrogen

atom to meet another radical site and to recombine that way, a more likely reaction is that it abstracts another hydrogen atom from a complete chain. In a nutshell, the splitting of the C-H-bond leaves in this case two secondary radicals and a hydrogen molecule.

Another case may happen when the splitting occurs at the end of the terminal group (middle graph of figure 97) and a primary radical is formed. The hydrogen atom will again disappear with analogous consequences. But here the initially formed primary radical becomes a tertiary radical at room temperature. This is the same situation as if the C-H-bond breaks at the branching (right graph of figure 97). When these radicals are irradiated with UV light, the reaction will be revoked [IIT67] as shown in the next graph.

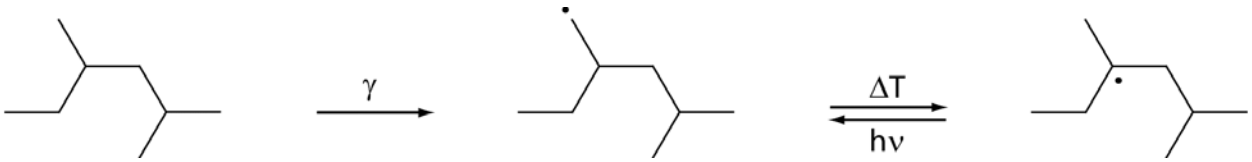

Figure 98: rearrangement of primary and tertiary radicals in Polypropylene

This reversal of the reaction should not occur when the tertiary radical encounters a plasma electron (because of its charge).

- ***Splitting of the main chain under formation of two primary radicals***

  The two resulting radicals of such a splitting (see figure 53) can be stabilised by secondary processes. Supposing that the polymer is treated below the temperature of the glass transition, the chains have only a small mobility, these two radicals are trapped and can be stabilised by recombination, disproportionation or hydrogen cession. For the case of the recombination, the main chain is established again and therefore there is no change in the polymer. The disproportionation leads to the formation of a C=C double bond and a methyl group. The chain is split and as a consequence the molecular weight of the polymer is lowered. WILKEN found a similar concentration of C=C double bonds and trans-vinylene bonds and concluded, that this reaction path plays only a minor role [Wilk98].

  The last possibility of stabilisation is the abstraction of a hydrogen atom from the directly neighboured polymer chains, which build up a cage around the pair of radicals. But as this reaction is less unlikely than the disproportionation, only a small effect on the polymer can be concluded for the splitting of the main chain.

For Polypropylene another variation of the reaction path exists. The radicals are trapped (figure 99 above) and can stabilise in two different ways (figure 99 below).

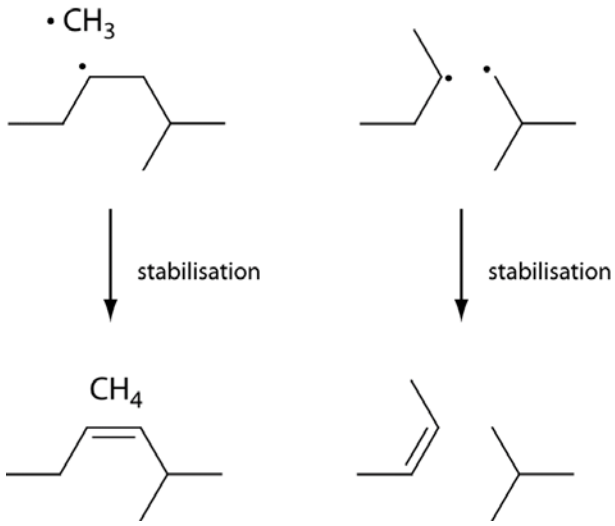

Figure 99: trapped radicals and their stabilisation in a Polypropylene chain

Both end products lead to a removal of polymeric material: directly through the splitting of methane (left) or in an indirect way of degradation of the molecular weight, which leads to the splitting of oligomeric chains.

- ***Thermal relaxation*** and ***fluorescence***.
  These last two processes do not change the composition of the polymer and therefore cannot be measured with the available equipment.

The microscopic explanation for the peak in the photoelectron spectrum (figure 95) after 10eV treatment is that electrons rupture the polymer chain between a carbon and a hydrogen atom. The intensity of this nitrogen signal in an oxime group suggests that this reaction is very likely.
The second kind of chemical surrounding at the 12eV experiment could not be explained with the three types of radicals. Instead BROWN suggested some reaction paths [Brow57] (taken up again by STRAUSZ and GUNNING [StGu63]) which lead from the tertiary type of radical to the found nitrogen groups, shown in figure 100.

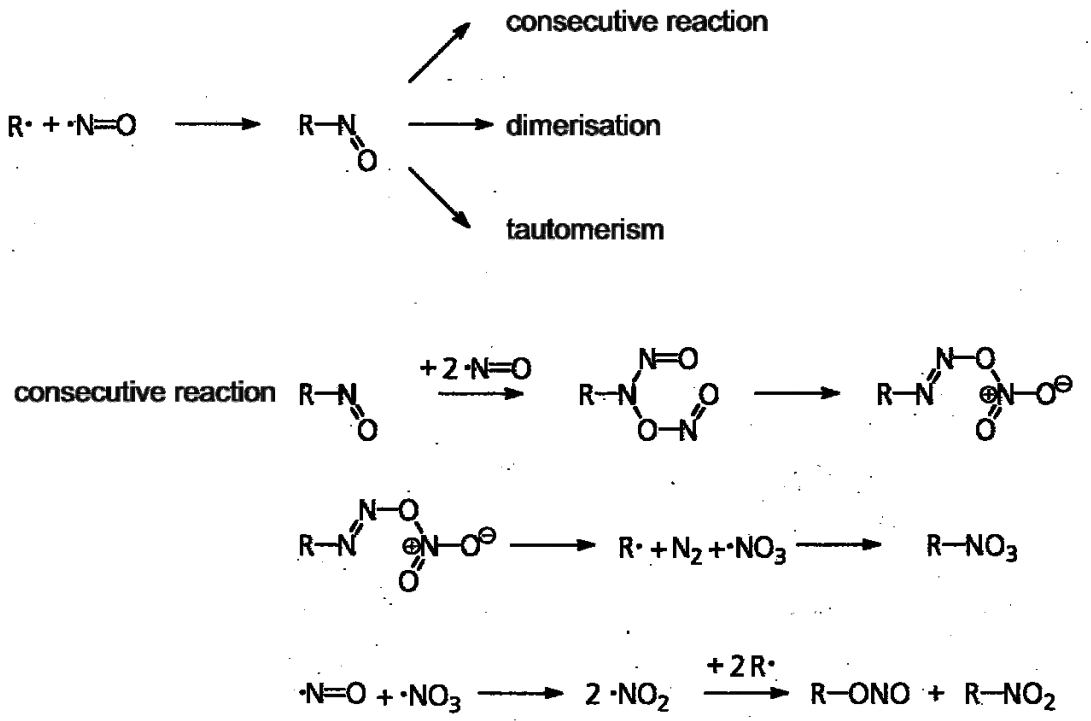

Figure 100: further reactions of a nitroso group

The application of is reaction scheme for the tertiary type of radicals would indicate a cross-linkage of polymer by the electron treatment. Therefore all occurring peaks in the spectra can be explained by the different radicals and their passivation reactions.

With higher electron energies also new nitrogen lines appear in the photoelectron spectra shown in figure 101. When the polymer is treated with 18eV electrons and radicals are passivated immediately after the modification with nitrogen monoxide (upper graph), a former unseen line appeared at 403.5eV. After table 15 this kind can be identified as a nitroso (C-N=O) group, the direct proof for tertiary radicals. The signal resulting from the oxime (C=NOH) group at 400.5eV is also present while the nitro (C-NO_2) and nitrite (C-ONO) groups at a binding energy of about 406eV became the most intensive signal.

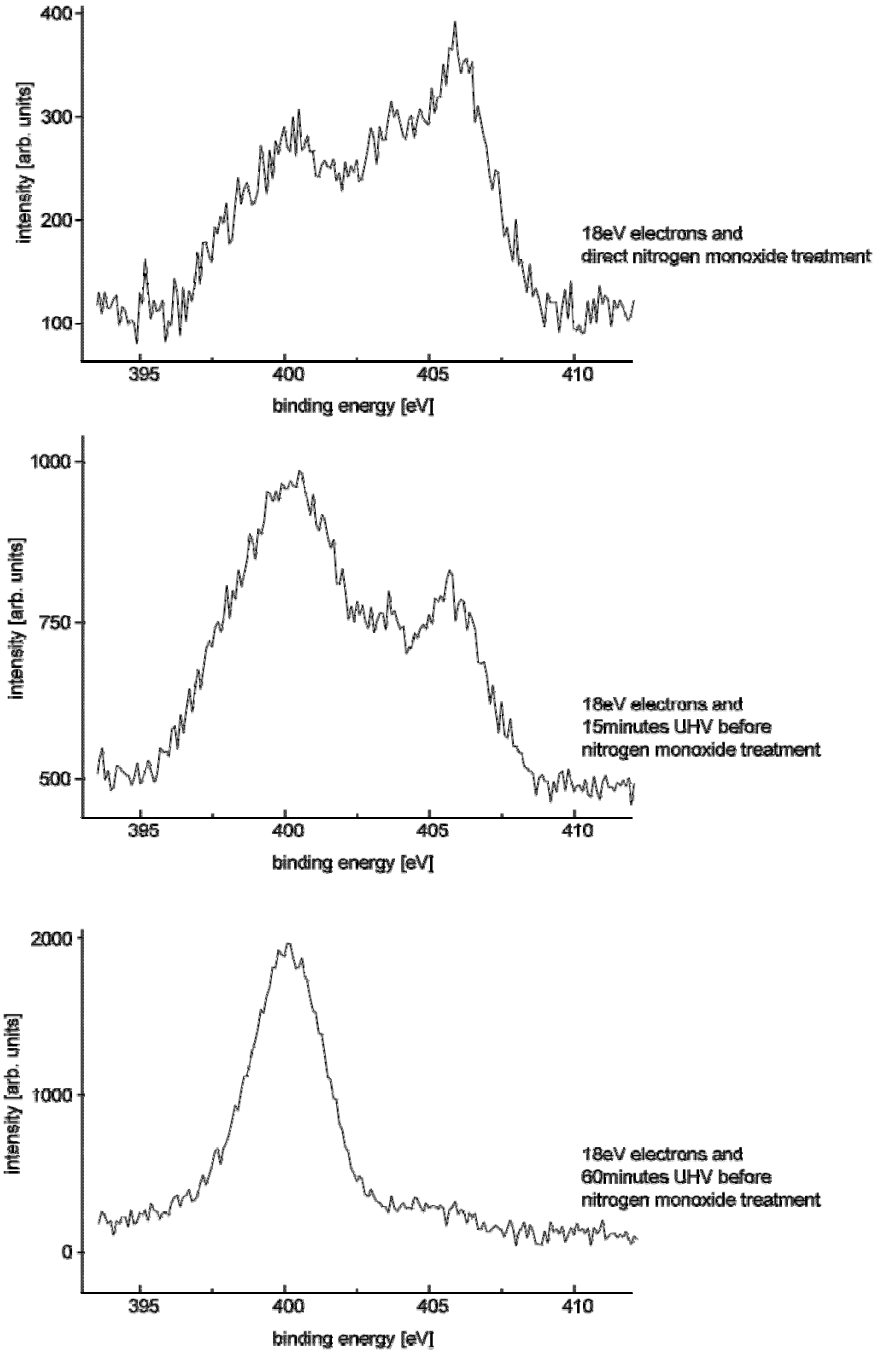

Figure 101: nitrogen monoxide after electron treatment with time

The spectrum shown in the middle of figure 101 was prepared under the same modification conditions, but stored afterwards for 15 minutes inside the UHV. While the nitrogen line at 406eV still exists, the intensity is less than before. Referred to the nitrile or oxime group, the nitroso group also diminished, but shows more intensity than the line with higher binding energy. The graph at the bottom of figure 101 corresponds to a derivatisation reaction with nitrogen monoxide one hour after the treatment with 18eV electrons. Here the intensity of the nitroso as well as for the nitro or nitrite group nearly vanished.

The intensities are fitted for the three groups. Their values are displayed in Table 16.

Delay between treatment and chemical labelling	oxime (C=NOH)	nitroso (C-N=O)	nitro ($C-NO_2$) and nitrite (C-ONO)
Immediately	31%	22%	47%
After 15 minutes	53%	20%	27%
After 60 minutes	93%	5%	2%

Table 16: different groups of the nitrogen signal

The measurements indicate a relative stability of secondary radicals while storage time leads to a passivation of tertiary radicals, as it can be concluded from the values of nitroso respectively nitro and nitrite groups. Remarkable is the slower decay of nitroso groups, as they only occur for the higher energetic electrons.

The experiments show that the electrons are splitting different bonds and consecutive reaction occur. As some reactions are exclusive dependent on tertiary radicals, cross-linkage must have been occurred. All resulting chemical groups can be explained by theoretical reaction paths, but the experiments need a lot of pre-work and the set-up has to be very elaborate to get such kinds of results.

After the presentation and discussion of so many different aspects of surface modification through plasma and separated effects of photons and electrons, the work will be summarised in the next chapter. Also some remarks will be given according to the further proceeding in this scientific field and the conclusions of this study for industrial applications.

5. Summary and Conclusions

In the previous chapters a wide range of aspects concerning to plasma analysis and modifications of polymers have been touched. This was necessary in order to work out *a fundamental analysis of the interaction of low pressure plasmas with polymer surfaces*:

- analysing different species inside an argon microwave discharge and their physical values;
- investigating the effects of these species towards a polymer surface on a microscopic scale;
- describing the modification by the isolated effects and modelling the plasma treatment through them.

Although this is a complex task, the whole process could be successfully demonstrated by a simplified model system of a microwave argon discharge. With this work new ideas for further investigations and finishing process applications also arose.

The first aspect of analysing the different species in an argon microwave was done by a LANGMUIR probe. This leads only to information about the particles. Data about the energy, charge carrier densities or potentials could be obtained. The results explain the role of electrons and therefore they are essential for modelling such a complex process like a microwave plasma.

Although the distribution of photons gives relevant information about the processes inside a discharge, it could not yet be investigated. On one hand the usage of a UV spectrometer with a resolution for vacuum ultraviolet is planned because even small amounts of contamination can be detected and even more important the radiation of the plasma can be characterised in a precise way. This examination will lead to more reliable information about the effect of radiation in the surface modification.

On the other hand a pure UV treatment could be achieved by using a crystal window to cover the sample from the influence of particles. Only the effects of high energy photons are neglected by this experimental set-up. To model these effects one can think of continuously tuneable light as it exists at synchrotron facilities.

At last, but not least, the ions need to be considered in more detail. With the LANGMUIR probe the ion density and the kinetic energy could be detected. While the usage of a noble process gases leads to little or no lasting interaction with the surface, impurities of the gas or small leaks of the apparatus spoil such “pure” modifications. The ions can be traced by their emission spectrum or by mass spectroscopy.

The second aspect was handled by using the available measurement techniques after modifying the polymer with plasma and the different species. In the procedure first the polymers were treated inside the discharge by different process gases (argon, oxygen, nitrogen) as well as just with UV-radiation or an electron beam. After the treatment the samples were brought in contact with air or labelling chemicals so created radical sites could react. The different labelling groups at the surface of the polymer were analysed by x-ray photoelectron spectroscopy according to their concentration and the angular (respectively depth) distribution.

All treatments lead to a change in the composition of the polymer surface, but the modifications differ between the treatments. For the oxidation of modified samples the plasma treatment gives the highest concentration and a weak angle distribution, while the separated effects show small changes and only for electrons an angle distribution could be observed. This distribution became more clear when the samples were stored inside the vacuum allow self-passivation reaction. Later they were chemically labelled with bromine and this label attacks the double bonds so that from the bromine distribution one can conclude the distribution of this binding type. All modifications show bromine in their analysis, but only plasma treatment shows a light and electron treatment a strong correlation with the electron emission angle. This can be understood with respect to the different penetration depths of radiation and particles (especially electrons) within the sample.

To cover another aspect in order to be more selective towards the fundamental modification processes, a radical passivation has been studied. The surface modification of polymers with electrons and a nitrogen monoxide treatment afterwards reveals the emergence of different nitrogen groups. While the treatment shows a threshold energy of 10eV before the peaks (respectively the radicals) appear due to the breakage of C-H-bonds, a higher electron energy give rise to tertiary radicals, which indicate cross-linkage reactions. Storing the electron modified polymers inside the vacuum before degassing them with nitrogen monoxide leads to a primary decay of the tertiary radicals.

The third aspect was achieved by comparing the different modifications and combining them in an accurate way. The depth distribution of double bonds through the argon microwave discharge therefore can be modelled by the addition of “normalised” electron and UV treatments. This was demonstrated by the chemical change in the surface composition after labelling with bromine as well as by the structural changes measured with the atomic force microscope.

This sequence of experimental steps will help in other discharge systems to gain a better understanding of the modification process and therefore this modelling could be a point of origin for a whole series of further investigations. The industrial application especially will have more possibilities by separated modifications of the bulk through UV and the surface through electrons. Also splitting the modification into several steps and functionalising the sample with different process gases between those steps could be interesting.

The complex theme of surface modification can only be approached by analysing the basic interactions between sample and discharge. Technological challenges are manifold and begin with the scaling-up of plasma processes. Coating at atmospheric pressure represents a major problem for plasma technology nowadays while other important topics of further research and development will be non-stationary, periodically or pulse-excited plasmas, reaction kinetics of multi-component plasmas and the computational simulation of plasmas to understand fundamental plasma processes and to design real systems.

The importance of the inner plasma parameters cannot be overestimated. Knowledge of them can be the key aspect to tailor surface properties and therefore this theme will be of major interest for the finishing industry. So far mainly outer parameters are used to characterise discharges which may lead to a wrong interpretation of measurements. Therefore the data obtained in plasma diagnostics can be used to enhance the quality of products by simulations or controlling the occurring processes [BMBF01]. Also a comparison of treatment processes becomes difficult without knowing the inner plasma parameters.

From a scientific point of view the next steps will lead in two directions. One is that a better correlation between plasma parameters and surface modifications is needed in the realm of the separated effects, especially the diagnostic of the UV radiation lack so far of experimental knowledge – at least to transfer the manifold results to the respective set-ups. The second aspect would be the extension of the chemical labelling to other basic reactions. For the used system of nitrogen monoxide labelling further measurements in an angle-resolved mode will give more details about the consecutive reactions.

6. Acknowledgement

In the first place I would like to thank apl. Prof. Dr. Manfred Neumann for his support and encouragement. The freedom he gave to me for my scientific development was not in vain. His help in the interpretation of results showed great experience.
Dr. Alfred Baalmann from the Fraunhofer Institute of Production Technology and Material Research was also a constant resource of profound questions and answers. Without him this work would probably became pathetic.

Former and actual colleagues are acknowledged for a pleasant atmosphere and several advises over all the years: Bolormaa Sanduijav, Stefan Bartkowski, Sorin Chiuzbãian, Daniela Hartmann, Karsten Küpper, Thorsten Meyer, Andreas Selinger, Albert Takacs, Werner Dudas, Sven Mähl, Mihaela Demeter, Bernd Schneider, Helmut Schürmann, Stefan Plogmann, Ralph Wilken, Volker Schlett, Stefan Dieckhoff, Lars Höper, Michel Reininger, Martin Görlich and others.
Special thanks in this list belong to Bolormaa, Helmut and Stefan. We shared over a long time the same “think tank” and had fruitful discussions about science and other relevant aspects of human life.
For helping with all the administrative work I would like to thank Marion von Landsberg and Birgit Guss. I will never forget your commitment at the end of the year 2000.
Lars Töben, Jenny Harris and Susan Kremer read parts of the manuscript. Thanks for helping me to improve my English.

This co-operation between the University of Osnabrück and the Fraunhofer Institute of Production Technology and Material Research received financial support from the Deutsche Forschungsgemeinschaft (NE276/11-1), which is gratefully acknowledged.

I am especially grateful for the support of my wife (she knows how much), my lovely son (who actually supported me by his deep sleep) and our families (who were forced to listen to my long monologues about plastics and plasma treatments).

I want to conclude with one of my favourite bible verses in Proverbs 1:7

> ***The fear of the LORD is the beginning of knowledge,***
> ***but fools despise wisdom and discipline.***

Appendix

In this appendix further information about polymers and the effects of different process gases as well as bibliography links will be presented.

Polymers

Polyethylene is composed of a multiplicity of ethylene blocks. Ethylene itself is a gaseous hydrocarbon with a double bond. The polymer is produced by linkage of a large number of ethylene molecules in a polymerisation process in two different procedures.

The high-pressure method was discovered in the thirties of the last century. The polymerisation of the ethylene is started by radicals at a pressure of 1500 to 3000bar and temperatures from 150 to 320°C and runs in a radical nuclear chain reaction. The formed Polyethylene results thereby as melted mass, which can be continued to process directly after the synthesis. The PE manufactured by this method consists of branched, bulky chains and indicates a relatively low density from 0.92 to 0.94 g/cm^3.

In the low pressure procedure at 60bar and 60 to 240°C, the polymerisation is achieved by catalysts. Those contain frequently titanium or magnesium. With this procedure, the formed PE results as insoluble powder which is converted for further applications to granulates. It contains a large proportion of linear chains which can be interpreted as regular structures (also mentioned as high crystallinity degree). According to its highly arranged structure it has fewer cavities and thus a high density from 0.94 to 0.97 g/cm^3 (called HDPE or PE-HD for high density). For the process development of the low pressure polymerisation with titanium KARL ZIEGLER and GIULIO NATTA received the Nobelprice for chemistry in 1963.

Polyethylene can be described in a chemical formula as $(C_2H_4)_n$, where the index n indicates the number of the track links which can amount to up to some hundred thousand. The next figure shows some unordered chains of PE and an ethylene molecule (white corner).

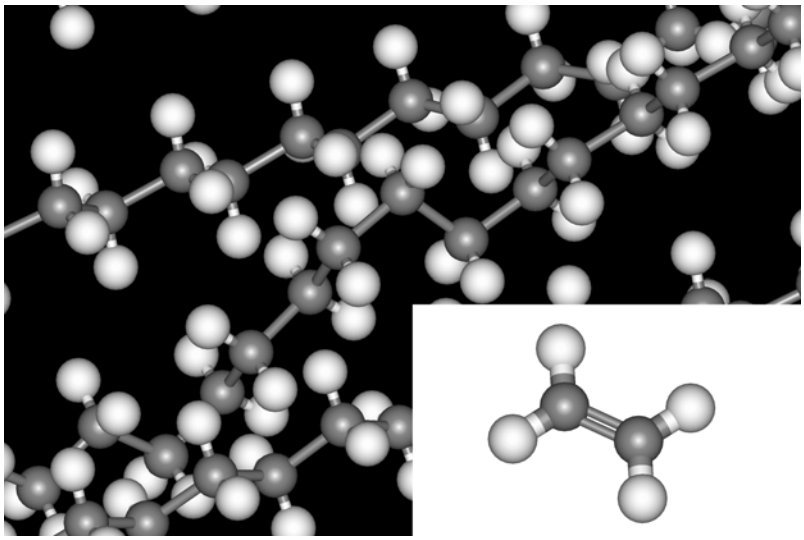

Figure 102: chains of PE and ethylene molecule

These large chain lengths correspond to the molecular mass of more than 5 million g/mol. Polyethylene shows an opposition to water, acids and bases as well as the usual chemical solvents. It is thermoplastic, i.e. it will became soft at temperatures about 130°C, and therefore can be processed easily. The mechanical characteristics such as hardness with ambient temperature, tenacity, transparency and melting temperature depend strongly on the chain length and the branch degree of the PE.

Polypropylene is a collective term for the chemical compounds made of the building block propylene, which is a gaseous hydrocarbon with three carbon atoms and a double bond (formula CH_3-CH=CH_2).

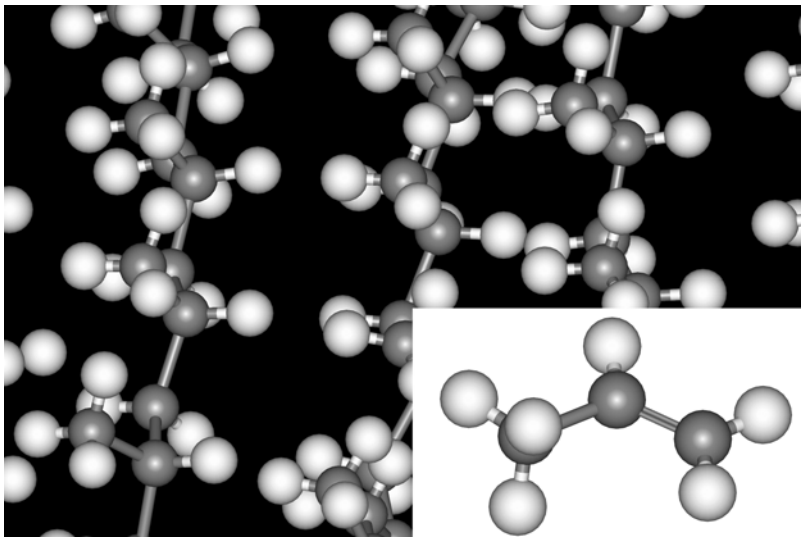

Figure 103: chains of PP and propylene molecule (white corner)

Polypropylene is manufactured at pressures of about 5 bar and at temperatures of about 50°C by aluminum or titan containing catalysts (ZIEGLER NATTA type). From the gaseous

propylene, chains are produced by the polymerisation, which consist of up to 20000 members. Its density is around 0.90g/cm³.

The Polypropylene can be produced in spatial different forms on molecular level in opposite to the chemically similar Polyethylene by the arrangement of the methyl group (CH_3). A regular sequence of orientation is called *isotactical*. This geometric structure is of large industrial importance because of its high crystallinity (which microscopically leads to hardness, stiffness and stability against temperatures up to 150 °C).

When two sequential groups of methyls arrange in an alternating form, this is called syndiotactic (Greek ISO: directly; syn: together; dio: two). A third arrangement is called atactic for an irregular sequence of orientation. By the selection of a suitable catalyst a large influence on the tacticity can be taken.

These configurations can be compared in the next figure, in which the rest group (R) must be replaced by a CH_3 group.

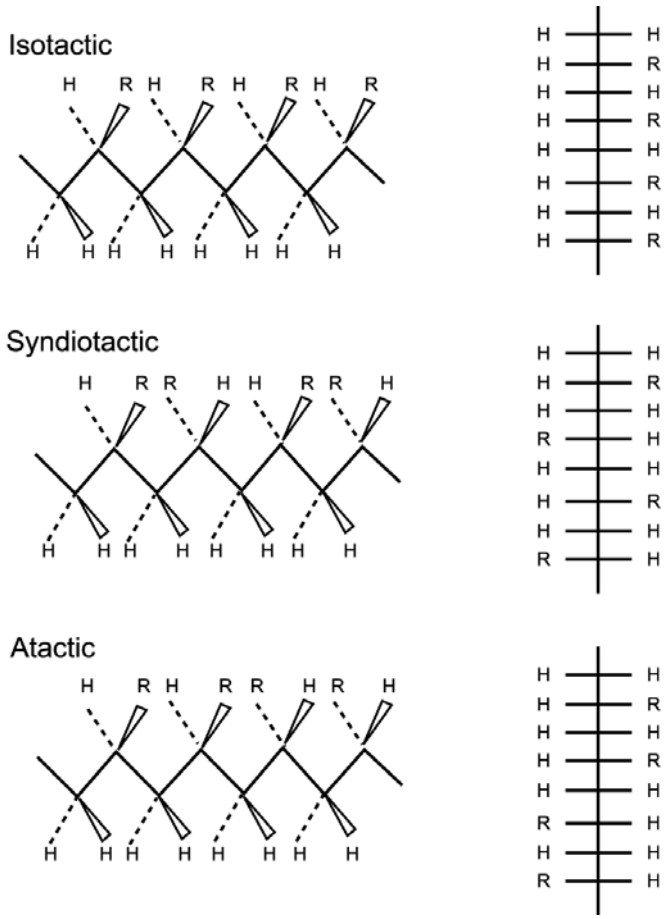

Figure 104: configuration of mono-substituted Polyethylene

Surface modifications for different process gases

The following table is a compilation of surface modifications. The references were collected by RIESS [Ries01] and extended by own inquiries.

Process gas	Surface modifications	Reference
Inert gases (Argon, Helium, Neon)	• Intense cross-linkage due to UV-radiation • Chain breakage • Incorporation of oxygen groups after contact with air • Formation of C=C-bonds • Improvement of wettability • Removal of adhesion decreasing layer	[FKG80] [Betz93] [Gere90] [HaSc66] [Tama93] [LoCo86] [RoIn95] [Coul93] [BVBG94]
Water	• Intense erosion • Incorporation of oxygen groups after contact with air • Improvement of wettability	[FKG80] [Viss93]
Oxygen	• Cross-linkage • Incorporation of oxygen • Formation diminishing from C=C. • Intense erosion of layers. • Modifications of crystallinity through selective corrosion of the amorphous areas • Improvement of wettability	[FKG80] [Gere90] [LaWa83] [Viss93] [Bisc88] [FBB91] [MOG90] [FoHu92] [FrEr94] [PaKi94] [CaJo92] [HBZ93] [ChBr91] [ITA92] [ChGa93] [VaGa89] [BVBG94]
Nitrogen	• Intense cross-linking due to UV-radiation • Improvement of wettability • Incorporation of oxygen and nitrogen containing groups • Creation of C=C-bonds • Mild decomposing • Mild increase of amorph parts • Removal of adhesion decreasing layer	[Gere90] [FBB91] [Bisc88] [HoBe93] [FoHu92] [FIH91] [Anto87] [FoIn90] [Coul93]
Hydrogen	• Intense cross-linkage due to UV-radiation • Incorporation of oxygen groups after contact with air • Creation of C=C-bonds • Mild decomposing • Mild increase of amorph parts • Improvement of wettability • Removal of adhesion decreasing layer	[FKG80] [FLG81] [Küpp95]
CO and CO_2	• Incorporation of oxygen groups • Improvement of adhesion for fibres • Creation of C=C-bonds • Mild decomposing • Long time surface modifications • Improvement of wettability • Removal of adhesion decreasing layer	[PoCh90] [ITO90a]
NO and NO_2	• Incorporation of oxygen and nitrogen containing groups • Improvement of wettability	[ITO90b]
NH_2 and NH_3	• Cross-linking • Improvement of wettability and adhesion • Incorporation of oxygen and nitrogen containing groups • Creation of C=C-bonds • Mild decomposing • Bio compatibility	[ChBr91] [Merc94] [CoLo73] [ITK89] [HoSt69] [WuGu95] [LiCo93] [FLG86]
Air	• Incorporation of oxygen and nitrogen containing groups • Creation of C=C-bonds • Improvement of wettability (long time) and adhesion	[OgPo85] [Merc94] [BhJo94] [CoLo73]

Table 17: surface modifications of different process gases

Bibliography

ACW90	S. Akhter, K. C. Cannon, J. M. White. Distribution of compositional defects in solvent cast polyvinyl alcohol films: angular dependent xps and reactivity study. Appl. Surf. Sci. 44 (1990) 49-57
Albe94	T. Albers. Untersuchung stoßinduzierter Effekte bei der Tiefenprofilanalyse an oxidischen Multischichtsystemen mittels Röntgenphotoelektronen-Spektroskopie. Thesis, University of Osnabrück (1994)
Andr85	J. D. Andrade. Surface and Interfacial Aspects of Biomedical Polymers, Volume 1, J. D. Andrade Ed., Pleum Press, New York, (1985)
Anto87	K. Antolin. Effect of Nitrogen Plasma on Polypropylene. ANTEC ´87, S. 1522-1524
Auge25	P. Auger, J. Phys. Radium. 6 (1925) 205
AWvS90	W. A. M. Aarnink, A. Weishaupt and A. van Silfhout, Appl. Surf. Sci., 45 (1990) 37
Basc91	O. A. Baschenko, M. A. Tyzykhov, V. I. Nefedov, G. Polzonetti, M. V. Russo, A. Furlani. Iodine incorporation into polymeric films investigated by angle-resolved XPS. J. Electron Spectrosc. Relat. Phenom. (1991), 203-209
BBK77	D. Briggs, D. M. Brewis and M. B. Konieczko. J. Mater. Sci. 12 (1977), 429ff
Bear90	B. C. Beard. Cellulose Nitrate as a Binding Energy Reference in N(1s) XPS Studies of Nitrogen-Containing Organic Molecules. Appl. Surf. Sci. 45 (1990), 221
BeBr92	G. Beamson, D. Briggs, High Resolution XPS of Organic Polymers, J. Wiley & Sons, Chichester 1992
BeSp64	C. N. Berglund, W. E. Spicer. Photoemission Studies of Copper and Silver: Theory. Phys. Rev. 136 A (1964), 1030
Betz93	Betz, W.: Polyoxymethylen im neuen Gewand. Kunststoffe 83 (1993) 7, S. 527-530
BhJo94	Bhat, N.V.; Joshi, A.H.: Surface modification of polyethylene films by low temperature plasma. Polym. Sci.: 2 (1994), S. 839-844
Bika71	N. Bikales. Characterization of Polymers. Encyclopedia of Polymer Science and Technology, Wiley-Interscience, New York, 1971, p.91
Binn87	G. Binnig, Ch. Gerber, E. Stoll, T.R. Albrecht und C.F. Quate. Atomic Resolution with Atomic Force Microscope Europhys. Lett. 3 (12), (1987) 1281
Bisc88	Bischoff, R.: Einfluß unterschiedlicher Oberflächenvorbehandlungen auf Klebbarkeit, Alterung und Oberflächenbeschaffenheit von Polypropylen. Hinterwaldner Verlag, München 1988
BMBF01	Plasma Technology - Process Diversity and Sustainability.German Federal Ministry of Education and Research. November 2001
Bors85	G. Borstel, Theoretical aspects of photoemission, Appl. Phys. A 38 (1985),193-204
Bove72	F. Bovery. High Resolution NMR of Macromolecules. Academic Press, New York, 1972
BQG86	G. Binnig, C.F. Quate und Ch. Gerber. Atomic Force Microscope Phys. Rev. Lett. 56 (1986) 930.
Brai00	N. St. J. Braithwaite. Introduction to gas discharges. Plasma Sources Sci. Technol. 9 (2000) 517-527
BrBa79	C. R. Brundle and A. D. Baker, Electron Spectroscopy: Theory, Techniques and Applications, John Wiley & Sons, Bristol, 1979
BRGW82	G. Binnig, H. Rohrer, Ch. Gerber und E. Weibel. Tunneling through a controllable vacuum gap Appl. Phys. Lett. 40 (1982) 178.
Brig98	D. Briggs. Surface Analysis of Polymers by XPS and Static SIMS. Cambridge University Press. 1998
Brow57	H. E. Brown. The reaction of nitric oxide with isobutylene. J. Amer. Chem. Soc.79 (1957), 2480
BrSe83	D. Briggs and M. P. Seah, Practical Surface Analysis by Auger and X-ray Photoelectron Spectroscopy, John Wiley & Sons, 1983
BuCo93	N.A. Burnham und R.J. Colton. Force Microscopy aus D.A. Bonnell : Scanning tunneling microscopy and spectroscopy VCH Publishers Verlagsgesellschaft (1993).
BuHo85	T. D. Bussing and P. H. Holloway. Deconvolution of concentration depth profiles from angle resolved x-ray photoelectron spectroscopy data. J. Vac. Sci. Technol., A3 (1985) 1973

Burk54	C. A. Burkhard, J. F. Brown, C. S: Herrick, R. L. Myers, D. T. Hurd, Abstract of Papers, 126th Meeting American Chemical Society (September 12-17, 1954, 42
BVBG94	A. Baalmann, K. D. Vissing, E. Born, A. Gross. Surface Treatment of Polyetheretherketone (PEEK) Composites by Plasma Activation. J. Adhesion 46 (1994)
CaDi99	B. Cappella, G. Dietler. Force-distance curves by atomic microscopy. Surf. Sci. Reports 34 (1999) 1-104
CaJo92	C. M. Carlsson, K. S. Johansson. Plasma modification and its effect on polymer-polymer and polymermetal adhesion. Polym. Mat. Sci. Eng. 67 (1992), S. 21/22
Carl67	T. Carlson. Double electron ejection resulting from photoionization in the outermost shell of He, Ne, and Ar, and its relationship to electron correlation. Phys. Rev. 156, 142 (1967)
CGNS95	M. Coullaud, P. Groening, S. Nowak, L. Schlapbach. Plasma treatment of polymers: the effect of the plasma parameters on the chemical, physical, and morphological states of the polymer surface and on the metal-polymer interface. In: K. L. Mittal (Ed.). Polymer Surface Modification: relevance to Adhesion, VSP 1995
CGS78	P. Chadman, G. Gosserge, J. D. Scott. The determination of the photoelectron escape depths in Polymers and other materials. J. Electron Spectosc. Relat. Phenom. 13 (1978) 1
Chap80	B. Chapman, Glow Discharge Processes, John Wiley & Sons, New York (1980)
ChBr91	P. J. Chappell. J. R. Brown. Surface modification of extended chain polyethylene fibres to improve adhesion to epoxy and unsaturated polyester resins. Surface and Interface Analysis 17 (1991), S. 143-150
Chen65	F. F: Chen, Plasma Diagnostic Techniques, R. H. Huddlestone (Editor), Academic Press, New York (1965)
ChFu00	T. Chevolleau, W. Fukarek. Ion flux, ion energy distribution and neutral density in an inductively coupled argon discharge. Plasma Sources Sci. Technol. 9 (2000) 568-573
ChGa93	Y. Chaoting, S. Gao. Effect of low-temperature-plasma surface treatment on the adhesion of ultra-highmolecular-weight-polyethylene fibres. J. of Mat. Sci. 28 (1993), S. 4883-4891
CKH96	C.M. Chan, T. M. Ko, H. Hiraoka. Polymer surface modification by plasmas and photons, Surface Science Reports 24 (1996) 1-54
CoLo73	G. Collins, A. C. Lowe. An analysis of PTFE surfaces modified by exposure to glow discharge. European Polymer J. 9 (1973), S. 1173-1185
Coul93	M. Coullaud, S. Nowak, O. M. Küttel, P. Gröning, L. Schlapbach. Surface modifications of polypropylene after in–situ Ar and N2 plasma treatments: an XPS study. Applied Surface Science 72 (1993) 19-29
CTT75	P. M. Chung, L. Talbot, K. J. Touryan, Electrical Probes in Stationary and Flowing Plasmas, Springer Verlag, Berlin (1975)
Cump95	P. J. Cumpson. Angle resolved XPS and AES: depth-resolution limits and a general comparison of properties of depth-profile reconstruction methods. Journal of Electron Spectroscopy an Related Phenomena, 73 (1995), 25-52
DaFe81	L. C. Davis, L. A. Feldkamp. Resonant photoemission involving super-Coster-Kronig transitions. Phys. Rev. B 23 (1981) 6239
Deke73	W. Dekeyser, L. Fiermans, G. Vanderkelen, and J. Vennik, Electron Emission Spectroscopy, D. Reidel Publishing Company, Dordrecht-Holland, 1973
Deme01	M. Demeter, Thesis, Spectroscopic study of transition metal compounds. University of Osnabrück (2001)
Dilk77	A. Dilks. Thesis. The application of ESCA to structure, bonding and reactivity of some polymer systems with particular reference to surface modification. University of Durham, 1977
DoSu70	S. Doniach and M. Sunjic, Many-electron singularity in X-ray photoemission and X-ray line spectra from metals, J. Phys. C: Solid St. Phys. 3 (1970), 285-291.
Dros78	H. Drost. Plasmachemie, Akademie-Verlag, Berlin 1978, S. 20/21
Druy30	M. J. Druyvesteyn. Der Niedervolt Bogen. Z. Phys. 64, 781 (1930)
Eins05	A. Einstein. Über einen die Erzeugung und Verwendung des Lichts betreffenden heuristischen Gesichtspunkt. Annalen der Physik, 17 (1905), 132ff.
EvRe81	D. S. Everhart, C. N. Reilley. Functional Group Mobility. Surface Interface Analysis 3, 126-133 (1981)

Extr94	C. W. Extrand. Spin coating of very thin polymer films. Polym. Eng. Sci. 34 (5). 1994 390-394
Fadl78	C. S. Fadley: Basic concepts of X-ray Photoelectron Spectroscopy, in Electron Spectroscopy: Theory, Techniques and Applications Vol. 2. Brundle, Baker (Ed.), Academic Press London 1978
Fadl84	C. S. Fadley. Angle-Resolved X-Ray Photoelectron Spectroscopy. Progress in Surface Science 16, 275-388, 1984
FaSh70	C. S. Fadley and D. A. Shirley, Multiplet splitting of metal-atom electron binding energies, Phys. Rev. A 2 (1970), no. 4, 1109-1120
FBB91	R. Foerch, G. Beamson, D. Briggs. XPS valence band analysis of plasma-treated polymers. Surface and Interface Analysis 17 (1991), S.842-846
FeLo00	C. M. Ferreira, J. Loureiro. Electron kinetics in atomic and molecular plasmas. Plasma Sources Sci. Technol. 9 (2000) 528-540
FeSm85	J. Ferrante, J.R. Smith. Theory of the bimetallic Interface Phys. Rev. B 31 (1985) 3427
FIH91	R. Foerch, N. S. Intyre, D. H. Hunter. Plasmamodifikation von Kunststoffoberflächen on line. Kunststoffe 81 (1991) 3, S. 260-262
FKG80	J. Friedrich, G. Kühn, J. Gähde. Untersuchungen zur Plasmaätzung von Polymeren. Teil 1, Acta Polymerica 30 (1979) 8, S. 470-477; Teil 2, Aca Polymerica 31 (1980) 1, S. 52-58; Teil 3, Acta Polymerica 31 (1980) 1, S. 59-62
Flen93	U. Flender. Messung von Ionenenergieverteilungen hinter der Randschicht einer Hochfrequenz-Entladung in Verbindung mit Langmuirsondenmessungen. Thesis. Universität Bochum 1993
FLG81	J. Friedrich, I. Loeschke, J. Gähde. Untersuchungen zur Plasmaätzung von Polymeren. Teil 6: Veränderungen an der Oberfläche von Polypropylen. Acta Polymerica 32 (1981) 48, S. 337-343
FLG86	J. Friedrich, I. Loeschke, J. Gähde. Zur Adhesion von Aluminium auf Polypropylen. Acta Polymerica 37 (1986) 11/12, S. 687-695
FoHu92	R. Foerch, D. H. Hunter. Remote Nitrogen Plasma Treatment of Polymers. J. of. Polym. Sci.: Part A: Polym. Chem. 30 (1992), S. 279-286
FoIn90	R. Foerch, N. S. Intyre. Nitrogen Plasma Treatment of Polyethylene and Polystyrene in a Remote Plasma Reactor. J. of Appl. Polym. Sci. 40 (1990), S. 1903-1915
Fran94	G. Franz. Oberflächentechnologie mit Niederdruckplasmen. Springer Verlag, Berlin Heidelberg 1994
FrEr94	J. F. Friedrich, J. Erdmann. Vorbehandlung von Polymeren mit Normal- und Niederdruckplasmen zur Herstellung hochfester Verklebungen mit Polyurethan. GAK 47 (1994) 6, S. 382-388
Frey95	Helmut Frey (Hrsg.) Plasmaphysik, Plasmadiagnostik, Analytik. Düsseldorf, VDI Verlag, 1995
GAM95	H.-J. Güntherodt, D. Anselmetti und E. Meyer. Forces in scanning probe methods. NATO ASI Series, Series E: Applied Sciences Vol. 286 (Kluwer Academic Publishers 1995)
Gere90	L. J. Gerenser. XPS studies of plasma-modified polymer surfaces. Polym. Mater. Sci. Eng. (1990) 62, 125-129
GeSc87	K. W. Gerstenberger, D. Schön in: G. Spur, Th. Stöferle (eds.), Handbuch der Fertigungstechnik, Band 4, Kapitel 2.3.5., Carl Hanser Verlag, München (1987)
Ghos83	P. K. Ghosh, Introduction to photoelectron spectroscopy, John Willey & Sons, New York/ Chicester/ Brisbane/ Toronto/ Singapore, 1983
Gies97	F.J. Giessibl. Forces and frequency shifts in atomic-resolution dynamic-force microscopy. Phys. Rev. B 56 (1997) 16010
GoGa91	F. O. Goodman und N. Garcia. Roles of attractive and repulsive forces in atomic force microscopy Phys. Rev. B 43 (1991) 4728
GoHa76	J. J. Gonzales. P.C. Hammer. Polym. Lett. 14, 645 (1976)
Grab93	M. G. Grabherr, H. Ebel, M. F. Ebel, R. Svagera and G. Baron, J. Electron Spectrosc. Relat. Phenom., 63 (1993) 43
Greu98	W. Greulich. Lexikon der Physik. Spektrum Akademischer Verlag 1998
GrKü95	P. Gröning, O. M. Küttel, M. Collaud-Coen, G. Dietler, L. Schlapbach. Interaction of low-energy ions (<10eV) with polymethylmethacrylate during plasma treatment. Applied Surface Science 89 (1995) 83-91

GüWi92	H. J. Güntherodt, R. Wiesendanger. Scanning Tunneling Microscopy I Springer Series in Surface Sciences 20. Berlin 1992
Haef91	R. Haefer. Oberflächen- und Dünnschichttechnologie. Teil 2, Kap. 5: Modifizierung von Oberflächen durch Plasma-Verfahren. Springer Verlag, Berlin 1991
Hall89	W. Hallwachs, Über Den Zusammenhang Des Electricitätsverlustes Durch Beleuchtung Mit Der Lichtadsorption, Annalen der Physik, 37 (1889), 666-675
HaSc66	R. H. Hansen, H. Schonhorn. Technique for preparing low surface energy polymers for adhesive bonding. J. Polym. Sci. Polym. Letters 4 (1966), S. 203-209
Hazl90	R. D. Hazlett. Fractal Applications: Wettability and Contact Angle. Journal of Colloid and Interface Science, Vol 137, No 2 (1990)
HBZ93	A. Holländer, J. Behnisch, H. Zimmermann. Surface modification of poly(ethylene) in an rf downstream remote plasma reactor. J of Appl. Polym. Sci. 49 (1993), S. 1857-1863
HeHo99	W. F. Heinz, J. H. Hoh. Spatially resolved force spectroscopy of biological surfaces using the atomic force microscope. Tibtech April 1999 (Vol. 17)
Hert87	H. Hertz. Über Einen Einfluß Des Ultravioletten Lichtes Auf Die Electrische Entladung, Annalen der Physik, 31 (1887), 983-1000
Hide97	Hiden Analytical Ltd. Electrostatic Plasma Probe Operating Instructions. ESP V3.12 Manual (1997)
HiLe39	R. Hill, J. R. Lewis. Tranc. Faraday Soc. 35, 1073 (1939)
HLMG95	L. Howald, R. Lüthi, E. Meyer und H.-J. Güntherodt. Atomic force microscopy on the Si (7x7) surface. Phys. Rev B 51 (1995) 5484
HoBe93	A. Holländer, J. Behnisch. Surface Modifikation of Poly(Ethylene) in an rf Downstream Remote Plasma Reactor. J. of Appl. Polym. Sci. 49 (1993), S. 1857-1863
Holl82	J. M. Hollas, High resolution spectroscopy, Butterworths & Co, London, 1982
Hörs99	I. Hörsch. Experimentelle Aspekte der Mikroskopie und Spektroskopie im optischen Nahfeld. Dissertation (Ulm 1999).
HoSt69	J. Hollahan, B. B. Stafford. Attachment of Amino Groups to Polymer surfaces by Radiofrequency Plasmas. J. Appl. Polym. Sci. 13 (1969), S. 807-816
Hüfn95	S. Hüfner, Photoelectron spectroscopy, Springer-Verlag, Berlin Heidelberg, 1995
Hutc87	I. H. Hutchinson, Principles of Plasma Diagnostics, Cambridge University Press, Cambridge (1987)
HWS72	J. Haslam, H. A. Willis, M. Squirrell. Identification and Analysis of Plastics, 2nd edition. Ileffe, London. 1972
IIT67	M. Iwasaki, T. Ichkawa, K. Toriyama. J. Polym. Sci, Polym. Letters 5 (1967), 423
ITA92	N. Inagaki, S. Tasaka, H. Abe. Surface Modification of Polyethylene Powder using Plasma Reactor with Fluidized Bed. J. of Appl. Polym. Sci.: 46 (1992), S. 595-601
ITK89	N. Inagaki, S. Tasaka, H. Kawai. Improved adhesion of poly(tetrafluoroethylene) by NH – plasma 3 treatment. J. Adh. Sci. Technol. 3 (1989) 8, S. 637-649
ITO90a	N. Inagaki, S. Tasaka, J. Ohkubo. Hydrophilic surface modification of polyethylene by plasma exposure. Polym. Prep. 31 (1990) 2, S. 380-381
ITO90b	N. Inagaki, S. Tasaka, J. Ohkubo. Hydrophilic surface modification by plasma of nitrogen oxides. Poly. Mater. Sci.: Eng. 62 (1990), S. 145-149
Kami97	W. Kaminsky. Polymersiation von Olefinen mit Metallocenen. Spektrum der Wissenschaft. 2/97, 85ff
Kers01	H. Kersten. Modeling of plasma-wall interaction in Low Temperature Plasma Physics. Fundamental Aspects and Applications von Rainer Hippler, Sigismund Pfau, Martin Schmidt and Karl H. Schoenbach. Wiley-VCH Verlag. 2001
Keud00	A. von Keudell. Surface Processes during thin-film growth. Plasma Sources Sci. Technol. 9 (2000) 455-467
KhOv00	M. H. Khater, L. J. Overzet. A new inductively coupled plasma source design with improved azimuthal symmetry control. Plasma Sources Sci. Technol. 9 (2000) 545-561
Koen80	J. L. Koenig. Chemical Microstructure of Polymer Chains. Wiley-Interscience, New York. 1980
Koen99	J. L. Koenig. Spectroscopy of Polymers, 2nd edition. Elesevier. Amsterdam 1999
KoMa70	H. R. Koenig and L.J. Maissel. Application of RF-Discharges to Sputtering, IBM J. Res. Develop. 14, 168-171 (1970)

Konu92	M. Konuma. Film Deposition by Plasma Techniques. Springer Verlag, Berlin (1992)
Koop33	T. Koopmans. Über die Zuordnung von Wellenfunktionen und Eigenwerten zu den eizelnen Elektronen einer Atoms, Physica 1 (1933), 104-113
Kort00	Korth Kristalle GmbH, Datasheet (2000)
KrCa67	M. O. Krause, T. A. Carlson. Vacancy Cascade in the Reorganization of Krypton Ionized in an Inner Shell. Phys. Rev. 158, 18, (1967)
Küpp95	J. Küppers. The Hydrogen Surface Chemistry of Carbon as a Plasma Facing Material. Surf. Sci. Reports 22 (1995) 249-321
Kuzm98	H. Kuzmany, Solid state spectroscopy- an introduction, Springer-Verlag, Berlin Heidelberg, 1998
LaMS26	I. Langmuir, H. M. Mott-Smith. The Theory of Collectors in Gaseous Discharges. Phys. Rev. 28, 727 (1926)
LaWa83	N. H. Ladizesky, I. M. Ward. A study of the adhesion of draw polyethylene fibre/polymeric resin systems. J. Mat. Sci. 18 (1983) 2, S. 533-544
LBP60a	E. J. Lawton, J. S. Balwit, R. S. Powell. Paramagnetic-Resonance Studies of Irradiated High-Density Polyethylene. I. Radical Species and the Effect of Environment on Their Behaviour. Journal of Chemical Physics. Vol 33 No 2, 1969
LBP60b	E. J. Lawton, J. S. Balwit, R. S. Powell. Paramagnetic-Resonance Studies of Irradiated High-Density Polyethylene. II. Effect of Irradiation Dose on the Radical Species Trapped at Room Temperature. Journal of Chemical Physics. Vol 33 No 2, 1969
LiCo93	J. C. Lin, S. L. Cooper. Plasma Surface Modification of the Inner Surface of LDPE-Tubing for Biomedical Application. Polym. Prep. 34 (1993) 1, S. 659/660
LoCo86	Loh, I.H.; Cohen, E.: Plasma Surface Modification of Polymer Powders with Application to Thermal Energy Storage. J. of Appl. Polym. Sci. 31 (1986), S. 901-910
LoHo68	W. Lochte-Holtgreven, Plasma Diagnostics, North-Holland Publishing Company, Amsterdam (1968)
Lu75	C. S. Lu. Mass determination with piezoelectric quartz crystal resonators. J. Vac. Sci. Technol. 12 (1975), 578
Luet93	H. Lueth. Surfaces and interfaces of solid materials, Springer, Berlin,1993
Lütk97	S. Lütkehoff. Thesis, University of Osnabrück (1997)
Mähl94	S. Mähl. Diploma, University of Osnabrück (1994)
Mähl96	S. Mähl, J. Lachnitt, R. Niemann, M. Neumann, A. Baalmann and V. Schlett. Innovative Methods for a Deconvolution of XPS-Spectra from Plasma Oxidized Polyethylene. Surf. Interface Anal. 24, 405-410 (1996)
Mähl97	S. Mähl. Grundlegende Untersuchungen zur Charakterisierung plasmamodifizierter Polyolefinoberflächen mittels Röntgen-Photoelektronenspektroskopie. Thesis, University of Osnabrück (1997)
Mähl99	S. Mähl, M. Neumann, B. Schneider, V. Schlett, A. Baalmann. Analysis of XPS Valence Band Spectra of Polymers using DFT Band Calculations of Model Oligomers. J. Polymer Science A37, 95 - 103 (1999)
Mare00	J. Marec. Mircowave Plasmas. Lecture at CLTPP Socrates Course 2000 in Eindhoven
Merc94	F. P. M. Mercx. Improved adhesive properties of high-modulus polyethylene structures. Polymer 35 (1994) 10, S. 2098-2106
MMB97	S. Molitor, J. Miltat und L. Belliard. MFM Messungen an Co/Pt Multischichten OMICRON Vakuumphysik GmbH / Université Paris-Sud (F) (1997)
MNSB98	Some Aspects to the Fitting of XPS Core Spectra of Polymers. S. Mähl, M. Neumann, V. Schlett, A.Baalmann. Surf. Interface Anal. 26, 204-212 (1998)
MOG90	Morra, M.; Ochiello, E.; Gila, L.: Surface dynamics of adhesion in oxygen plasma treated polyolefins. J. Adhesion 33 (1990), S. 77-88
Moli00	S. Molitor. Thesis, University of Osnabrück (2000)
Nano03	Nanosensors Datasheet (2003)
Natt60	G. Natta. Progress in the Stereospecific Polymerization. Makromol. Chem. 35 p94 (1960)
NeBa88	V. I. Nefedov and O. A. Baschenko. Relative intensities in ESCA and qualitative depth profiling. J. Electron Spectrosc. Relat. Phenom., 47 (1988) 1
NeKo00	N. Nestle and B. Koslowski in an essay “Ober- und Grenzflächenphysik”, Lexikon der Physik, 2000

Nors79	H. Norstrøm. Langmuir Probe Studies of the Glow Discharge in an RF Sputtering System at various Frequencies, Vacuum 29 (11/12), 443-445 (1979)
Öchs97	R. Öchsner. Modifikation der Oberflächeneigenschaften von Polymeren durch Ionenimplantation. Thesis University of Erlangen-Nürnberg Shaker Verlag 1997
OgPo85	T. Ogita, A. N. Ponomarev. Surface structure of low-density polyethylene film exposed to air plasma. J. Macromol. Sci.: - Chem. A 22 (8) (1985), S. 1135-1150
OkKo92	K. Okada and A. Kotani, Interatomic and intra-atomic configuration interactions in core-level X-ray photoemission spectra of late transition metal compounds, J. Phys. Soc. Jpn. 61 (1992), no. 12, 4619-4637.
PaKi94	S. H. Park, S. D. Kim. Plasma surface treatment of HDPE-powder in a fluidized bed reactor. Polymer Bulletin 33 (1994), S. 249-256
Paul60	L. C. Pauling. The Nature of the Chemical Bond and the Structure of Molecules and Crystals. Ithaca, N. Y. , Cornell university Press, 1960
PECB94a	F. Poncil-Epaillard, B. Chevet, J. C. Brosse. Study of Aramid Surface Reactivity: Modification with a Cold Plasma or a Electron Beam followed by a Postgrafting Reaction. J. Appl. Polym. Sci. 52 (1994), 1047
PECB94b	F. Poncil-Epaillard, B. Chevet, J. C. Brosse. Modification of Isotactic Polypropylene by a Cold Plasma or an Electron Beam and Grafting of the Acrylic Acid onto these activated Polymers. J. Appl. Polym. Sci. 53 (1994), 1291
PeEl91	Perklin-Elmer, ESCA: Technical Manual, 5600 technique, 1991
PGE86	J. M. Pochan, L. J. Gerenser and J. F. Elman. An e.s.c.a. study of the gas-phase derivatization of poly(ethylene terepthalate) treated by dry-air and dry-nitrogen corona discharges. Polymer 27 (1986), 1058ff
PlEb82	E. W. Plummer and W. Eberhardt, Angle-resolved photoemission, Adv. In Chem. Phys. 49 (1982), 533-649
PoCh90	F. Poncin-Epaillard. B. Cheret. Functionalization of polypropylene by a microwave (433 MHz) cold plasma of carbon dioxide. Eur. Polym. J. 26 (1990) 3, S. 333-339
Povs94	V. I. Povstugar, A. M. Lyakhovich, A. A. Shakov. Bromination reaction in C=C double bond determination by XPS, Journal of Electron Spectroscopy an Related Phenomena, 68 (1994), 565-568
Ques02	Quesant Instrument Corporation. Operator's Manual. Q-ScopeTM 250/350/400/850 and NomadTM. V4.00 April 2002
Rein01	M. Reiniger. Rasterkraftmikroskopie an dünnen organischen und metall/organischen Schichten auf Siliziumoxid. Osnabrück, Univ., Diss., 2001
RiDw74	W. M. Riggs and D. W. Dwight. Characterization of Fluoropolymer Surface. J. Electron Spectrosc. Rel. Phenom. 5 (1974), 447ff
Ries01	K. Rieß. Thesis. Plasmamodifizierung von Polyethylen. Martin Luther Universität Halle-Wittenberg 2001
RME88	D. Rugar, H.J. Mamin, R. Erlandsson, J.E. Stern und B.D. Terris. Force microscope using a fiber - optic displacement sensor. Rev. Sci. Instrum. 59 (1988) 2337.
Robe80	R. F. Roberts, D. L. Allara, C. A. Pryde, D. N. E. Buchanan, N. D. Hobbins, Surf. Interface Anal. 2 (1980) 5
RoIn95	A. Rossi, L. Incarnato. Modification of barrier properties of polymeric films of LDPE and HDPE by cold plasma treatment. J. of Polym. Eng. 14 (1995), S. 191-197
Roos91	A. J. van Roosmalen. J.A.G. Baggerman and S. J. H. Brader Dry Etching for VLSI. Plenum Press New York 1991
Ruts84	A. Rutscher. Plasmatechnik. Carl Hanser Verlag. Munich (1984)
Saue59	G. Z. Sauerbrey. Schwingquarze zur Wägung dünner Schichten. Zeit. Physik 155 (1959), 206
Schn01	B. Schneider. Untersuchungen zur elektronischen und geometrischen Struktur ausgewählter oxidischer und sulfidischer Materialien mittels Photoelektronen und Röntgenspektroskopie. Thesis, University of Osnabrück (2001)
Schr00	D. C. Schram. Plasma Characterstic Dimensions and Time Constants. Lecture at the CLTPP Socrates Intensive Course 2000 in Eindhoven
SeTa72	T. Seguchi, N. Tamura. Mechanism of Decay of Alkyl Radicals in Irradiated Polyethylene on Exposure to Air as Studies by Electron Spin Resonance. Journal of Physical Chemistry. Vol 77 No 1, 1972

Shir72	D. A. Shirley, High-resolution X-ray photoemission spectrum of the valence band of gold, Phys. Rev. B 5 (1972), no. 12, 4709-4714
ShMö95	S.S. Sheiko, M. Möller. Scanning Force Microscopy on the Orientation of Gel-Crystallized Ultrahigh Molecular Weight Polyethylene in "Oriented Polymer Materials" S. Fakirov (Ed.), Hüthig & Wepf, Basel 1995
Sieg67	K. Siegbahn, C. Nordling, R. Fahlman, R. Nordberg, K. Hamrin, J. Hedman, G. Johansson, S. E. Karlsson, I. Lindgren, and B. Lindberg, ESCA, Atomic, Molecular and Solid State Structure Studies by Means of Electron Spectroscopy, Nova Acta Regiae Soc. Sci., Upsaliensis 20 (1967)
Sigg63	S. Siggia, Quantitative Organic Analysis via. Functional Groups, 3rd ed., Wiley, New York, 1963
Simo99	A. C. Simonsen, M. Schleberger, A. Nylandsted Larsen. Thin Solid Films 339(1999) 165
Somo94	G. A. Somorjai, Introduction to surface chemistry and catalysis, Wiley & Sons, Chichester (1994)
SpCh78	H. L. Spell and C. P. Chistenson. Surface Analysis of corona treated polyethylene – bonding and printability problems. In: TAPPI Papaer Synthetics Conference Proceedings, 283-291, Atlanta, 1978
Sper01	L. H. Sperling. Introduction to Physical Polymer Science. Third Edition 2001, John Wiley and Sons, New York
Spic58	W. E. Spicer, Photoemissive, photoconductive and optical absorbtion studies of alkali-antimony compounds, Phys. Rev. 112 (1958), no. 1, 114-122
SSKJ00	T. Schwarz-Selinger, A. von Keudell, W. Jacob. Novel method for absolute quantification of the flux and angular distribution of a radical source for atomic hydrogen. J. Vac. Sci. & Technol. A. 18 (3), 995 (2000).
Stei83	P. Steiner, T. Straub, F. Reinert, R. Zimmermann, S. Hüfner. Elastic and inelastic contributions to the XPS photoelectron diffraction pattern of Ni(100) and NiO(100). Surface Science 291 (1983) 154
StGu63	O. P. Strausz, H. E. Gunning. Reaction of electronically excited nitric oxide molecules with hydrocarbons. Can. J. Chem. 41 (1963), 1207
SwSc70	J. D. Swift, M. R. J. Schwar, Electrical Probes for Plasma Diagnostic, ILIFFE Books, London (1970)
Tama93	Y. Tamada. Cell adhesion to plasma-treated polymer surfaces. Polymer 34 (1993) 10, S. 2208-2212
TNS75	M. Tanaka, F. Nishimura, T. Shono. Anal. Chim. Acta 74. 119 (1975)
ToSi82	S. Tougaard and P. Sigmund, Inuence of elastic and inelastic scattering on energy spectra of electrons emitted from solids, Phys. Rev. B 25 (1982), no. 7, 4452-4466.
Toug89	S. Tougaard. Practical Algorith for Background Substraction. Surface Science 216 (1989) 343
Toug90	S. Tougaard. Inelastic background correction and quantitative surface analysis, J. Elelctron Spectrosc. Relat. Phenom. 52 (1990), 243-271
Toug96	S. Tougaard. Surface Nanostructure Determination by X-ray Photoemission Spectroscopy Peak Shape Analysis. J. Vac. Sci. Techn. A 14 (1996) 1415
Toug97	S. Tougaard. Surface Interf. Anal. 25 (1997) 137
UGM97	Manual V 2.0 The AFM/STM Users Guide OMICRON Vakuumphysik GmbH (1997).
VaGa89	T. G. Vargo, J. A. Gardella. Multitechnique surface spectroscopiec studies of plasma modified polymers III. J. of Poly. Sci.: Part A 27 (1989), S. 1267-1286
Vale00	H. B. Valentini. Sheath formation in low-pressure discharges. Plasma Sources Sci. Technol. 9 (2000) 574-582
Viss93	K. Vissing. Neue Möglichkeiten durch Niederdruckplasmen. Adhäsion 37 (1993) 12, S. 32-36
Vlec34	J. H. van Vleck. The Dirac Vector Model in Complex Spectra. Phys. Rev. 45 (1934), 405
Voge97	H. Vogel, Gerthsen Physik, Sonderauflage der 19. Ausgabe, 1997
WiGü92	R. Wiesendanger, H.-J. Güntherodt. Scanning Tunneling Microscopy II Springer Series in Surface Sciences 28. Berlin 1992
WiGü93	R. Wiesendanger, H.-J. Güntherodt. Scanning Tunneling Microscopy III Springer Series in Surface Sciences 29. Berlin 1993

Wilh95	J. Wilhelm. Plasma, der vierte Aggregatzustand der Materie. Stand und Perspektiven der Plasmatechnologie. 1994 Endbericht. Greifswald 1995
Wilk98	R. Wilken. Thesis. Untersuchungen zur Oberflächenmodifizierung ausgewählter Modellpolymere durch VUV-Photolyse. Potsdam, 1998
WuGu95	D. Y. Wu, W. Gutowski. Ammonia plasma treatment of polyolefins for adhesive bonding with a cyanoacrylate adhesive. J. of Adhesion Sci. And Technol. 9 (1995) 4, S. 501-525
www00	http://www-cxro.lbl.gov/optical_constants/atten2.html
www01	http://home.achilles.net/~jtalbot/data/elements/
www02	http://www.nanotec.es/
www03	http://www.newphotons.com/MgF2.htm
Yoff53	A. D. Yoffe, Research 6 (1953), 12
Zubr95	C. Zubrägel. Die elektronischen und geometrischen Eigenschaften von geordneten organischen Schichten. Thesis, University of Osnabrück (1995)